PIPELINE FLOW OF COARSE PARTICLE SLURRIES

A Thesis Submitted to the College of

Graduate Studies and Research

in Partial Fulfilment of the Requirements

for a Degree of Doctor of Philosophy

in the Department of Chemical Engineering

University of Saskatchewan

Saskatoon

by

Randall Gordon Gillies

In presenting this thesis in partial fulfilment of the requirements for a Postgraduate degree from the University of Saskatchewan, I agree that the Libraries of this University may make it freely available for inspection. I further agree that permission for copying of this thesis in any manner, in whole or in part, for scholarly purposes may be granted by the professor or professors who supervised my thesis work or, in their absence, by the Head of the Department or the Dean of the College in which my thesis work was done. It is understood that any copying or publication or use of this thesis or parts thereof for financial gain shall not be allowed without my written permission. It is also understood that due recognition shall be given to me and to the University of Saskatchewan in any scholarly use which may be made of any material in my thesis.

Requests for permission to copy or make use of material in this thesis in whole or part should be addressed to:

Head of the Department of Chemical Engineering

University of Saskatchewan

Saskatoon, Saskatchewan S7N 0W0

ABSTRACT

The horizontal pipeline flow of coarse-particle slurries has been examined. The study includes an evaluation of previous work, an experimental investigation and a presentation of improved modelling techniques for determining pipeline design parameters.

The experimental investigation was carried out to obtain an improved database for modelling the flow of coarse-particle slurries. Tests were conducted using sand slurries and coal slurries in pipes of industrial scale. Frictional headlosses, delivered solids concentrations, concentration distributions and velocity distributions were measured as functions of *in situ* solids concentration and mean velocity. Solids deposition velocities were determined visually using transparent pipe sections.

The experimental results were used to develop an improved two layer model for estimating frictional headlosses, a force balance model for concentration distributions and a method for predicting deposition velocities. The fraction of contact load, which contributes sliding friction at the pipe wall, was found to be primarily dependent on the ratio of the mean flow velocity to the settling velocity of the mass median coarse (+0.074 mm) particle size.

The models contain empirical correlations which incorporate a wide range of experimental conditions but are restricted to mixtures containing less than 35% coarse particles by volume. The correlations were tested using carrier fluids which were essentially Newtonian with viscosities less than 4 mPa.s.

ACKNOWLEDGEMENTS

I would like to acknowledge Dr. W.H.W. Husband, recently retired Director of Research and Development, Saskatchewan Research Council and Dr. C.A. Shook, Professor of Chemical Engineering, University of Saskatchewan for their cooperative effort to establish and maintain a pipeline research program in Saskatoon. Their outstanding contributions to the development of slurry pipelining technology are widely recognized in Canada and elsewhere.

More specifically, I would like to express my sincere gratitude to Dr. Shook for supervising this project and for providing invaluable guidance and encouragement.

I would like to thank Mr. M.H. Small, Senior Research Technologist, Saskatchewan Research Council, for his sound advice and assistance with the experiments.

In regard to modelling the flows, I would like to acknowledge the very helpful suggestions made by Dr. K.C. Wilson, Professor of Civil Engineering, Queen's University.

Energy Mines and Resources Canada provided funding for some of the pipeline experiments and this contribution is gratefully acknowledged.

TABLE OF CONTENTS

LIST OF TABLES

LIST OF FIGURES

LIST OF SYMBOLS

A	Cross-section area
Ar	Particle Archimedes number, $C_D\ Re^2$
c	Local value of the solids spatial volume fraction
C_{max}	Solids volume fraction in a loosely packed bed
C_c	Contact load concentration
C_D	Particle drag coefficient
C_f	Fine solids volume fraction
C_{lim}	Solids volume fraction in the lower layer (two layer model)
C_r	Mean *in situ* or spatial volume fraction of coarse solids
C_t	Mean *in situ* or spatial volume fraction of total solids
C_v	Solids volume fraction in the delivered mixture
C_w	Solids mass fraction in the delivered mixture
D	Pipe internal diameter
d	Particle diameter
d_{50}	Particle mass median diameter
F_D	Force acting on a particle due to fluid drag
F_G	Force acting on a particle due to gravity
F_L	Dimensionless deposit velocity, $V_c\ [g\ D\ (S_s - 1)]^{-0.5}$
F_p	Force per unit volume of particles due to particle interactions
F_t	Force per unit volume of particles due to turbulence
f	Fanning friction factor

f_{ij}	Interaction force acting on phase i due to j (per unit volume of i)
Fr_p	Froude number for the particles, V^2 / g d.
g	Acceleration due to gravity
h	Elevation above a datum
i	Headloss, m carrier fluid / m pipe
k	Pipe wall equivalent roughness
L	Length of a pipe section
m	Correlating parameter for the hindered settling velocity
P	Pressure
Q	Volumetric flowrate
R	Pipe radius
R	Slurry electrical resistance
r	Radial coordinate position
R_1	Inner cylinder radius (concentric cylinder viscometer)
R_2	Outer cylinder radius (concentric cylinder viscometer)
Re	Reynolds number for pipe flow
Re_p	Reynolds number for the particle
Ri	Richardson number
S	Segment length
S_s	Ratio of solids to liquid density, ρ_s / ρ_L
T	Torque per unit length
t	Time

u_*	Friction velocity
v	Local velocity
v'	Velocity fluctuation
V	Mean velocity of pipe flow
V_c	Deposition velocity
V_s	Hindered settling velocity for a slurry
V_∞	Particle settling velocity at infinite dilution
x	Axial coordinate position
y	Vertical coordinate position (positive upward)
y_0	Vertical position, $y_0 = - y / R$ where R is the pipe radius
α	Angle of internal friction of the particles
α_{ij}	Coefficients used to define turbulent stresses
β	Angle defining the location of the hypothetical interface for layer models
$\dot{\gamma}$	Shear rate
ϵ_s	Particle eddy diffusivity
η_s	Coefficient of particle-wall friction
θ	Angular coordinate position
κ	The fraction of the solids which are supported by particle interactions
μ	Viscosity
μ_p	Plastic viscosity (Bingham fluid model)
μ_r	Relative viscosity (mixture viscosity / carrier fluid viscosity)

ρ	Density
σ	Normal stress
τ	Stress
τ_w	Mean wall shear stress
τ_y	Yield stress (Bingham fluid model)
Φ	Excess headloss, $(i - i_L) / i_L C_v$
ω	Angular velocity

Subscripts:

f	Refers to the fluid
L	Refers to the liquid
m	Refers to the mixture
s	Refers to the solids

1 INTRODUCTION

1.1 Characterizing Slurries

For slurry pipelining applications it is convenient to categorize mixtures as "fine-particle" or "coarse-particle" where the distinction depends on the particle settling rates. Fine-particle slurries contain only non-settling or slowly settling particles which are completely suspended by the fluid during normal pipeline operation. Coarse-particle slurries, which are sometimes called "settling" slurries, contain particles which are too large to be fully suspended by fluid forces.

For fine-particle slurries, the particles and the carrier liquid are considered to form a pseudo-continuous phase so that single-phase fluid flow models can be used for predicting their pipeline behaviour. These models are often non-Newtonian, however. Coal-water fuel mixtures and finely divided mineral tailings mixtures are examples of fine-particle slurries. These slurries are sometimes called "non-settling" although in fact the particles may settle if the flow is stopped.

If the particles are too large to be fully suspended by the fluid then a portion of the immersed weight of these particles is transmitted to the wall of the pipe. During pipeline flow of these mixtures, energy is consumed by fluid-like friction and also by processes resulting from particle-wall interactions. The additional component of friction can be considerably larger than the fluid-like friction so that single-phase fluid models are not appropriate for estimating the flow behaviour of such slurries. The pipeline flow of these coarse-particle slurries is the focus of this study.

1.2 Coarse-Particle Slurry Applications

The vast majority of slurry pipelining designs are intended for short distance transportation of solids. These may include mine to mill haulage of mineral ores, mine to wash plant transportation of raw coal, in-plant transfers, and tailings disposal operations. For short distance applications, the pipeline design engineer will rarely have the freedom to specify that the particle size of the solids be reduced in order to improve the flow characteristics of the slurry. Instead, the pipeline will have to be designed to handle whatever the upstream process provides and this may include a substantial concentration of coarse particles.

Although the pipeline may be only a few kilometres in length, a coarse-particle slurry pipeline system may well require more than one centrifugal pump to generate the required pipeline pressure. Therefore, the capital cost of the project will be sensitive to the pipeline flow characteristics of the mixture. The design engineer will require a good estimate of the mixture's frictional pressure gradient before the economic feasibility of a proposed project can be evaluated.

1.3 The Need for Improved Models

In their present state of development, the two-phase flow models used to describe coarse-particle slurry flows are filled with empirical terms and actual pipeline flow data are usually required to verify these terms. The effects of pipe size are not well understood and therefore costly and time-consuming full-scale pipeline flow experiments are often required. There is such a wide variety of industrial slurries and so many

parameters contribute to their flow behaviour that it is unlikely that the need for testing can be eliminated entirely. However, with the development of better, mechanistically-based two-phase flow models, it should be possible to reduce the cost of a laboratory test program.

In slurry technology, it has been customary (eg. Wasp et al., 1970) to consider a mixture as being composed of two parts; a pseudo-continuous phase (or "carrier fluid"), which consists of the liquid and the fine solids and a dispersed phase which contains only the coarse solids. The fine particles affect the slurry behaviour by altering the density and the viscosity of the "fluid" but do not contribute directly to particle-wall friction. Depending on the fines concentration and the nature of particle-liquid surface interactions, the carrier fluid rheology may be similar to that for the liquid or it may be altered quite dramatically. Industrial slurries often contain surfactants as flocculants, flotation agents or dispersants and these frequently affect the carrier fluid rheology.

For the coarse solids fraction, the particle settling tendency is of dominant importance. Particle settling velocities are affected in a predictable manner by the particle diameter and shape, particle and fluid densities and by the solids concentration in the mixture. The particle settling tendency is also strongly dependent on the rheological nature of the carrier fluid.

In the design of a pipeline, the selection of a pipe diameter is usually based on economic considerations. The capital costs are lowest for small pipe diameters and the energy requirements are reduced by using diameters as large as possible. For settling slurries, there is a critical pipeline operating velocity, V_c at which a stationary deposit

of solids will form on the bottom of the pipeline. If the velocity is reduced below the critical value, the thickness of the stationary layer will increase, occluding part of the pipe cross-section from flow. The frictional headloss will tend to increase as the thickness of the stationary solids layer increases. Therefore, particle deposition imposes an additional constraint on the selection of a suitable operating velocity. In a typical design situation, the volumetric flowrate will be fixed and the design engineer will, based on an estimate of the deposition velocity, select a pipe diameter which gives the desired operating velocity. Therefore, it is essential that reliable estimates of the deposition velocity are available during the early stages of a pipeline design.

For coarse-particle slurry pipeline operations a large number of variables must be considered by the designer. The following variables are known to affect the pressure drop or energy consumption:

- Pipe diameter
- Average particle size of the coarse solids fraction
- Solids volume fraction (concentration)
- Particle to carrier fluid density ratio
- Carrier fluid viscosity
- Pipeline velocity

These parameters have always been reported in experimental investigations. Other parameters whose effects are known to be significant, but whose magnitudes have often been omitted, include pipe wall surface roughness, particle shape and the coefficient of friction between the particles and the pipe wall.

Although there is considerable information in the open literature on coarse-particle slurry flows much of it is restricted to small (less than 100 mm) pipes. Unfortunately, little of the published data for larger pipes are useful for model development because of the omissions noted above. An experimental program has been carried out at the Saskatchewan Research Council's pipeline laboratory to generate as much data as possible to rectify this deficiency. This experimental program is an important component of this thesis.

1.4 Key Elements of this Study

In this investigation, experiments were conducted to examine slurry flow behaviour for a wide range of pipe diameters (50 to 500 mm), average particle sizes (0.18 mm to 2.4 mm), solids volume fractions (0 to 0.4) and pipeline operating velocities. The constraints of cost and time limited the range of particle-fluid density ratios and carrier fluid viscosities. Sand-in-water slurries were used for most of the tests so that the particle-fluid density ratio was approximately 2.65. Coal-water slurries with a density ratio of approximately 1.4 were used in a few of the tests. The carrier fluid viscosity varied from 0.5 mPa.s for hot water to approximately 4 mPa.s for cold water containing fine solids.

The results of this study are directly applicable to a large number of slurry pipelining situations of industrial importance in Canada. These include ore hydrotransport and tailings disposal for the oil sand, metallurgical and potash industries and run-of-mine coal pipelining. Because of the carrier fluid viscosity limitation, the

results of this study are not directly applicable to slurry pipeline situations where the carrier liquid has a viscosity which is substantially higher than that of water or where the carrier liquid is non-Newtonian. The so-called long-distance coal-water or coal-oil slurry pipelines would fall into the latter category.

This study contains the following:

1. A review of the basic concepts for slurry flows,
2. A review of previous work in the area of coarse-particle slurry pipelining,
3. A presentation of the results of new coarse-particle slurry pipeline experiments,
4. An improved model for estimating frictional headlosses for pipeline flow of coarse-particle slurries,
5. A model for estimating the concentration distribution for mixtures flowing in pipelines,
6. A correlation for estimating the solids deposition velocity for pipeline flow of coarse-particle slurries.

2 BASIC CONCEPTS FOR SLURRY FLOWS

2.1 Definitions

Several definitions are commonly used by design engineers to describe slurry pipeline flows. The capacity of the pipeline is of primary importance: a slurry pipeline delivers solids at a volumetric flowrate Q_s and carrier liquid at a volumetric flowrate Q_L. Both quantities are considered to be fixed in a typical design situation.

The mean (bulk) velocity V is an important slurry pipeline design variable because it must exceed the deposition velocity of the slurry. For a pipe of diameter D, the cross sectional area A is $\pi D^2 / 4$ and the mean velocity of the slurry is

$$V = \frac{Q_s + Q_L}{A} \tag{2.1}$$

Most slurry pipelines operate over a relatively narrow range of mean velocities near their optimum. For turbulent flows, the frictional headlosses will be unnecessarily large if the mean velocity exceeds the deposition velocity substantially.

For the pipe section shown in Figure 2.1, the solids and liquid flowrates can be written in terms of time-averaged local concentrations and velocities:

$$Q_s = \int_A v_s c \, dA \tag{2.2}$$

$$Q_L = \int_A v_L (1-c) \, dA \tag{2.3}$$

During steady state operation of a once-through pipeline system, the mean solids concentration in the delivered mixture is fixed by the feed rates of solids and carrier liquid. The solids volume fraction in the delivered mixture is

$$C_v = \frac{Q_s}{Q_s + Q_L} \tag{2.4}$$

For slurry flow experiments conducted in recirculating pipeline flow loops, the total *in situ* or spatial concentration is more often the quantity which is fixed during an experiment. At the start of the experiment, a measured volume of solids is placed in a pipeline loop of known volume. The mean *in situ* concentration remains constant during the test and the delivered concentration may vary as the flowrate is altered. In terms of a pipe of cross sectional area A, the *in situ* concentration is

$$C_r = \frac{1}{A}\int_A c \, dA \tag{2.5}$$

and the mean solids velocity is

$$V_s = \frac{1}{AC_r}\int_A c v_s \, dA = \frac{Q_s}{AC_r} \tag{2.6}$$

Similarly, the mean velocity for the carrier liquid is

$$V_L = \frac{Q_L}{A(1-C_r)} \tag{2.7}$$

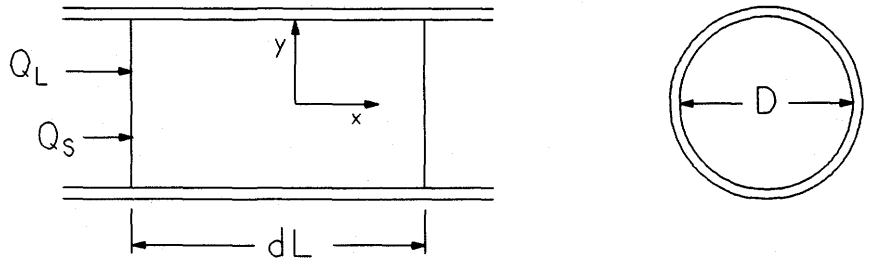

Figure 2.1: An elemental control volume for pipeline flows.

Although v_s and v_L may have similar values at any point in the flow in horizontal pipes (i.e. the local values of particle-fluid slip, $v_L - v_s$, are often small), the variations in c and v_s (or v_L) over the cross section often results in significant differences between V_s and V_L for coarse-particle slurry flows.

The solids mass fraction in the delivered mixture is often specified in design situations:

$$C_w = \frac{\rho_s Q_s}{\rho_s Q_s + \rho_L Q_L} \tag{2.8}$$

where ρ_s is the solids density and ρ_L is the liquid density.

The density of a mixture of solids concentration c is

$$\rho_m = \rho_s c + \rho_f (1-c) \tag{2.9}$$

2.2 Conservation of Mass

Assuming matter to be continuous, the rate of mass accumulation in a stationary volume element is equal to the rate of mass input minus the rate of mass output. Using vector notation, this is written as

$$\frac{\partial \rho}{\partial t} = -\nabla \cdot (\rho V) \tag{2.10}$$

$\nabla \cdot (\rho V)$ is the divergence of the vector ρV and represents the net rate of loss of mass per unit volume by fluid flow.

In the rectangular coordinate system, the mass conservation equation is

$$\frac{\partial \rho}{\partial t} + \frac{\partial}{\partial x}(\rho v_x) + \frac{\partial}{\partial y}(\rho v_y) + \frac{\partial}{\partial z}(\rho v_z) = 0 \tag{2.11}$$

For a system where solids are dispersed in a liquid, the solids volume fraction c may be defined in a time averaged sense as the probability of finding the dispersed phase at the particular point of interest. This definition of c allows us to visualize the two-phase system as two interpenetrating continua so that we can write continuity equations for each phase. For the solids

$$\frac{\partial}{\partial t}[c\rho_s] = -\nabla\cdot[c\rho_s V_s] \tag{2.12}$$

and for the liquid

$$\frac{\partial}{\partial t}[(1-c)\rho_L] = -\nabla\cdot[(1-c)\rho_L V_L] \tag{2.13}$$

2.3 Conservation of Momentum

Momentum is conserved when the rate of momentum accumulation in a stationary volume element is equal to the net rate of momentum input by convection plus the sum of the forces acting on the system. If gravity is the only body force, the conservation of momentum equation may be written as

$$\frac{\partial}{\partial t}(\rho V) = -\nabla\cdot(\rho VV) - \nabla\cdot T - \nabla P - \rho g \nabla h \tag{2.14}$$

The left hand side of Equation 2.14 represents the rate of increase of momentum per unit volume. ρVV is the convective momentum flux (nine components) and $-\nabla\cdot(\rho VV)$ represents the net rate of momentum gain by convection per unit volume. T is

the stress tensor with nine components of the form τ_{ij} where i denotes the surface on which the stress component acts and j denotes the direction of the component. $\nabla \cdot T$ represents the rate of momentum loss by viscous transfer. The vector ∇P is the pressure force and ρ g ∇h is the gravitational force on the element per unit volume. h is the elevation above a datum.

For a constant density fluid flowing in a pipe section, the equation for momentum conservation in the x (axial) direction may be written in rectangular coordinates as:

$$\rho \frac{Dv_x}{Dt} = -\left(\frac{\partial \tau_{xx}}{\partial x} + \frac{\partial \tau_{yx}}{\partial y} + \frac{\partial \tau_{zx}}{\partial z} \right) - \frac{\partial P}{\partial x} - \rho g \frac{\partial h}{\partial x} \qquad (2.15)$$

Here, the combined momentum accumulation and convective momentum terms are represented by the substantial derivative D /Dt:

$$\frac{Dv_x}{Dt} = \frac{\partial v_x}{\partial t} + v_x \frac{\partial v_x}{\partial x} + v_y \frac{\partial v_x}{\partial y} + v_z \frac{\partial v_x}{\partial z} \qquad (2.16)$$

2.4 Turbulent Stresses

The momentum equations for a fluid, such as Equation 2.14, can be written in terms of the instantaneous values of the velocity components. However, it is often more convenient to think in terms of time-averaged values of velocities. The inertial forces associated with turbulent flows are then considered to be contributions to the stress components of Equation 2.14. For the simple pipe flow situation, where the x-wise

velocity varies only with radial position r, the stress τ_{rx} in turbulent flow is expressed in terms of the velocity fluctuations associated with the turbulence, v'_x and v'_r, by

$$\tau_{rx} = \rho \overline{v'_x v'_r} - \mu \frac{dv_x}{dr} \tag{2.17}$$

The first term on the right hand side of Equation 2.17 represents the inertial stress which is also referred to as the turbulent Reynolds stress. The bar superscript indicates that the quantity is time-averaged. The second term on the right hand side of Equation 2.17 is the viscous contribution to the total stress and v_x is the time-averaged velocity component. For turbulent pipe flow, the inertial stresses are much larger than the viscous stresses everywhere except very near the pipe wall.

An eddy kinematic viscosity, ν_t, is sometimes used to represent the inertial contribution:

$$\nu_t \frac{dv_x}{dr} = -\overline{v'_x v'_r} \tag{2.18}$$

Longwell (1966) showed that Equation 2.15 may be integrated over the cross section of a pipe of diameter D to give

$$\rho\left(\frac{\partial V}{\partial t} + V\frac{\partial V}{\partial x}\right) + \frac{4\tau_w}{D} = -\frac{\partial P}{\partial x} - \rho g \frac{\partial h}{\partial x} \tag{2.19}$$

where V is the time and area averaged mean velocity and τ_w is the value of τ_{rx} at the wall of the pipe. τ_w includes the effect of the inertial stress in the flow.

The friction velocity, $u_* = (\tau_w/\rho)^{0.5}$, is a useful correlating parameter because it provides an indication of the intensity of turbulence during pipe flow (Laufer, 1954). The time averaged values of the velocity fluctuations scale nearly as u_*.

2.5 Interaction Forces

For pipeline flow of solid-liquid mixtures, there are forces acting on each phase because of the presence of the pipe wall. In the notation of Wallis (1969) f_{sw} and f_{Lw} are the forces acting on the solids and the liquid respectively because of the wall. It is sometimes convenient to separate the wall interaction forces for the solids into those resulting from direct particle-wall contact (also represented by the symbol f_{sw}) and those transmitted to the wall as a result of particle-particle interactions (f_{ss}).

In addition to the wall-related forces, there are interfacial forces acting on the solids (f_{sL}) and on the liquid (f_{Ls}) because of the slip velocity. Each of these interaction forces is expressed per unit volume of the phase upon which the force acts. The net interfacial interaction force per unit volume of mixture must of course be zero. Therefore,

$$c f_{sL} + (1-c) f_{Ls} = 0 \tag{2.20}$$

The stress components of Equation 2.15 may be related to the wall interaction forces. Assuming that turbulence effects are included in the stresses, the momentum equation for a single-phase fluid may be written as

$$\rho_L \frac{Dv_{Lx}}{Dt} = f_{Lw} - \frac{\partial P}{\partial x} - \rho_L g \frac{\partial h}{\partial x} \tag{2.21}$$

For a two phase mixture, momentum equations may be written for each phase using the interpenetrating continuum model described by Wallis (1969) by including the interfacial forces. For the liquid phase, Equation 2.21 is re-written as

$$\rho_L \frac{Dv_{Lx}}{Dt} = f_{Lwx} + f_{Lsx} - \frac{\partial P}{\partial x} - \rho_L g \frac{\partial h}{\partial x} \tag{2.22}$$

and for the solids as

$$\rho_s \frac{Dv_{sx}}{Dt} = f_{swx} + f_{sLx} - \frac{\partial P}{\partial x} - \rho_s g \frac{\partial h}{\partial x} \tag{2.23}$$

The forces in Equations 2.22 and 2.23 are expressed per unit volume of the particular phase while the stress components of Equation 2.15 are averaged over the appropriate surface of the elemental volume. Therefore, for a solid-liquid mixture, the wall interaction forces and the stress components are related as follows:

$$f_{Lwx} = -\left(\frac{1}{1-c}\right)\left(\frac{\partial \tau_{Lxx}}{\partial x} + \frac{\partial \tau_{Lyx}}{\partial y} + \frac{\partial \tau_{Lzx}}{\partial z}\right) \tag{2.24}$$

$$f_{swx} = -\left(\frac{1}{c}\right)\left(\frac{\partial \tau_{sxx}}{\partial x} + \frac{\partial \tau_{syx}}{\partial y} + \frac{\partial \tau_{szx}}{\partial z}\right) \tag{2.25}$$

2.6 Particle Drag Coefficient

The interfacial force exerted on a particle by the fluid is calculated from an expression which defines the particle drag coefficient C_D.

$$F_D = 0.5\, C_D\, A_p\, \rho_L\, (v_L - v_s)|v_L - v_s| \tag{2.26}$$

A_p is the cross-sectional area of the particle and $v_f - v_s$ is the velocity of the fluid relative to the particle. The drag force acts in the direction of the relative velocity.

2.7 Coulombic Friction

For granular solids the particle stresses τ_{syx} and τ_{syy} are considered to be related. If τ_{syy} is fixed, say by gravity, and if motion occurs in the x direction, then the stresses are related by a coefficient of Coulombic friction, η_s.

$$\tau_{syx} = \eta_s \tau_{syy} \tag{2.27}$$

The coefficient of friction depends on the nature of the two surfaces. For particles flowing parallel to a pipe wall, the coefficient of friction is reduced by lubrication effects if the particles and the wall are separated by a liquid layer. For pipe flow, the value of η_s between particles and the pipe wall will be independent of the mean velocity provided that the lubrication force is small.

2.8 Frictional Headloss

For macroscopically steady state operation of a pipeline of constant cross sectional area transporting a constant density mixture, the inertial and kinetic energy terms in Equation 2.19 are zero. The simplified equation for this situation is

$$\frac{4\tau_w}{D} = -\frac{dP}{dx} - \rho g \frac{dh}{dx} \tag{2.28}$$

The right hand side of Equation 2.28 is often written (i ρ_L g) where i is the headloss with units (m liquid / m pipe length). If the pipe is horizontal, the

measurement of the pressure drop $P_1 - P_2$ over a pipe section of length L provides a direct measure of the frictional headloss:

$$\frac{4\tau_w}{D} = i\rho_L g = \frac{P_1 - P_2}{L} \tag{2.29}$$

It is convenient to use a friction factor to estimate the wall shear stress for pipeline flow of fluids. The Fanning friction factor f is defined by the following equation:

$$i\rho_L g = \frac{2fV|V|\rho_L}{D} \tag{2.30}$$

The simplest flow behaviour is that of Newtonian fluids. Using cylindrical coordinates, the time rate of shear strain in laminar pipe flow is

$$\dot{\gamma}_{rx} = -\frac{dv_x}{dr} = \frac{\tau_{rx}}{\mu} \tag{2.31}$$

For Newtonian fluids, the Fanning friction factor can be determined from the Reynolds number $Re = D\ |V|\ \rho / \mu$ and the equivalent sand roughness of the pipe wall k (Churchill, 1977).

$$f = 2\left[(8/Re)^{12} + (A+B)^{-1.5}\right]^{1/12} \tag{2.32}$$

where

$$A = \left[-2.457\ \ln\left(\left(\frac{7}{Re}\right)^{0.9} + \frac{0.27k}{D}\right)\right]^{16}$$

and

$$B = (37530/Re)^{16}$$

A Fanning friction factor may also be defined for the flow of mixtures:

$$i\rho_L g = \frac{2 f_m V|V| \rho_m}{D} \tag{2.33}$$

For fine-particle slurries at low solids concentration, satisfactory estimates of the headloss are often obtained by assuming that the Fanning friction factor for the mixture is the same as that for the fluid flowing in the same pipe at the same mean velocity. In this case, the slurry to carrier liquid headloss ratio is

$$\frac{i}{i_L} = 1 + C_v(S_s - 1) \tag{2.34}$$

where S_s is the density ratio ρ_s / ρ_L. Strictly, Equation 2.34 applies only if the mixture is effectively Newtonian with a kinematic viscosity $\nu = \mu / \rho$ which is equal to the kinematic viscosity of the carrier liquid. However, as the slurry concentration increases, measurements show that the slurry viscosity can be substantially greater than that of the liquid.

While this study is concerned mainly with coarse-particle slurry flows, some consideration has to be given to fine-particle (non-settling) slurry behaviour. A coarse-particle slurry often contains a substantial amount of fine solids and at high concentrations, fine-particle slurries often exhibit non-Newtonian shear-thinning behaviour. The two most useful shear thinning models are the Bingham fluid model and the power law model. In the Bingham model the fluid is assumed to have a yield stress

τ_y and a plastic viscosity μ_p. The power law fluid model also uses two coefficients (K and n) to characterize the slurry. For pipe flow these models are

$$-\frac{dv_x}{dr} = \frac{\tau_{rx} - \tau_y}{\mu_p} \tag{2.35}$$

$$\frac{dv_r}{dr} = \left(\frac{\tau_{rx}}{K}\right)^{1/n} \tag{2.36}$$

3 PREVIOUS STUDIES OF COARSE-PARTICLE SLURRY FLOW

3.1 Introduction

From observation of the flows through transparent pipe sections, early investigators (Newitt et al., 1955) defined at least three regimes: "homogenous suspension", "heterogeneous suspension" and flow with a "sliding bed" of solids in the lower part of the pipe. With improved instrumentation, it is now possible to measure the velocity and concentration distributions within flowing mixtures. These measurements show that what appears to be a "sliding bed" is almost always the flow of a sheared mixture. It now seems more appropriate to regard "settling" slurry flows to be bounded by two limiting cases. The first situation is pseudohomogeneous flow, in which fluid lift forces are strong enough to support the entire immersed weight of the particles. At the other extreme form of behaviour, the particles are so coarse that practically the entire immersed weight of the particles is supported by contact with the pipe wall. The latter case is sometimes described as "completely segregated" flow.

Although pipelines of various sizes are used throughout the world to transport coarse-particle slurries, the vast majority of reliable pipe flow data have been collected in small laboratory pipeline flow loops less than 100 mm in diameter. A large number of correlations have been proposed for estimating frictional headlosses and deposition velocities. Unfortunately, these correlations are limited by a shortage of good quality data for flow in large pipes. This chapter discusses a few of the correlations; those which are particularly useful because they incorporate large databases or because they

illustrate important aspects of coarse-particle slurry flows. Also, predictive methods which have a mechanistic basis are reviewed.

Industrial coarse-particle slurries often contain significant concentrations of fine particles. When modelling the mixture flows, consideration has to be given to the effects of the fine particles on the rheological properties of the carrier liquid. For this reason, a brief review of non-settling slurry flows is included in this chapter.

3.2 Headloss for Non-settling Slurry Flows

Fine-particle slurries which are non-settling or which settle slowly upon standing are usually assumed to behave like homogeneous fluids during pipe flow. Normally laminar flow experiments are conducted to determine a suitable fluid flow model. The relative viscosity of a mixture ($\mu_r = \mu_m / \mu_L$) depends on the solids volume fraction c, the particle size and size distribution, particle shape, particle-particle interactions and fluid-particle interactions. In 1906, Einstein presented a theoretical equation relating μ_r to c for very dilute suspensions of spherical particles.

$$\mu_r = 1 + 2.5c \tag{3.1}$$

Based on the results of a number of experimental studies with deflocculated monosized spheres, D.G. Thomas (1965) developed an empirical equation to extend Einstein's equation to higher concentrations.

$$\mu_r = 1 + 2.5c + 10.05c^2 + 0.00273\exp(16.6c) \tag{3.2}$$

If the mixture is essentially Newtonian, Churchill's equation may be used to estimate headlosses for turbulent flows. For non-Newtonian fluids, the shear strain rate

and possibly the shear history are important. The Metzner and Reed (1955) method is useful for scaling laminar pipe flow data to larger pipes for time independent non-Newtonian mixtures. An alternative method is to curve-fit the data from a tube viscometer or concentric cylinder viscometer to a model (Bingham fluid, power law fluid, etc.) and use the correlating coefficients to calculate headlosses for other pipe sizes. Several methods including those of Dodge and Metzner (1959) and Wilson and Thomas (1985) have been proposed for estimating turbulent flow headlosses from laminar flow data for non-Newtonian slurries.

3.3 Headloss Correlations for Settling Slurries

Single-phase fluid models are inappropriate for slurries which contain coarse particles. The Durand-Condolios approach to modelling coarse-particle slurry flows is widely quoted and many efforts have been made to improve this correlation since its introduction in 1952. The Durand-Condolios correlation contains two useful dimensionless variables, an excess headloss Φ and a dimensionless grouping of the independent variables Ψ. Φ relates the actual slurry frictional headloss i to i_L, the frictional headloss for the carrier liquid travelling in the same pipe at the same mean velocity.

$$\Phi = \frac{i - i_L}{C_v i_L} \tag{3.3}$$

Using the particle drag coefficient, C_D, the independent variables are grouped as

$$\Psi = \frac{V^2\sqrt{C_D}}{gD(S_s - 1)} \tag{3.4}$$

A commonly used version of the Durand-Condolios correlation is

$$\Phi = 81\,\Psi^{-3/2} \tag{3.5}$$

From Equation 2.34 we see that for pseudohomogeneous flows (high values of Ψ) the excess headloss Φ should approach (S_s - 1) rather than zero as it does with the Durand-Condolios correlation. Charles (1970) attempted to rectify this deficiency with the following modification:

$$\Phi = 120\,\Psi^{-3/2} + (S_s - 1) \tag{3.6}$$

To account for broad size distributions, Wasp et al. (1970) suggested that the slurry be divided into "homogeneous" and "heterogeneous" fractions. The solids in the homogeneous fraction were considered to increase the viscosity and the density of the "equivalent liquid vehicle". This approach leads to several modifications to the Durand-Condolios equation:

1. The liquid headloss, i_L, is replaced by i_f, the headloss for the liquid-fines mixture.
2. C_v is replaced by $C_{v,\,het}$, the heterogeneous solids volume fraction in the mixture.
3. S_s and C_D are modified because of the effects of the fine particles on the density and viscosity of the carrier vehicle.

Wasp's method divides the solids into several size intervals and uses an empirical equation to estimate the "homogeneous" solids fraction for each size interval. The Wasp procedure is equivalent to

$$\frac{x_{i,hom}}{x_i} = \exp\left(-\frac{bV_{i\infty}}{u_*}\right) \tag{3.7}$$

where u_* is the friction velocity, $V_{i\infty}$ is the terminal settling velocity of the particles in interval i in the "equivalent liquid" and b is a dimensionless constant.

As an alternative method for determining the cut-off point between fines and coarse particles, Faddick (1982) suggested that particles that settle with values of C_D greater than 24 should be considered to be part of the "homogeneous" fraction.

Shook et al. (1982) showed that the Durand-Condolios approach badly overestimates the headlosses for coarse-particle slurries flowing in large diameter pipes. This deficiency is unfortunate because indiscriminate use of correlations based on the Durand-Condolios approach could make potentially viable slurry pipelining projects appear to be uneconomic.

The Wasp method is an improvement over the Durand-Condolios correlation because the effects of fine particles on the carrier fluid properties are considered. However, the Wasp method shares the shortcomings of the Durand-Condolios correlation for large pipe flow predictions.

Newitt et al. (1955) distinguished the resistance contributions of the carrier liquid from that associated with particles whose immersed weight is transmitted to the pipe

wall. They reasoned that the excess headloss should be approximately proportional to the solids immersed weight. Their expression for the excess headloss is

$$\Phi = \frac{66gD(S_s - 1)}{V^2} \tag{3.8}$$

which in terms of i is approximately

$$i = i_L + 0.8C_v(S_s - 1) \tag{3.9}$$

Unlike the Durand-Condolios equation, Equation 3.9 has a theoretical basis and may be regarded as an upper limit to the headloss for fully stratified flows. For these flows, fluid turbulence is ineffective in suspending the coarse particles and the entire immersed weight of the solids fraction is supported through particle-wall contact.

3.4 Mechanistic Models for Settling Slurries

Correlations are gradually being replaced by mechanistically-based models for estimating pipeline frictional headlosses for coarse-particle slurries. Two modelling approaches are in current use:

1. a macroscopic approach in which the flow domain is perceived to be divided into layers which are coupled by hypothetical horizontal interfaces and
2. a microscopic approach in which the flow domain is divided into elemental volumes and the equations of continuity and motion are applied to each element.

3.4.1 Layer Models

Newitt and coworkers (1955) were the first to recognize that, in addition to fluid-like friction, there is friction due to transmission of the immersed weight of particles to

the pipe wall. Their analysis was not rigorous, however. An improved analysis, the force-balance model, was used to estimate the limit of stationary deposition (Wilson, 1970) and headlosses for dense-phase flow (Wilson, Streat and Bantin, 1972).

The force balance model led to the development of a two layer model to describe the flows of more dilute coarse-particle mixtures (Wilson, 1975 and Wilson, 1976). Basically, the two layer model consists of coupled force balance and mass balance relationships for the two layers. The force balance includes contributions due to fluid-wall friction in each layer and the friction due to particle-wall friction in the lower layer. Wilson used a kinematic coefficient of friction conceptually similar to the coefficient of particle-wall friction, η_s, defined in Equation 2.21, to determine the frictional contribution resulting from the particle-wall normal forces. In addition to the wall forces, there are interfacial forces acting on each layer at the horizontal interface between the two layers.

Televantos et al. (1979) published a version of the two layer model, conceptually identical to that of Wilson, which contains a concise presentation of the methods of calculation. As shown in Figure 3.1, the pipe is divided into an upper layer of area A_1 containing only carrier fluid and a lower layer of area A_2 which contains the solids at a concentration C_2.

By assuming steady and incompressible flow Televantos et al. wrote the conservation of mass equations for the fluid and the particles in the following form:

$$AV = A_1V_1 + A_2C_2V_{s2} + A_2(1-C_2)V_{f2} \tag{3.10}$$

$$C_vAV = C_2A_2V_{s2} \tag{3.11}$$

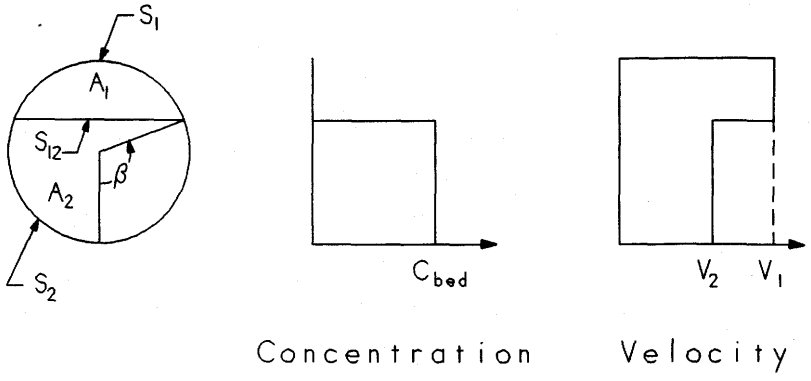

Figure 3.1: An early version of the two layer model (Televantos et al., 1979).

The mass balance relationships may be simplified by assuming that the particle-fluid slip velocity in the lower layer is small so that approximately $V_{s2} = V_{f2}$.

By integrating the momentum equations over A_1 and A_2 separately and by assuming steady and horizontal flow, Televantos et al. wrote force balances for each layer:

$$i \rho_L g - (\tau_1 S_1 + \tau_{12} S_{12})/A_1 = 0 \tag{3.12}$$

$$i \rho_L g + (\tau_{12} S_{12} - \tau_2 S_2)/A_2 = 0 \tag{3.13}$$

For the upper layer, a friction factor, f_1, is used to compute the shear stress τ_1.

$$\tau_1 = f_1 V_1^2 \rho_1 / 2 \tag{3.14}$$

Televantos et al. used a modified Colebrook friction factor for turbulent flow over rough boundaries to estimate the interfacial friction factor, f_{12}.

$$f_{12} = \frac{1}{[\, 4 \log(D/d) + 3.36]^2} \tag{3.15}$$

Here d is the mean particle diameter and D is the pipe diameter.

The lower layer shear stress τ_2 is comprised of two effects, fluid-boundary friction and particle-boundary friction. The particle-boundary friction effect contains two terms, one which is due to the immersed weight of the solids and a second which is due to the transmission of the interfacial stress through the sliding bed of solids. Both of these effects were recognized by Wilson (1970). The solids which are supported by the pipe wall generate a normal interparticle stress which increases with depth, y, as

$$\frac{d\sigma_2}{dy} = (\rho_s - \rho_f) g C_{lim} \tag{3.16}$$

where C_{lim} is the concentration of the supported bed of solids. The interfacial shear stress produces a normal stress in the solids bed $\sigma_{12} = \tau_{12} / \tan \alpha$ where α is the angle of internal friction of the particles. Integrating σ_2 from the interface to the pipe wall, the combined wall shear stress in the lower layer is

$$\tau_2 S_2 = \frac{f_2 V_2^2 \rho_f S_2}{2} + \frac{\rho_f (S-1) g C_2 D^2 (\sin\beta - \beta\cos\beta)\eta_s}{2} + \frac{\tau_{12} C_2 S_2 \eta_s}{\tan\alpha} \tag{3.17}$$

Wilson (1976) extended the two layer model for use with mixtures of finer particles where only a fraction of the immersed solids weight is supported by the pipe wall. In this case, the upper layer is assumed to contain suspended solids and the lower layer contains solids which are supported through contact with the pipe wall. The suspended solids and carrier fluid contribute fluid-like friction while the contact load fraction contributes a kinematic friction component. Using coarse-particle mixture data available at the time, Wilson (1976) proposed the following relationship to estimate the contact load concentration, C_c:

$$C_c = \sum_{i=1}^{N} C_{ci} \tag{3.18}$$

where

$$C_{ci}/C_v = 0.36(V_{\infty i}/u_*)^2 \exp(90 d_i/D) \tag{3.19}$$

The strength of the layer modelling approach is that it provides a relatively simple mechanistic method for dealing with the pipe wall stress components which arise from fluid-like friction and particle-induced friction. In addition to providing frictional headloss estimates, the model is a useful tool for estimating solids delivered concentrations for coarse-particle flows and for understanding the nature of solids deposition in pipelines.

It is likely that layer models will eventually be replaced by more sophisticated microscopic models. Microscopic models are capable of providing truer representations of the nature of coarse-particle slurry pipeline flows. However, at their present stage of development, microscopic models contain numerous empirical coefficients of doubtful generality. When attempting to generalize experimental results, the number of empirical coefficients which must be inferred from a set of experiments is considerably smaller for layer models than for microscopic models. This is a major advantage of the layer modelling approach.

3.4.2 Microscopic Models

In homogeneous pipeline flow, the point of maximum velocity is located at the centre of the pipe and the shear stress τ_{rx} varies linearly with radial position in the pipe:

$$\tau_{rx} = \tau_w r/R \tag{3.20}$$

Here τ_w is the shear stress at the wall and R is the radius of the pipe. The situation is much more complex for non-vertical pipeline flow of settling slurries, however. A concentration gradient will exist due to the settling tendency of the solids and the dilute mixture in the upper portion of the pipe will travel at a higher velocity than the dense mixture in the lower portion. The shear stress in these flows is zero at some point above the centre of the pipe. Since the local concentration will affect the rate of momentum transfer, in solving the equations of motion over the flow domain, the modeller will require a method for estimating the concentration distribution.

Schmidt (1925) and Rouse (1937) used a diffusion model to estimate the concentration gradient for open channel flows. The model relates the concentration gradient to V_∞, the particle settling velocity at infinite dilution and ϵ_s, a solids diffusion coefficient. With y positive upward, the diffusion model is

$$\epsilon_s \frac{dc}{dy} = -V_\infty c \tag{3.21}$$

The solids diffusion coefficient was considered to be analogous to ν_t, the eddy kinematic viscosity used to describe momentum diffusion during turbulent flow.

The Schmidt-Rouse equation was found to be appropriate for low concentrations where hindered settling effects can be neglected. Daniel (1965) examined the effects of higher concentrations in a series of coarse particle slurry flow experiments. He used a rectangular channel 2.5 cm deep and 10 cm wide and found that, at low concentrations, the gradient was approximately exponential as predicted by the Schmidt-

Rouse equation. However, if the concentration was high, the gradient was much lower than predicted. An improvement to the Schmidt-Rouse equation was obtained by replacing V_∞ with a hindered settling velocity correction of the type proposed by Richardson and Zaki (1954). Wallis (1969) suggested that the hindered settling velocity for a slurry could be estimated as

$$V_s = V_\infty (1-c)^m \tag{3.22}$$

where

$$m = \frac{4.7\left(1+0.15\,Re_\infty^{0.687}\right)}{1+0.253\,Re_\infty^{0.687}}$$

and the particle Reynolds number, Re_∞ is written in terms of the particle diameter d as

$$Re_\infty = d\,V_\infty\,\rho_f / \mu$$

Equation 3.22 does not reflect the fact that the settling velocity approaches zero as the solids concentration approaches the limiting value for a packed bed, C_{max}. Roco and Frasineanu (1977) showed that better results could be obtained at high concentrations by including the term $(1 - c / C_{max})$ in the Schmidt-Rouse equation.

Daniel also found that, in some experiments, the concentration passed through a maximum value so that the concentration gradient became negative near the bottom of the channel. This result shows that there are forces which tend to move particles from the region of low velocity near the wall to regions of higher velocity and these forces are great enough to exceed the gravitational force in some cases.

The observations of particle migration away from the region of the pipe wall have been verified by a number of other experimenters. Sumner et al. (1989) determined that the particle concentration was reduced at the wall for turbulent flow of nearly neutrally buoyant solid-liquid mixtures. Their experimental results showed that inward migration tendency is strongest when the particles are large, the solids concentration is high and the velocity is high. Wysoluzil et al. (1987) and Gillies and Shook (1992) found reduced dispersed phase concentrations near the pipe wall for laminar flow of mixtures consisting of oil droplets dispersed in water. Effects which would tend to repel particles from the wall include the lift force which occurs when slip and shear occur together (Saffmann, 1965).

A repelling or dispersive stress also occurs in slurry flows because of the interactions of particles moving in layers at different velocities. This repulsive normal stress was first revealed by the experiments of Bagnold (1954) who found that it was proportional to the shear stress. If the ratio of inertial to shear forces is low the shearing process is said to be "macroviscous" and the shear stress τ_{syx} and the normal stress were found to vary with the first power of the shear strain rate $\dot{\gamma}$:

$$\tau_{syx} = \mu_f f(c) \dot{\gamma}_{syx} \tag{3.23}$$

When the inertial to shear forces are high, the shear stress and normal stress are due to collisions between particles moving in layers at different velocities. In this case, the shear is said to be "inertial" and the strain rate-stress relationship was found to be

$$\tau_{syx} = K \rho_s f(c) d^2 \dot{\gamma}_{syx} |\dot{\gamma}_{syx}| \tag{3.24}$$

Here, d is the particle diameter and ρ_s is the density. The factor K has been found to depend on the coefficient of restitution of the particles and on velocity fluctuations (Hanes and Inman, 1985).

In both macroviscous and inertial regimes, the interparticle dispersive stress increases with the shear rate and the particle concentration. In the vicinity of the pipe wall, the shear rate decreases rapidly with distance from the wall so there will be a net force which tends to move particles inward. It seems reasonable to conclude that this dispersive stress can contribute to the observed reduced particle concentration near the pipe wall.

Roco and Shook (1983) and Shook and Roco (1990) presented a force balance approach to modelling the concentration distribution for pipeline flow of settling slurries. For horizontal pipe flow, the balance of dominant forces acting on the particles, and affecting the concentration gradient in the vertical direction, is written as

$$\frac{3\rho_f C_D}{4d}\,\frac{\epsilon_s^2}{c^2(1-c)^{2m-2}}\,\frac{dc}{dy}\left|\frac{dc}{dy}\right| = (\rho_s-\rho_f)g - \frac{1}{c}\,\frac{d}{dy}\left[\frac{\tau_{syxB}}{\tan\alpha} + \tau_{syyC}\right] \tag{3.25}$$

The left hand side of Equation 3.25 represents the diffusive force due to turbulence. The gravitational force is represented by the first term on the right hand side of the equation. The second and third terms on the right hand side of the equation are the particle interaction effects. The second term is the strain rate dependent interparticle stress of the type studied by Bagnold. τ_{syxB} is the dispersive stress arising as a result

of collisions between particles moving in layers at different velocities. The resulting normal stress which affects the concentration distribution in the y direction is τ_{syyB} and it is related to the dispersive stress through the constant of proportionality tan α. Bagnold (1956) defined α as the internal angle of friction for the sheared mass of particles. The third term represents the Coulombic (strain rate independent) forces transmitted between particles and ultimately to the pipe wall. Here τ_{syyC} is the normal stress resulting from the transmission of the contact load fraction to the pipe wall.

The terms ϵ_s, τ_{syyC} and τ_{syyB} are determined empirically and Shook and Roco (1990) indicate that more research is needed to quantify these terms for a wide range of flow conditions.

Other workers have presented variations of the Roco-Shook force balance model. In one version, Rasteiro et al. (1988) used a two dimensional model for situations where interparticle effects are negligible. In this case, the two dimensional concentration gradient is governed by the diffusion equation:

$$\frac{\partial}{\partial y}\left[\epsilon_s \frac{\partial c}{\partial y}\right] + \frac{\partial}{\partial x}\left[\epsilon_s \frac{\partial c}{\partial x}\right] = v_y \frac{\partial c}{\partial y} \qquad (3.26)$$

Rasteiro and coworkers neglected hindered settling effects by setting $v_y = v_\infty$ and used a position and concentration dependent function for ϵ_s.

Hsu et al. (1989) used a two dimensional approach similar to that of Rasteiro et al. to deal with the turbulent diffusion effect and included a Saffman lift force term in addition to the effects of Equation 3.25. Again, empirical equations were required for τ_{syyB} and τ_{syyC} and ϵ_s.

Wilson and Pugh (1988) considered the turbulent flow of coarse-particle slurries to be divided into three zones; a sliding bed in the bottom portion of the pipe, a shear layer above the bed and a turbulent zone in the upper portion of the pipe. In the sliding bed layer, there was assumed to be no shear and the solids concentration was assumed to be that of a loosely packed bed. It was further assumed that all the solids in the sliding bed were supported through contact with the pipe wall. In the shear layer, the particles were considered to be supported by both turbulence and contact load effects. The particles in the top layer were assumed to be supported entirely by turbulence effects.

Wilson and Pugh wrote the force balance as

$$\frac{(\rho_s - \rho_f) g}{c} \frac{\epsilon_s}{v_\infty} \frac{dc}{dy} = (\rho_s - \rho_f) g - \frac{1}{c} \frac{d\tau_{syyC}}{dy} \qquad (3.27)$$

which requires an empirical expression for τ_{syyC}. Wilson and Pugh assumed a linear contact load concentration variation with position in the sheared layer.

Roco and Shook (1983) used Equations 2.22 and 2.23, the momentum equations for each phase, to model velocity distributions for flowing mixtures. The interfacial drag force was eliminated by using Equation 2.20. Turbulent stresses τ_{ij} at a point were considered to be defined by six independent coefficients α_{ij} such that

$$\tau_{ij} = \frac{\partial\left(\alpha_{ij} \rho v_i^2\right)}{\partial x_j}; \qquad i,j = 1,2,3$$

In clear fluids, α values were functions of position within the pipe. For slurries, α values were assumed to be functions of solids concentration and position. In slurries, the distance from the pipe wall in the clear fluid expression for α was replaced by an "equivalent distance" to reflect the fact that the velocity distribution is distorted by the dense mixture in the lower portion of the pipe.

Over the years, Roco and coworkers have used increasingly more complex methods for estimating the eddy diffusivity. Roco and Balakrishnan (1983) replaced the algebraic solution of Roco and Shook with a one equation two phase eddy viscosity model. More recently, Roco and Mahadevan (1986) used a one equation kinetic energy turbulence model. Although several empirical coefficients must have been used in these models, the publications do not provide sufficient detail for the calculations to be verified.

Hsu et al. (1989) modelled the velocity distribution in a manner which differs from that of Roco and Shook in that axial slip is considered and multispecies particle interactions are included. The eddy viscosity was estimated from algebraic equations. In contrast with the publications noted above, their method is explained clearly. However, the number of empirical coefficients in this model is substantial. The data base examined by all these workers was essentially the same as that used by Roco and Shook (1983).

Wilson and Pugh (1988) modelled the velocity distributions for coarse-particle slurries by assuming that, in the shear layer, the shear stress available to produce turbulent fluid flow is the difference between the total shear stress and the interparticle

shear stress. The latter is considered to increase with depth in proportion with the normal interparticle stress. This approach resembles that proposed originally by Bagnold (1956) but is restricted to coarse particles. It is not appropriate when part of the immersed weight of the particles is supported by fluid lift forces.

3.5 Deposition Velocity

No aspect of the flow of settling slurries is more important than the limit-deposit velocity, V_c. To minimize energy consumption, slurry pipelines are usually designed to operate at velocities which are as low as possible and therefore, near V_c. For a specified volumetric throughput, the design engineer will have to make a selection of pipe diameter based on the available estimate of V_c.

Because of its importance, innumerable correlations have been proposed to predict V_c. Carleton and Cheng (1974) identified 55 correlations and many more have been proposed since that time. Some of these have a theoretical basis but their validity is entirely dependent upon the scope of the data base which they incorporate. The work of Carleton and Cheng showed that there is considerable disagreement between the numerous correlations proposed for estimating deposit velocities.

Wilson's (1979) nomogram provides a convenient method for estimating the upper limit of V_c. The nomogram considers the effects of pipe diameter, particle diameter and solids to carrier fluid density ratio. The effects of viscosity are not included so the nomogram is best for aqueous slurries with low fines contents. The

nomogram predicts that V_c is highest when the particle diameter is approximately 0.5 mm.

Using a data base which contained 864 experimental critical velocity data points, Turian et al. (1987) developed a correlation for V_c which includes the effects of carrier fluid viscosity. The correlation uses a large data base and includes both turbulent and laminar flows. The data base includes few results for large particles and large pipes, however. The correlation is

$$\frac{V_c}{\sqrt{2gD(S_s-1)}} = \chi_1 C_v^{\chi_2}(1-C_v)^{\chi_3}\left(\frac{\rho_L D\sqrt{gD(S_s-1)}}{\mu_L}\right)^{\chi_4}\left(\frac{d}{D}\right)^{\chi_5} \qquad (3.28)$$

where $\chi_1 = 1.7951$, $\chi_2 = 0.1087$, $\chi_3 = 0.2401$, $\chi_4 = 0.00179$ and $\chi_5 = 0.06623$. The correlation predicted V_c with an absolute average deviation of 20%. The deviation was over 50% for 69 of the 864 points.

The correlation of Turian and coworkers indicates that V_c is a very weak function of the particle size. In direct constrast, Wilson's nomogram indicates strong dependence on particle size. An improved correlation is required and this is one of principal goals of the present investigation.

4 EXPERIMENTAL PROCEDURES

4.1 Pipeline Flow Loop Operation

Four horizontal pipeline flow loops, nominally 50, 150, 250 and 500 mm in diameter, were used to collect the experimental data. Figure 4.1 illustrates the layout for the small 50 mm flow loop and Figure 4.2 is representative of the layouts used for the three large diameter flow loops.

The major components of each circuit are a pump with a variable speed drive, a pipeline and a feed tank through which the solids are admitted. Each test rig is operated as a closed loop in that the mixture discharged from the pump travels through the pipe loop and returns directly to the pump inlet.

Centrifugal slurry pumps were used to circulate the slurries. A Linatex pump with a 75 mm inlet and a 50 mm outlet was used on the 50 mm circuit. A Warman pump with a 250 mm diameter inlet and a 200 mm diameter discharge was used for both the 150 and 250 mm flow loops. An Allan-Sherman-Hoff pump with 400 mm diameter inlet and discharge sections was used to provide the flows for the tests in the 500 mm circuit. The Linatex pump was powered by a 12 kW electric motor and a variable diameter pulley drive system was used to adjust the pump speed. The Warman pump was powered by a 190 kW electric motor and a 250 kW electric motor was used to drive the Allan-Sherman-Hoff pump. Fluid couplings were used to adjust the speeds of the two large pumps.

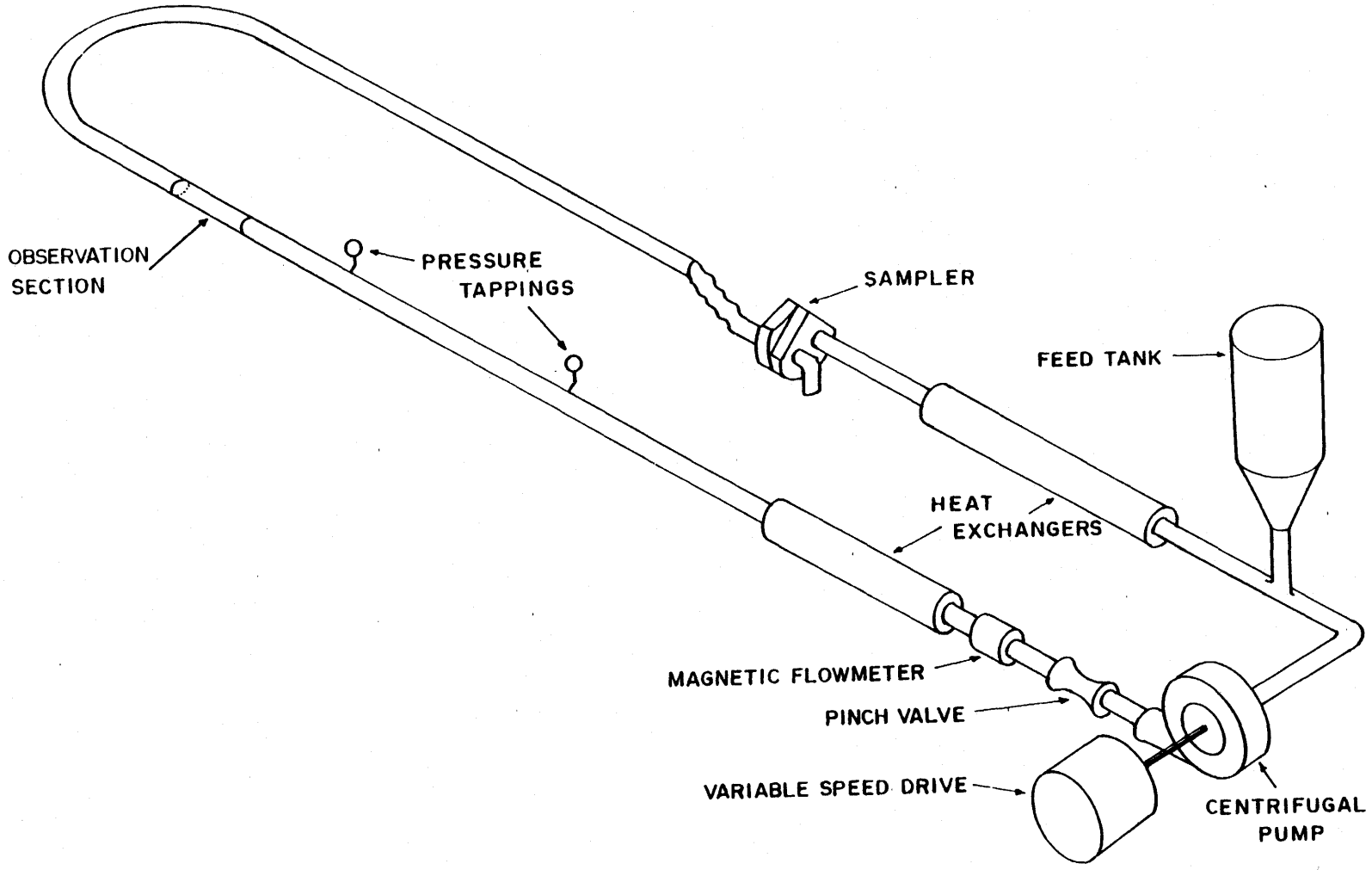

Figure 4.1: 50 mm slurry pipeline loop.

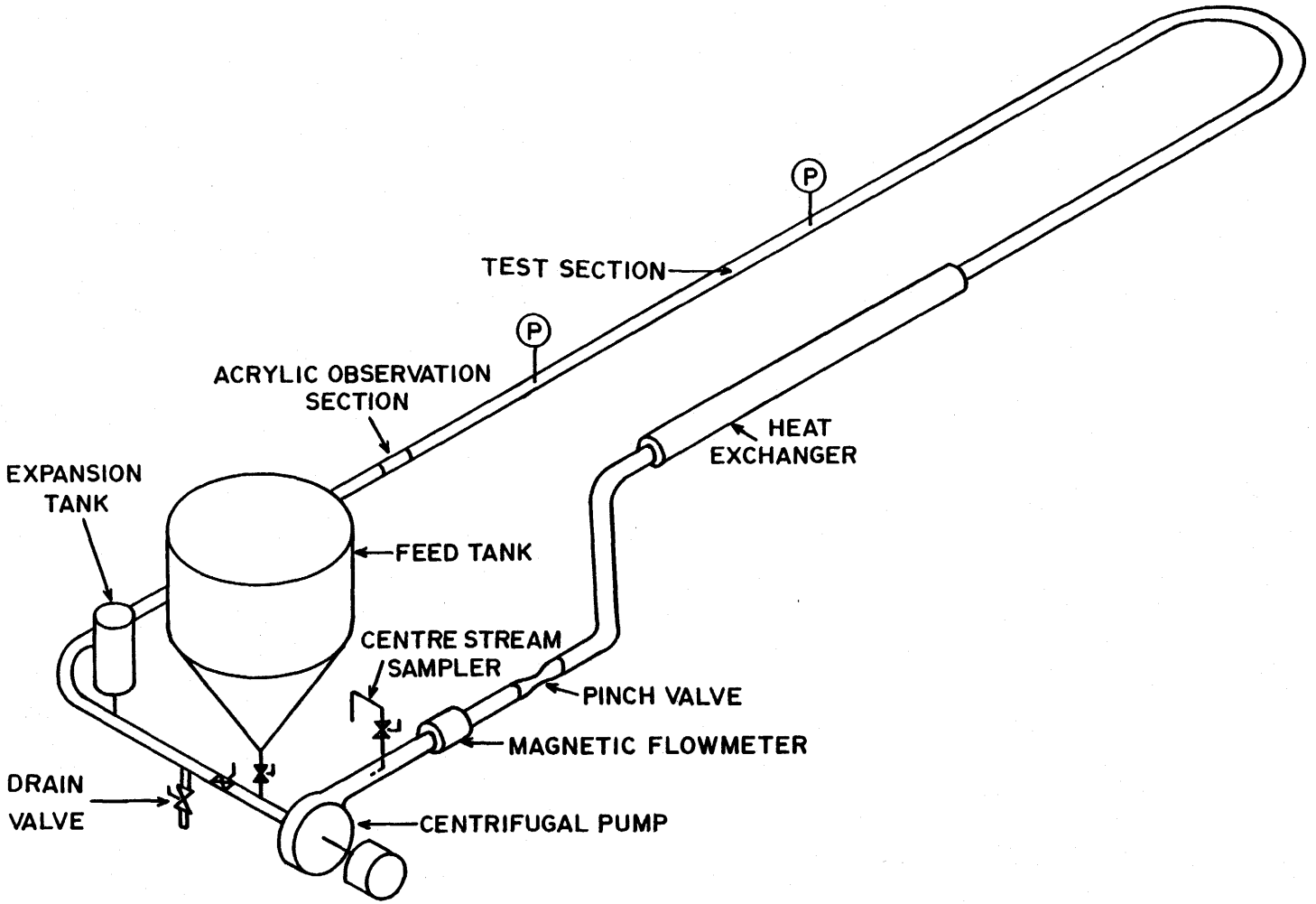

Figure 4.2: Large diameter slurry pipeline loops.

Electromagnetic flow meters were used to determine the mixture flowrates. For the 50 mm flow loop, the flow meter calibration was verified by collecting timed and weighed discharge samples. For the large flow loops, the flow meters were calibrated by measuring the pressure drops for water flowing through orifice plates. The orifice plates were constructed according to British Standard 1042 using D and D/2 pressure tappings. Differential pressure transducers were used to measure the pressure drops across the orifice plates. The differential pressure transducers were calibrated against U-tube manometers.

For each flow loop, temperature was controlled by circulating a heated or chilled mixture of ethylene glycol and water through the annulus of a double pipe heat exchanger. Temperature was controlled to within 1°C. Temperature control is a unique feature of these large loops. Although pipes of similar diameter are used in the United States, the United Kingdom, Germany and Australia, no other facility is capable of maintaining isothermal flow by absorbing the energy degraded by friction.

Transparent acrylic pipe sections were used to observe the flow and to allow visual determination of solids deposition. The transparent pipe sections were also useful for determining whether the mixture contained any air. Some air is usually entrained during the flow loop loading process but this was removed before any pipe flow data were collected.

Pipeline pressure drops were measured over straight horizontal pipe test sections for steady state flows. Differential pressure transducers were used to determine the pressure difference (P_1 - P_2) over a pipe section of length L. P_1 is the pressure at the

upstream end of the test section and P_2 is the pressure at the downstream end. Each test section was preceded by a long straight disturbance-free section of piping. These approach sections were included in the flow loop design to ensure that fully developed flow conditions existed in the test sections. Table 4.1 provides a summary of the important dimensions for each flow loop.

A computerized data acquisition system was used to collect and store output from the pipeline flow loop instruments. The system consisted of a NEFF 620 analog-to-digital converter and a Hewlett-Packard Model 9825A computer.

Each test consisted of the following steps:

1. The pipeline flow loop was filled with water which was circulated until the desired temperature was obtained. The flowrate was set and pipeline pressure drop measurements were made for steady state conditions. The instrument readings were collected for a two minute period to obtain average values for each setting. The procedure was repeated to obtain a series of pressure drop versus flowrate measurements.
2. With the water circulating around the flow loop, a pre-determined amount of solids was added through the feed tank. Water was displaced upward into the feed tank by the solids as they settled into the flow loop. After allowing time for the fine solids to settle into the flow loop, the excess water was drained to the level of the bottom of the conical section of the feed tank.
3. The mixture was circulated until the desired operating temperature was obtained. Steady state pipeline pressure drop versus flowrate measurements were collected

starting at a high flowrate. The flowrate was reduced step-wise until a stationary deposit of solids formed along the bottom of the horizontal pipeline.

4. Samples were removed to determine the density and the viscometric properties of the carrier fluid (water and fines).

5. Concentration and velocity distributions were determined at selected flowrates using methods described in Section 4.2.

The solids concentration was increased by adding more solids to the flow loop and the measurements were repeated to obtain a series of concentration-flowrate-pressure drop data points.

The solids concentration distributions were measured using a gamma ray density gauge. An electrical probe was used to measure the velocity distributions for the flowing mixtures. For some of the 50 mm pipeline tests, the same probe was also used to measure local solids concentrations.

Table 4.1 Flow loop dimensions.

Nominal Pipe Size (mm)	Test Section Internal Diameter (mm)	Test Section Length (m)	Approach Section Length (m)	Volume of Flowing Mixture (L)
50	53.2	4.88	6	65
150	158.5	23.77	15	2300
250	263	28.96	15	6600
500	495	22.86	25	27000

4.2 Specialized Equipment

4.2.1 Gamma Ray Density Gauge

The Beer-Lambert law describes the absorption of a monochromatic beam of radiation:

$$\frac{dN}{dx} = -\mu_j N \tag{4.1}$$

where N is the intensity of the beam and μ_j is the absorption coefficient. For a beam passing through a pipe containing a slurry, the intensity of the beam is found by integrating Equation 4.1 for each absorber and combining the results:

$$\ln\left(\frac{N}{N_1}\right) = -\mu_w x_w - \mu_L x_L - \mu_s x_s \tag{4.2}$$

In this expression, N_1 is the unattenuated beam intensity, w denotes the pipe wall, L the liquid and s the solids.

A traversing gamma ray density gauge, shown in Figure 4.3, was used to determine chord-average values of the solids concentration. The gauge uses a Cs-137 source. Slits were used to collimate the beam to a vertical thickness of 6 mm for the large flow loops and 2 mm for the 50 mm flow loop. The Cs-137 source was chosen because its absorption coefficient is almost proportional to the density of the absorber. An Ortec detection system was used to determine the degree of attenuation of the radiation. Synchronized stepping motors were used to move the source and the detector vertically between measuring locations.

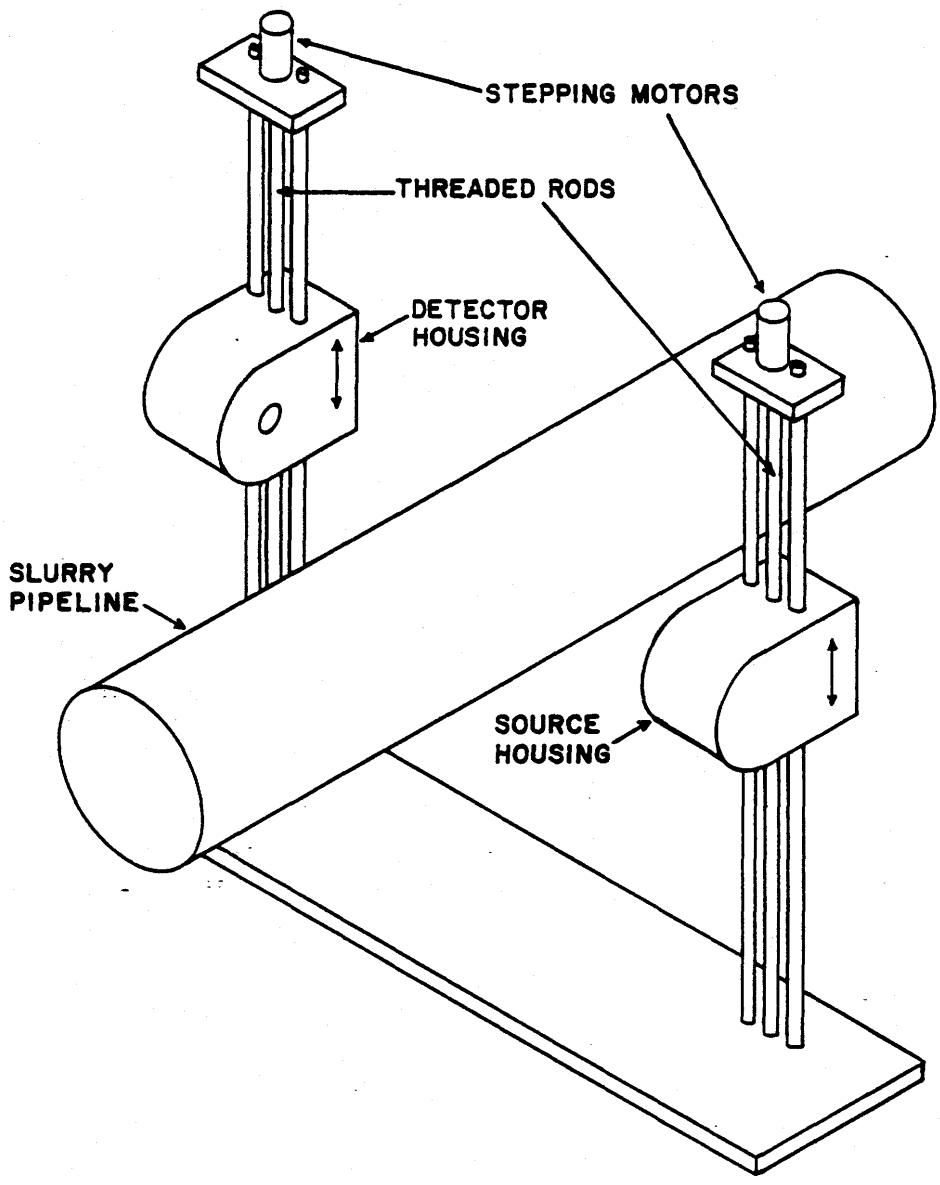

Figure 4.3: Traversing gamma ray absorption density gauge.

Absorption coefficients were determined for the pipe wall and the carrier liquid by performing traverses first across an empty pipe and then across a water filled pipe. Absorption coefficients for the solids were determined in separate calibration tests using dry solids packed into a cylindrical container. The path length for the solids calibration test was C_{max} L where C_{max} is the solids concentration for the packed bed and L is the length of the cylinder.

The average *in situ* solids fraction was determined by integrating the local solids fraction numerically over the pipe-cross section:

$$C_r = \sum_{j=1}^{n} c_j L_j \Big/ \sum_{j=1}^{n} L_j \qquad (4.3)$$

where C_r and c_j are the average and local volume fractions and L_j is the chord length at vertical position j. The measurements were made at ten equally spaced vertical positions.

4.2.2 Velocity/Concentration Probe

An electrical probe developed at the University of Saskatchewan (Brown et al., 1983 and Nasr-El-Din et al., 1987) was used to determine local particle velocities and local solids concentrations for flowing slurries. The probe, which is shown schematically in Figure 4.4, is described in detail by Sumner et al. (1989). The probe consists of a pair of field electrodes (the body of the probe is one electrode) and two sets of sensor electrodes. If a current source is applied to the field electrodes, the potential between the sensor electrodes will be directly proportional to the resistance in the region between them. Assuming that the solids are perfect insulators, the Maxwell

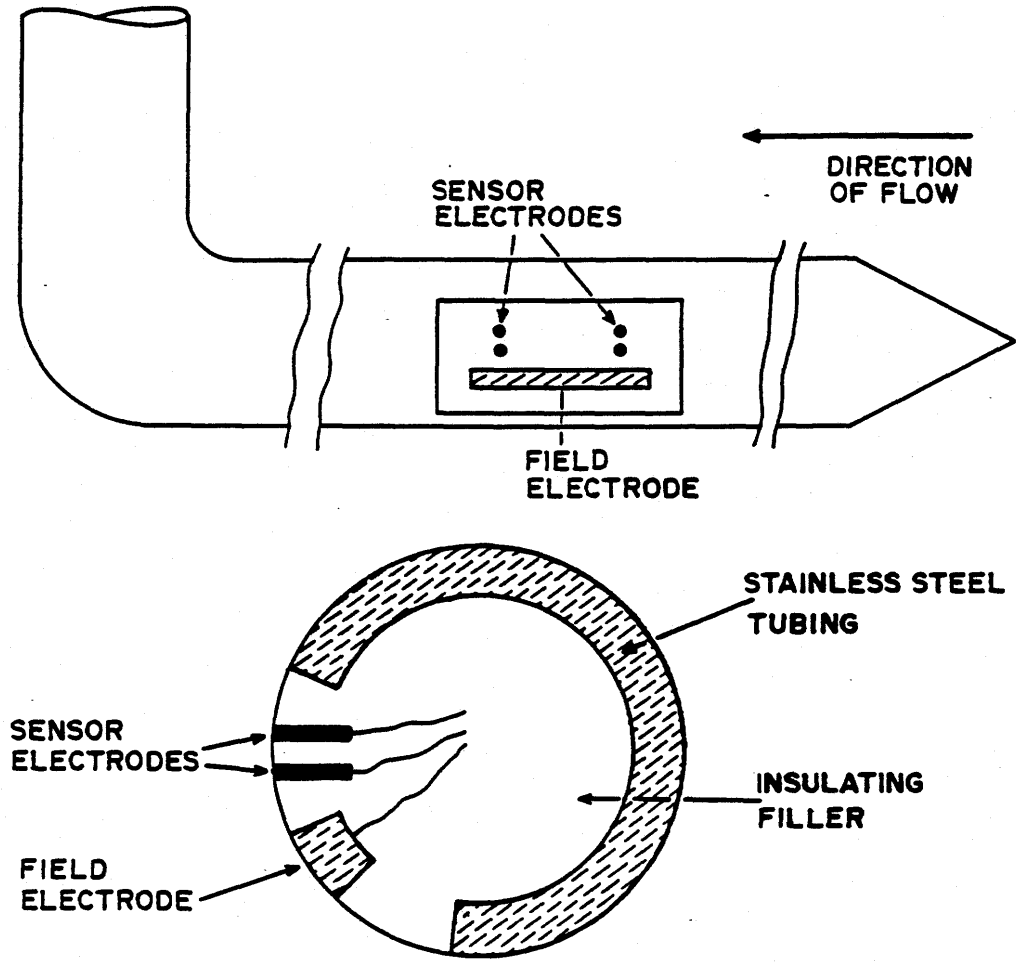

Figure 4.4: Probe for local velocity and concentration determinations.

equation (1892) gives the solids concentration from measurements of the electrical resistivity of the mixture, R and the resistance of the liquid, R_L:

$$\frac{R}{R_L} = \frac{2 + C}{2 - 2C} \tag{4.4}$$

Polarization at the electrodes can cause a problem with this type of probe. Nasr-el-din et al. (1987) found that polarization effects could be minimized by using a high-frequency alternating current supply.

Brown et al. (1983) showed that when a current is applied to the field electrodes the potential difference between a pair of sensor electrodes fluctuates as particles pass by the electrodes. The particles will cause a similar fluctuation to occur as they pass the second set of axially displaced sensor electrodes. A cross-correlation technique may be used to determine the time required for the particles to travel between the two sets of electrodes. Hence, the particle velocity may be measured for a flowing mixture. Here, the absolute magnitude of the fluctuations is not important so that polarization effects are not as critical as for concentration measurements.

In this study, a direct current was applied to the field electrodes for velocity determinations and an alternating current source (1 kHz square wave) was used for concentration measurements. A Hewlett-Packard Model 3721A correlator was used to determine the transit times for velocity determinations.

The velocity/concentration probes were installed in sections of pipe which could be rotated to allow sampling at any position. Figure 4.5 shows the locations of the samples points used during the present study. The thirteen sampling points were located

at the centroids of segments of equal area. Assuming the flow is symmetrical about the vertical axis of the pipe, the average particle velocity V_s may be determined from the local velocities v_j as follows:

$$V_s = \frac{1}{25}\left(2\sum_{j=1}^{12} v_j + v_{13}\right) \tag{4.5}$$

Similarly, the average *in situ* concentration is determined from the local concentrations c_j as follows:

$$C_t = \frac{1}{25}\left(2\sum_{j=1}^{12} c_j + c_{13}\right) \tag{4.6}$$

For the tests where measurements of local solids concentrations were not available, c_j values were estimated by interpolation of the gamma ray gauge data. In performing the interpolations, it was assumed that the solids concentration did not vary significantly with horizontal position.

The solids concentrations in the delivered mixtures were computed from the measured local particle velocities and measured or estimated local concentrations:

$$C_v = \frac{2\sum_{j=1}^{12} c_j v_j + c_{13} v_{13}}{2\sum_{j=1}^{12} v_j + v_{13}} \tag{4.7}$$

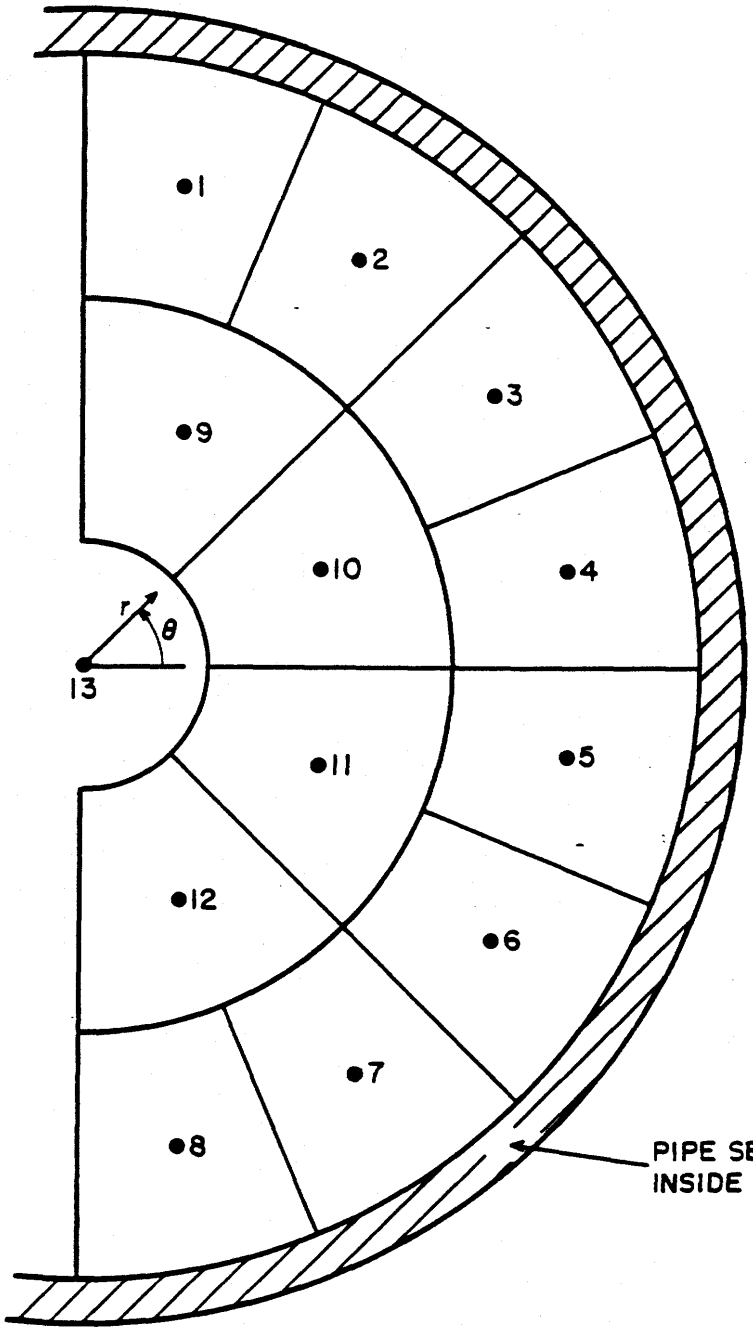

POSITION	θ	r/R
1	78.75°	0.8
2	56.25°	0.8
3	33.75°	0.8
4	11.25°	0.8
5	-11.25°	0.8
6	-33.75°	0.8
7	-56.25°	0.8
8	-78.75°	0.8
9	67.50°	0.4
10	22.50°	0.4
11	-22.50°	0.4
12	-67.50°	0.4
13	—	0.0

Figure 4.5: Sampling positions for particle velocity measurements.

4.3 Particle Property Determinations

4.3.1 Particle Size

Particle size distributions were determined by sieving. Samples were wet screened using a sieve with 0.074 mm openings (200 mesh) to remove the fines portion. The material passing through the sieve (-0.074 mm fraction) was collected and dried to determine the fines mass fraction. The +0.074 mm fraction was dried and screened using a series of Tyler sieves and a Ro-tap shaker.

4.3.2 Particle Density

The particle densities were determined using volumetric flasks. The flasks were partly filled with solids and the weight was determined. Water was added to cover the particles and a vacuum was applied to remove any gases. More water was added to fill the flask to the mark and the filled flask was weighed to determine, by difference, the total amount of water. The sand particle density ρ_s could then be determined from the weight of sand w_s, the weight of the water w_L and the volume of the flask:

$$\text{Volume} = \frac{w_s}{\rho_s} + \frac{w_L}{\rho_L} \qquad (4.8)$$

Special considerations are required for porous solids such as coals. These materials contain moisture in two forms; surface (or external) moisture and saturation (or internal) moisture. The internal water is considered to contribute to the volume of the particles and the surface moisture is considered to contribute to the continuous phase. To determine the effective density of coal particles, the particles must first be brought to their saturation moisture level. In this study, the coal was equilibrated in a

humidity chamber which operated at 25°C and 92 to 95% relative humidity. The coal was left in the chamber for several days until the sample reached a constant weight.

The sand sample density was found to be 2650 kg/m^3. The coal sample had an internal moisture content of 1.8% (mass) and an effective density of 1374 kg/m^3.

4.3.3 Drag Coefficients

Particle drag coefficients may be measured by determining the steady state settling velocities for individual particles falling through a quiescent column of liquid. At steady state, the drag force acting on the particle is balanced by the gravitational force ($F_D + F_G = 0$). The net gravitational force acting on a particle of diameter d and density ρ_s immersed in fluid of density ρ_f is

$$F_G = g(\rho_s - \rho_f)\left(\frac{\pi d^3}{6}\right) \tag{4.9}$$

For infinite dilution, the steady state settling velocity for a particle of cross sectional area $\pi d^2/4$ is

$$V_\infty = \left(\frac{4gd(\rho_s - \rho_f)}{3\rho_f C_D}\right)^{0.5} \tag{4.10}$$

It is convenient to use the Archimedes number $C_D Re_p^2$ to correlate particle drag coefficients.

$$C_D Re_p^2 = \frac{4gd^3\rho_f(\rho_s - \rho_f)}{3\mu_f^2} \tag{4.11}$$

Re_p is the particle Reynolds number:

$$Re_p = d \rho_f V_\infty / \mu \qquad (4.12)$$

Particle drag coefficients were determined by measuring the steady state settling velocities of individual particles in a quiescent column of water. The column had a diameter of 150 mm. Particle diameters were determined by sieving. For a series of sieves, the average particle diameter for sieve interval j was assumed to be the arithmetic mean of the sieve openings, $(d_{j-1} + d_j) / 2$.

The coal samples were submerged in water prior to the measurements to ensure that the particles were saturated.

4.3.4 Particle-Wall Kinematic Friction

For slurries of coarse particles, headlosses exceed those of the clear fluid by an amount which depends, according to theoretical explanations, on η_s, the coefficient of friction between the particles and the pipe wall. In their description of the particle-wall friction process, Wilson, Streat and Bantin (1972) suggested that a tilting tube could be used to determine η_s.

Shook et al. (1982a) showed that such a device could provide useful information about η_s but there are some experimental difficulties. The dynamics of motion of the sliding mass of particles are complicated and the measurements may be difficult to reproduce. The average values of η_s, as determined by Shook et al., were 0.5 for sand and gravel slurries and 0.4 for Western Canadian coal slurries.

4.4 Carrier Fluid Properties

4.4.1 Fluid Density

Samples of slurry were obtained from the pipeline flow loop during each test. The coarse particles were removed by using a sieve with 0.074 mm openings. Fluid densities were determined by weighing known volumes of the remaining (fines + water) mixtures.

4.4.2 Viscosity

Samples were collected from the pipeline flow loop and the coarse particles were removed by sieving through a screen with 0.074 mm openings. A Brookfield concentric cylinder viscometer was used to determine the viscosity for fine solids in water mixtures. The rotating inner spindle had a radius of $R_1 = 12.56$ mm and the stationary outer cup had a radius of $R_2 = 13.73$ mm. The viscometer provides a measure of T, the torque per unit length of spindle, required to rotate the inner cylinder at an angular velocity ω.

For concentric cylinder viscometers, it is assumed that the flow is one-dimensional (in the θ direction). The shear stress in the annular space between the cylinders is known to vary with radial position as follows:

$$r^2 \tau_{r\theta} = \text{constant} \tag{4.13}$$

For the tests reported here, the fluids were essentially Newtonian and the flow was laminar so,

$$\dot{\gamma}_{r\theta} = -r\frac{d(v_\theta/r)}{dr} = \frac{\tau_{r\theta}}{\mu} \qquad (4.14)$$

Using the facts that at $r = R_1$, $\omega = d(V_{r\theta}/r)/dr$ and $T = 2\pi R_1^2 \tau_{r\theta}$, Equation 4.14 can be integrated to give the well known equation describing the laminar flow of Newtonian fluids in a concentric cylinder viscometer:

$$\omega = \frac{T}{4\pi\mu}\left(\frac{1}{R_1^2} - \frac{1}{R_2^2}\right) \qquad (4.15)$$

Thus measurements of ω and T allow μ to be calculated. Non-linearity of the T-ω relationships would indicate non-Newtonian flow.

5 EXPERIMENTAL RESULTS

5.1 Introduction

Pipeline flow loop tests were performed using sand-in-water slurries in 50, 150, 250 and 500 mm diameter pipes and coal-in-water slurries in a 250 mm diameter pipe. Tables 5.1 and 5.2 provide a summary of the operating conditions for each test. C_t is the volumetric concentration of total solids including the coarse particles (+0.074 mm fraction) and the fines (-0.074 mm fraction). C_r is the volumetric concentration of the coarse solids and ρ_s is the density of the solid particles. ρ_f and μ_f are the density and viscosity of the carrier fluid which is comprised of the water and fine particles. Tables 5.1 and 5.2 also give the deposition velocity, V_c, determined experimentally for each test.

The frictional headlosses, particle size distributions, concentration distributions and velocity distributions are given in tabular form in Appendix A. The concentration distributions are presented graphically in Appendix B and the velocity distributions are shown in Appendix C.

In Appendix B, the local (horizontal chord-average) concentrations are plotted against vertical position (y/R). The dashed lines illustrate the effectiveness of the effort to model these distributions. The modelling effort is discussed in Chapter 6.

In Appendix C, the local velocities, normalized by the mean velocity, are plotted against vertical position (y/R). For clarity, only the velocities measured at r/R = 0.8 are shown. The entire set of measurements, which includes data at r/R = 0.4 and r/R = 0 as well, is given in the tables of Appendix A.

Table 5.1: Summary of slurry flow tests for solids with narrow size distributions.

Solids	D (mm)	d (mm)	C_t	C_r	T (°C)	ρ_s (kg/m^3)	ρ_f (kg/m^3)	μ_f (mPa.s)	V_c (m/s)
0.1 to 0.3 mm sand	53.2	0.18	0.15	0.15	15	2650	999	1.2	1.1
0.1 to 0.3 mm sand	53.2	0.18	0.30	0.30	15	2650	999	1.2	1.1
0.1 to 0.3 mm sand	53.2	0.18	0.45	0.45	15	2650	999	1.2	1.2
0.1 to 0.3 mm sand	158.5	0.19	0.06	0.06	11	2650	1000	1.3	2.1
0.1 to 0.3 mm sand	158.5	0.19	0.16	0.16	10	2650	1000	1.3	2.2
0.1 to 0.3 mm sand	158.5	0.19	0.30	0.30	10	2650	1000	1.3	2.1
0.1 to 0.3 mm sand	158.5	0.19	0.06	0.06	60	2650	983	0.5	2.5
0.1 to 0.3 mm sand	158.5	0.19	0.16	0.16	60	2650	983	0.5	2.7
0.1 to 0.3 mm sand	158.5	0.19	0.30	0.30	60	2650	983	0.5	2.7
0.1 to 0.3 mm sand	495	0.18	0.10	0.10	14	2650	999	1.2	3.1
0.1 to 0.3 mm sand	495	0.18	0.15	0.15	13	2650	999	1.2	3.1
0.1 to 0.3 mm sand	495	0.18	0.20	0.20	14	2650	999	1.2	3.1
0.1 to 0.3 mm sand	495	0.18	0.25	0.25	15	2650	999	1.2	3.0
0.1 to 0.3 mm sand	495	0.18	0.29	0.29	10	2650	1000	1.3	2.8
0.1 to 0.3 mm sand	495	0.18	0.34	0.34	9	2650	1000	1.3	2.7

Table 5.1 (continued)

Solids	D (mm)	d (mm)	C_t	C_r	T (°C)	ρ_s (kg/m^3)	ρ_f (kg/m^3)	μ_f (mPa.s)	V_c (m/s)
0.3 to 1 mm sand	53.2	0.55	0.15	0.15	15	2650	1001	1.2	1.3
0.3 to 1 mm sand	53.2	0.55	0.30	0.29	15	2650	1013	1.6	1.2
0.3 to 1 mm sand	53.2	0.55	0.40	0.39	15	2650	1024	3.3	1.3
0.3 to 1 mm sand	263	0.55	0.15	0.15	15	2650	1003	1.3	3.4
0.3 to 1 mm sand	263	0.55	0.25	0.25	15	2650	1010	1.5	3.2
0.3 to 1 mm sand	263	0.55	0.30	0.29	15	2650	1009	1.6	3.1
0.3 to 1 mm sand	263	0.55	0.30	0.29	40	2650	1007	0.9	3.2
2 to 6 mm sand	53.2	2.4	0.15	0.13	15	2650	1041	1.3	1.2
2 to 6 mm sand	53.2	2.4	0.30	0.22	15	2650	1173	2.1	1.2
2 to 6 mm sand	263	2.4	0.13	0.11	15	2650	1029	1.5	2.6
2 to 6 mm sand	263	2.4	0.22	0.19	15	2650	1068	2.0	2.4
2 to 6 mm sand	263	2.4	0.22	0.19	40	2650	1058	1.2	2.6

Table 5.2: Summary of slurry flow tests for solids with broad size distributions.

Solids	D (mm)	d (mm)	C_t	C_r	T (°C)	ρ_s (kg/m^3)	ρ_f (kg/m^3)	μ_f (mPa.s)	V_c (m/s)
0 to 1 mm sand	53.2	0.29	0.15	0.15	15	2650	1001	1.2	1.3
0 to 1 mm sand	53.2	0.29	0.30	0.30	15	2650	1003	1.4	1.4
0 to 1 mm sand	53.2	0.29	0.40	0.40	15	2650	1004	1.5	1.4
0 to 1 mm sand	263	0.29	0.16	0.16	15	2650	1000	1.3	3.1
0 to 1 mm sand	263	0.29	0.25	0.25	15	2650	1004	1.5	3.0
0 to 1 mm sand	263	0.29	0.34	0.34	15	2650	1007	1.8	3.0
0 to 1 mm sand	263	0.29	0.34	0.34	40	2650	999	1.0	3.1
0 to 6 mm sand	263	0.38	0.15	0.15	15	2650	1004	1.3	3.3
0 to 6 mm sand	263	0.38	0.25	0.24	15	2650	1019	1.3	3.4
0 to 6 mm sand	263	0.38	0.34	0.33	15	2650	1034	1.8	3.3
0 to 6 mm sand	263	0.38	0.34	0.32	40	2650	1045	1.0	3.5
0 to 10 mm coal	263	0.80	0.23	0.22	23	1374	1003	0.9	1.8
0 to 10 mm coal	263	0.85	0.35	0.23	23	1374	1057	2.1	2.0
0 to 10 mm coal	263	1.1	0.48	0.30	22	1374	1095	3.2	1.7

The pipeline headlosses are presented in graphical form in this chapter (Section 5.2). The particle properties are discussed in Section 5.3 and the fluid properties are discussed in Section 5.4. The pipeline headloss data are examined in greater detail as part of a modelling effort in Chapter 6.

5.2 Pipe Flow Data

5.2.1 General Observations

A preliminary examination of the data in Appendix A provides an indication of the vast range of pipeline frictional headlosses that may be encountered with coarse-particle slurries. The energy required to transport the 0.18 mm sand does not differ greatly from that for water alone while the energy requirement for the 0.55 mm sand and the 2.4 mm sand can be almost an order of magnitude higher than that for water.

From a cursory examination of the concentration and velocity distribution plots of Appendices B and C, it is apparent that coarse-particle slurry flows are much more complex than single phase fluid flows. At normal pipeline operating velocities, the particles are not uniformly distributed in the pipe. The concentrations in the lower portion of the pipe may approach the concentration of settled bed while the mixture in the upper portion may contain relatively few particles. The plots of Appendix C show that, at a fixed radial position, the slurry velocity increases with height in the horizontal pipe. Therefore, the location of the point of symmetry (the point where v is a maximum and $\tau_{rx} = 0$) is not at the centre of the pipe. For the numerical modeller, this is a serious complication which is not encountered with homogeneous flows.

For coarse-particle slurries, the local velocities depend strongly on the particle diameter and also on the local concentration. For the fine sand (d = 0.18 mm) the velocity gradients, d(v/V)/d(y/R) at r/R = 0.8, are small. For the coarse sand slurries (d = 0.55 mm and 2.4 mm) the velocity gradients are large in the lower part of the pipe. The velocity gradients approach zero in the upper part of the pipe in those instances when the local solids concentrations are low. The solids delivered concentrations (C_v), determined by using Equation 4.7, are given in Table 5.3. The delivered concentrations are somewhat lower than the *in situ* concentrations for all the sand slurries. The difference is greatest for the slurries which contain very coarse particles. A successful pipe flow model will have to be able to estimate the C_v / C_t ratio because the *in situ* concentration is usually the fixed parameter in pipeloop flow studies while the delivered concentration is of considerable interest in an actual pipeline system.

5.2.2 Narrow Particle Size Distributions

Several pipeline flow tests were performed with slurries composed of narrowly sized sand particles in water. The sand samples had mass-average particle sizes (d_{50}'s) of 0.18 mm, 0.55 mm and 2.4 mm. The particle size distributions are shown in Figure 5.1.

Table 5.3: Delivered concentrations for pipeline flow of coarse particle slurries.

Solids	T (°C)	D (mm)	d (mm)	C_t	V (m/s)	C_v/C_t
0.1 to 0.3 mm sand	15	53	0.18	0.15	1.83	0.93
0.1 to 0.3 mm sand	15	53	0.18	0.15	3.05	0.99
0.1 to 0.3 mm sand	15	53	0.18	0.30	1.83	0.98
0.1 to 0.3 mm sand	15	53	0.18	0.30	3.05	0.99
0.1 to 0.3 mm sand	15	53	0.18	0.45	3.05	1.00
0.3 to 1 mm sand	15	53	0.55	0.15	1.83	0.78
0.3 to 1 mm sand	15	53	0.55	0.15	3.05	0.86
0.3 to 1 mm sand	15	53	0.55	0.30	2.13	0.78
0.3 to 1 mm sand	15	53	0.55	0.30	3.05	0.88
0.3 to 1 mm sand	15	53	0.55	0.40	2.13	0.86
0.3 to 1 mm sand	15	263	0.55	0.15	3.94	0.74
0.3 to 1 mm sand	15	263	0.55	0.15	4.37	0.77
0.3 to 1 mm sand	15	263	0.55	0.25	3.90	0.83
0.3 to 1 mm sand	15	263	0.55	0.25	4.38	0.84
0.3 to 1 mm sand	15	263	0.55	0.30	3.90	0.87
0.3 to 1 mm sand	15	263	0.55	0.30	4.34	0.89
0.3 to 1 mm sand	40	263	0.55	0.30	3.95	0.87
0.3 to 1 mm sand	40	263	0.55	0.30	4.38	0.88
2 to 6 mm sand	15	53	2.4	0.15	1.83	0.61
2 to 6 mm sand	15	53	2.4	0.15	3.05	0.81
2 to 6 mm sand	15	53	2.4	0.30	1.83	0.77
2 to 6 mm sand	15	53	2.4	0.30	3.05	0.90
2 to 6 mm sand	15	263	2.4	0.13	4.52	0.69
2 to 6 mm sand	15	263	2.4	0.22	3.25	0.73
2 to 6 mm sand	15	263	2.4	0.22	4.08	0.75
2 to 6 mm sand	40	263	2.4	0.22	3.96	0.74

Table 5.3 (continued)

Solids	T (°C)	D (mm)	d (mm)	C_t	V (m/s)	C_v/C_t
0 to 1 mm sand	15	53	0.29	0.15	1.83	0.88
0 to 1 mm sand	15	53	0.29	0.15	3.05	0.97
0 to 1 mm sand	15	53	0.29	0.30	1.83	0.94
0 to 1 mm sand	15	53	0.29	0.30	3.05	0.98
0 to 1 mm sand	15	53	0.29	0.40	1.83	0.89
0 to 1 mm sand	15	53	0.29	0.40	3.05	0.97
0 to 1 mm sand	15	263	0.29	0.16	3.94	0.87
0 to 1 mm sand	15	263	0.29	0.16	4.68	0.91
0 to 1 mm sand	15	263	0.29	0.25	3.95	0.91
0 to 1 mm sand	15	263	0.29	0.25	4.65	0.95
0 to 1 mm sand	15	263	0.29	0.34	3.98	0.97
0 to 1 mm sand	15	263	0.29	0.34	4.68	0.98
0 to 1 mm sand	40	263	0.29	0.34	3.94	0.93
0 to 1 mm sand	40	263	0.29	0.34	4.60	0.95
0 to 6 mm sand	15	263	0.38	0.15	4.13	0.88
0 to 6 mm sand	15	263	0.38	0.15	4.87	0.88
0 to 6 mm sand	15	263	0.38	0.25	4.13	0.88
0 to 6 mm sand	15	263	0.38	0.25	4.83	0.92
0 to 6 mm sand	15	263	0.38	0.35	4.10	0.94
0 to 6 mm sand	15	263	0.38	0.35	4.83	0.96
0 to 10 mm coal	23	263	0.85	0.35	2.4	0.94
0 to 10 mm coal	23	263	0.85	0.35	3.1	0.94
0 to 10 mm coal	22	263	1.10	0.48	2.2	0.98
0 to 10 mm coal	22	263	1.10	0.48	2.9	0.99

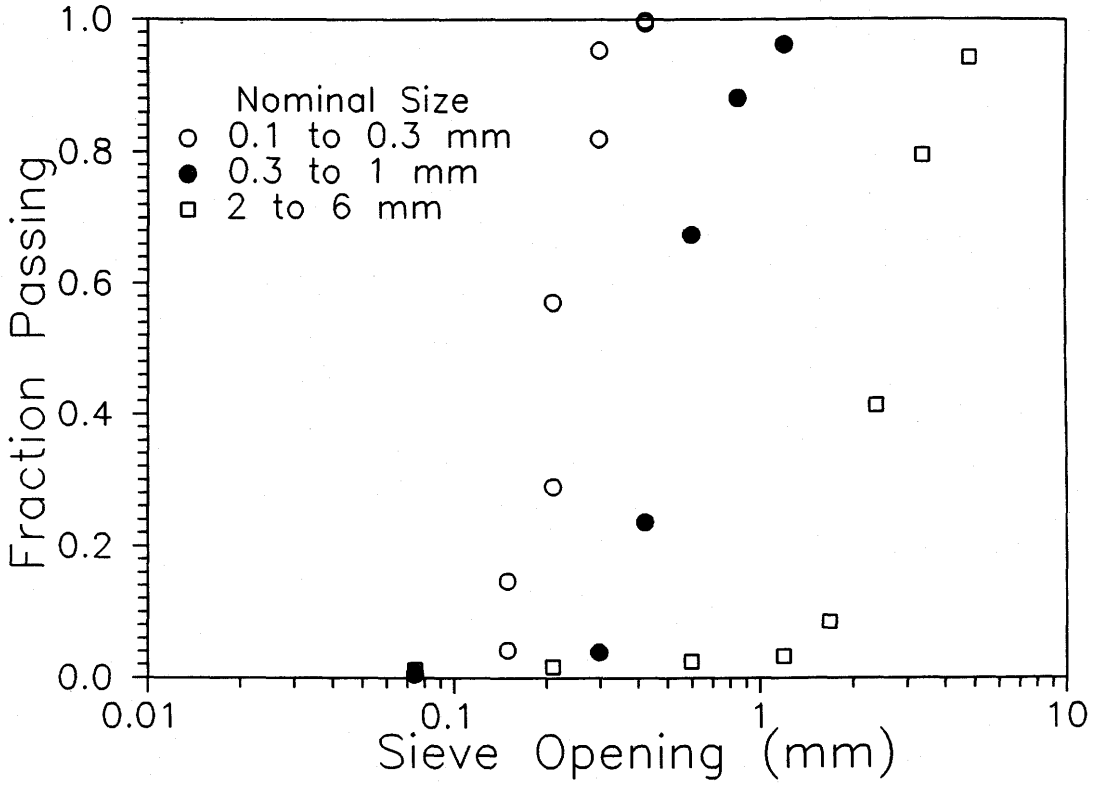

Figure 5.1: Particle size distributions for narrowly sized solids.

Figure 5.2 shows the frictional headlosses for 0.18 mm sand slurries flowing in the 53 mm pipe. In Figure 5.2, the solids concentration C_t ranges from 0.00 (clear water) to 0.45 which is near the maximum practical concentration for transportation of narrowly sized solids in pipelines. For each slurry concentration, there was a thin stationary deposit of solids at the bottom of the pipe at the lowest velocity. The pipe was free from stationary deposits for all the other data points.

Figure B1 (Appendix B) shows that, even for this relatively fine sand slurry, there is a variation in solids concentration with vertical position in the pipe. Increasing

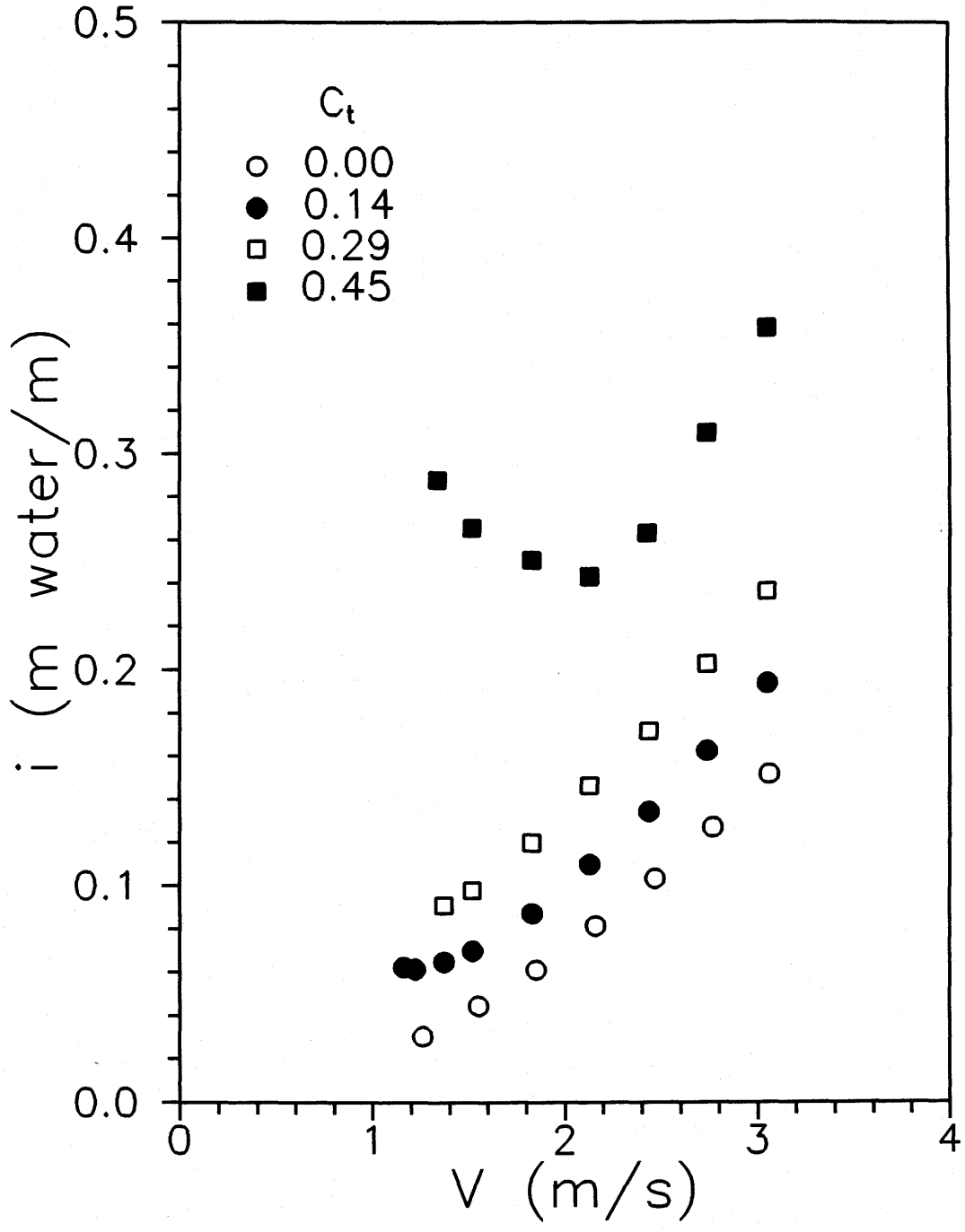

Figure 5.2: Frictional headlosses for 0.18 mm sand slurries flowing in a 53.2 mm pipe. T = 15°C.

the mean velocity from 1.8 m/s to 3.0 m/s results in a significant decrease in the amount of segregation.

The concentration distributions for 0.18 mm sand flowing in a 159 mm pipe are shown in Figure B2 (T=10°C) and Figure B3 (T=60°C). Again, the concentration gradients are reduced as the velocity increases. The operating temperature also has an effect on the concentration gradient. The warm water, with its lower viscosity and density, is less effective at suspending the particles than cold water.

Figure 5.3 shows the test results for the 0.18 mm sand flowing in a 495 mm diameter pipe. Figure B4 shows that once again there is considerable variation in the solids concentration with vertical position. Also, the effect of velocity is evident in that the concentration gradient is higher at a mean velocity of 3.1 m/s than at 3.8 m/s.

The frictional headlosses for a 0.55 mm sand are shown in Figure 5.4 for flow in the 53 mm pipe. The slurry headlosses are considerably higher than for the 0.18 mm sand. The coarser particles are more difficult to suspend than the 0.18 mm particles and particle-wall friction contributes significantly to the headloss. The concentration distributions for the 0.55 mm sand in the 53 mm pipe are shown in Figure B5. The concentration gradient is not very sensitive to the mean velocity for this coarse-particle slurry. The only noticeable effect of velocity is an apparent reversal in the concentration gradient near the bottom of the pipe for flow at a high mean velocity (3.1 m/s). This is presumably due to particle-particle interactions and other wall-repulsive effects which tend to move the particles away from the region of high velocity gradient near the pipe wall.

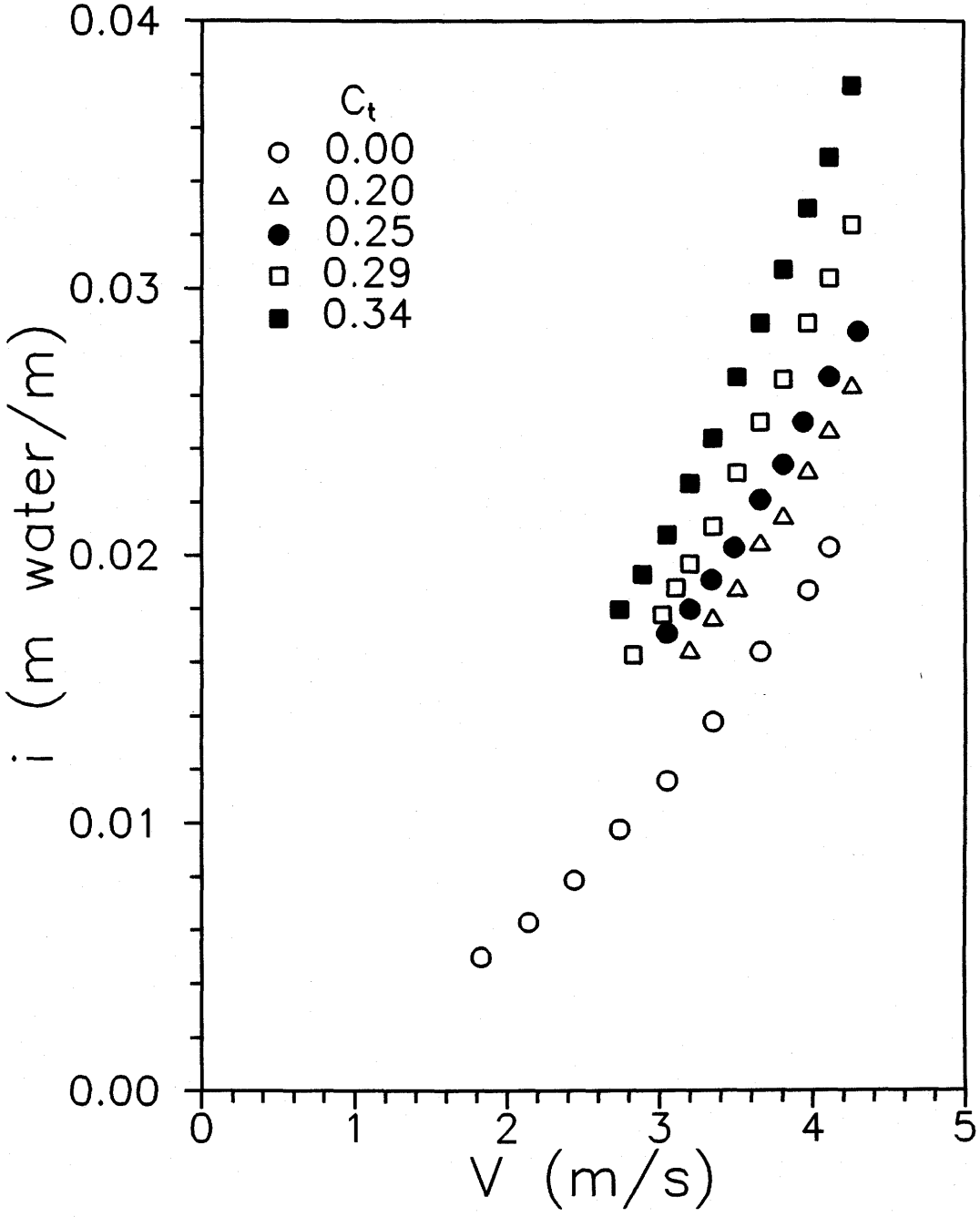

Figure 5.3: Frictional headlosses for 0.18 mm sand slurries flowing in a 495 mm pipe. T = 13°C.

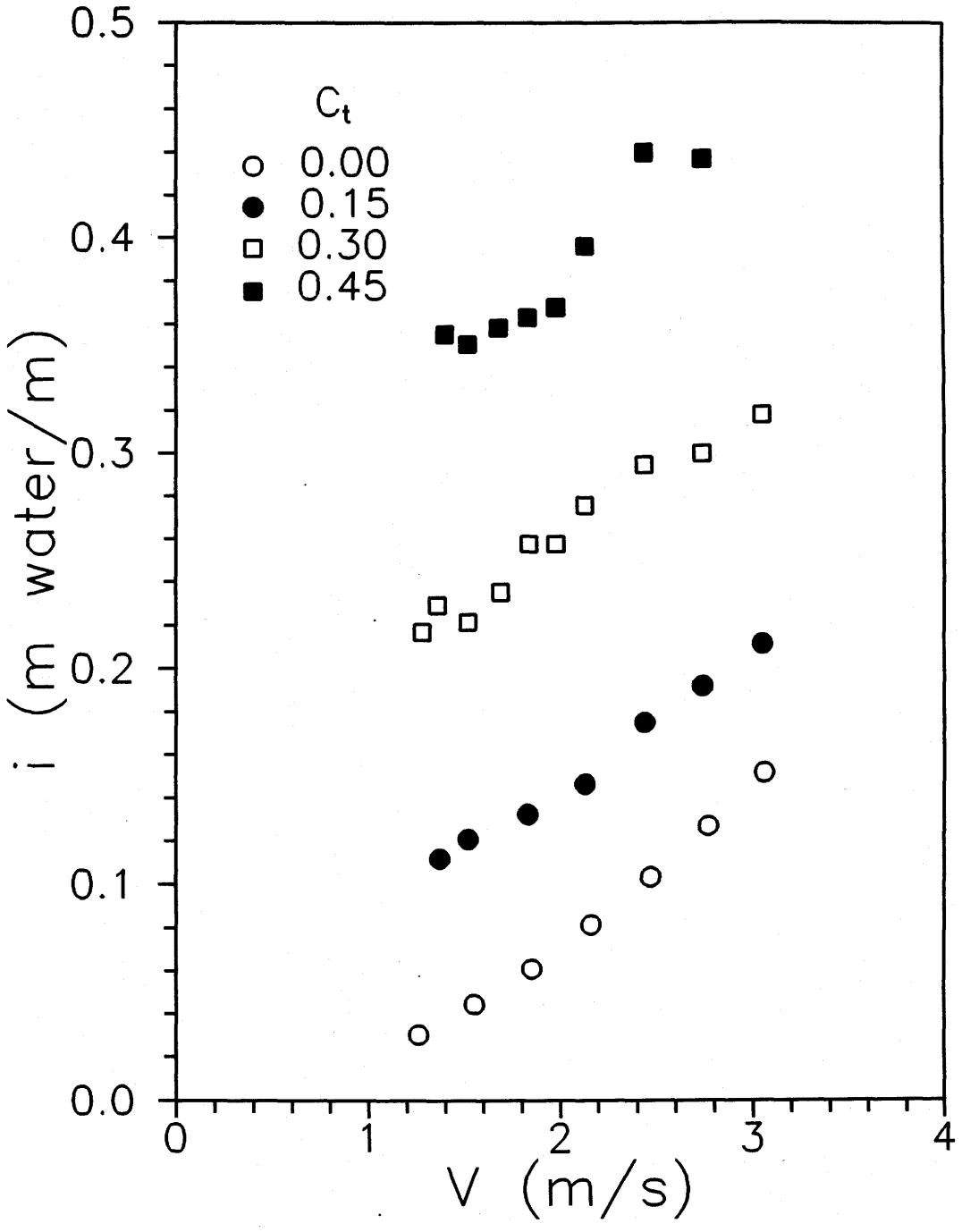

Figure 5.4: Frictional headlosses for 0.55 mm sand slurries flowing in a 53.2 mm pipe. T = 15°C.

Figure 5.5 shows the frictional headlosses for the 0.55 mm sand slurry flowing in a 263 mm pipe. Again, the slurry headlosses are high and the particle-wall friction component must be large. The frictional headloss increases substantially when the slurry temperature increases from 15°C to 40°C. Again, we see that the warm water is less effective at suspending the coarse particles. As was the case in the 53 mm pipe, the concentration distributions (Figure B6) are not strongly dependent on the mean velocity for the 0.55 mm sand slurry. The repulsive stresses are not strong enough to reverse the concentration gradient near the bottom of the pipe for flow in the large 263 mm pipe. There appears to be some effect of temperature with the solids concentration at the bottom of the pipe reaching a higher value at 40°C than at 15°C.

The pipe flow test results for 2.4 mm sand in the 53 mm pipe are given in Figure 5.6. The frictional headlosses are higher for the 2.4 mm sand than for the 0.55 mm sand for $C_t = 0.15$ but nearly identical for $C_t = 0.30$. Analysis of slurry samples showed that the carrier fluid density had increased substantially during the test with 2.4 mm sand at $C_t = 0.30$. A significant amount of fines were generated by interparticle abrasion during the test and, as shown in Table 5.1, the actual coarse solids concentration, C_r, was only 0.22. The presence of the fines is evident in the concentration distribution plots (Figure B7) where the measured solids concentration reaches a minimum value of 0.1 in the upper portion of the pipe.

The test results for 2.4 mm sand in the 263 mm pipe are given in Figure 5.7. The frictional headlosses are very high for this coarse-particle slurry. The concentration

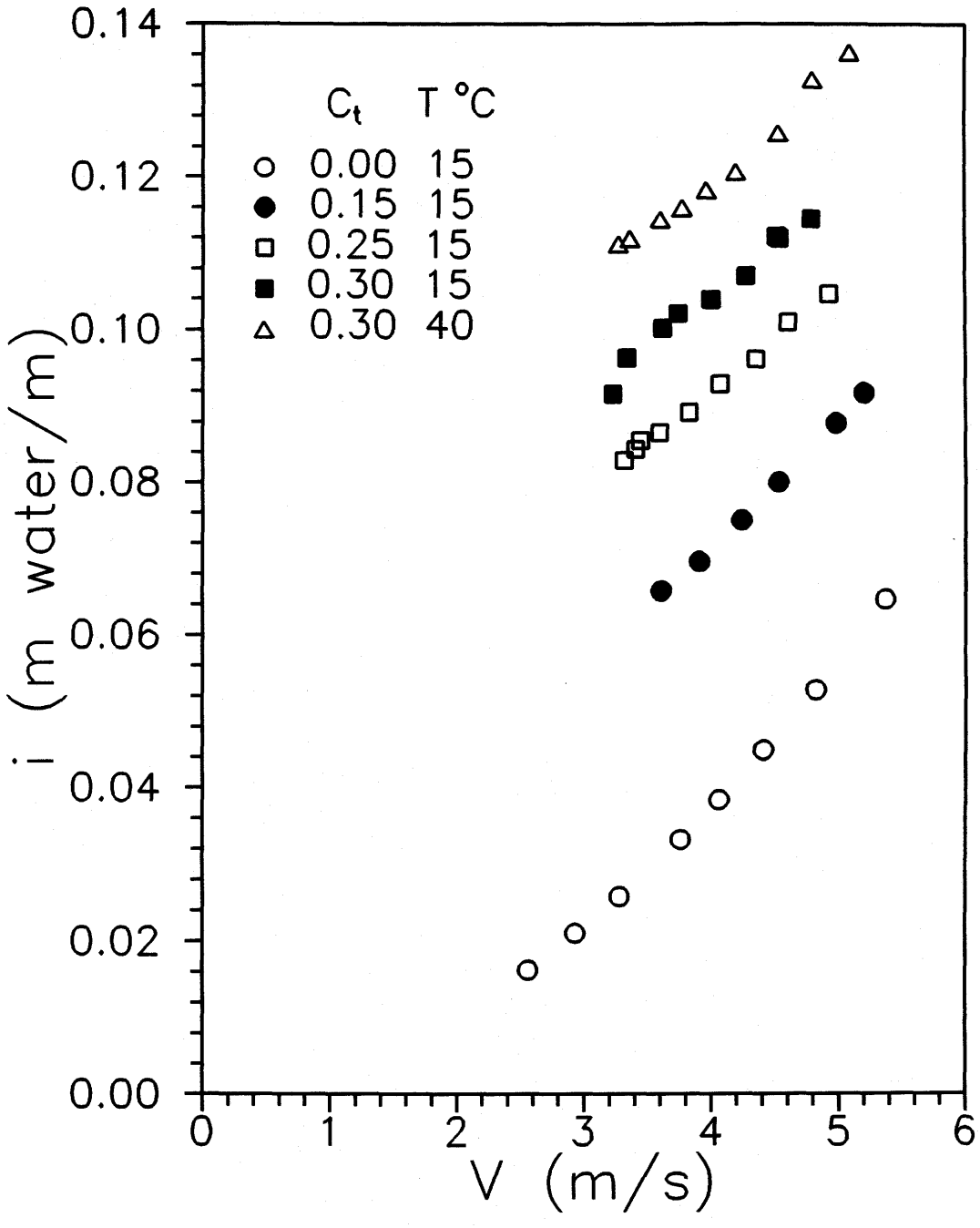

Figure 5.5: Frictional headlosses for 0.55 mm sand slurries flowing in a 263 mm pipe.

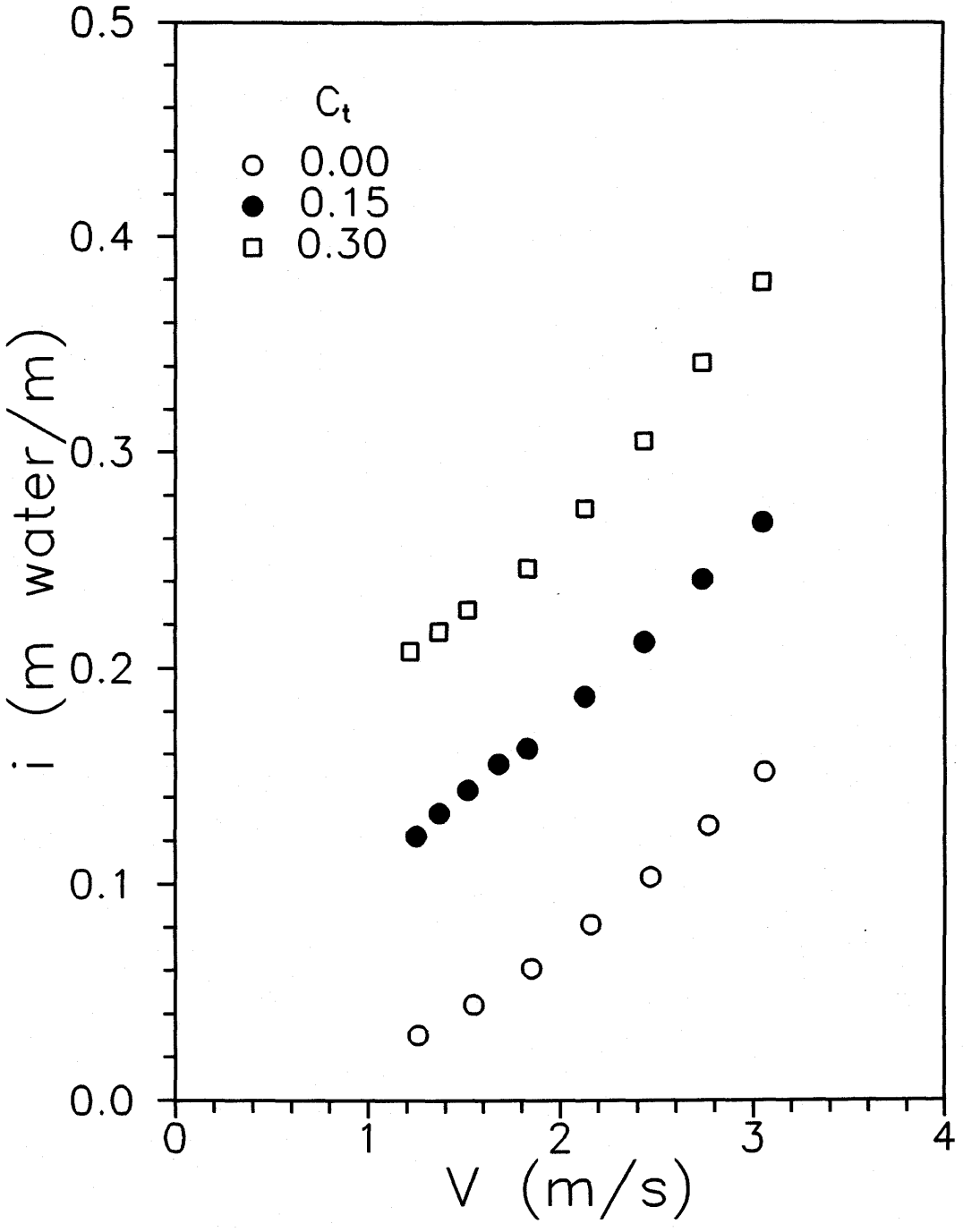

Figure 5.6: Frictional headlosses for 2.4 mm sand slurries flowing in a 53.2 mm pipe. T = 15°C.

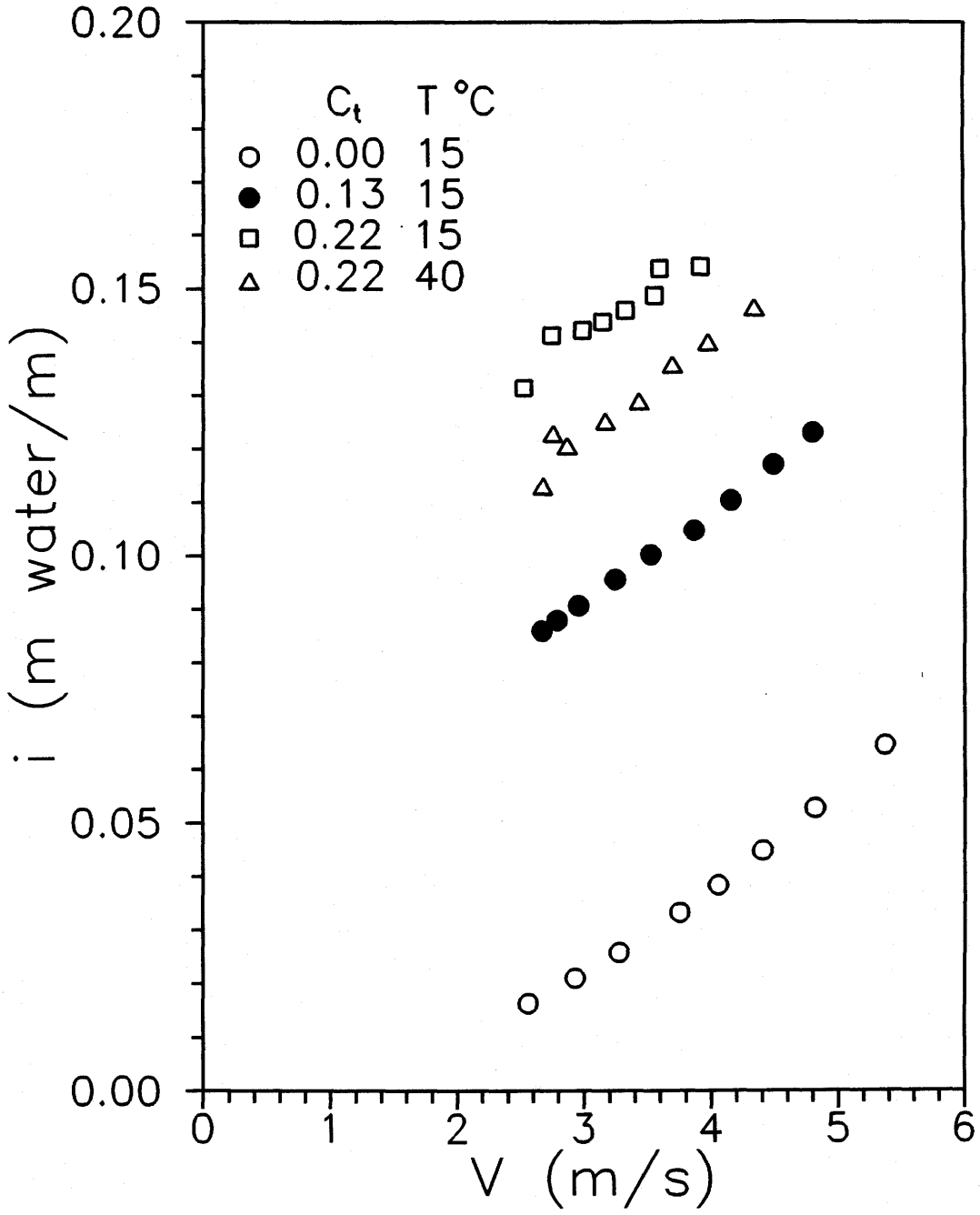

Figure 5.7: Frictional headlosses for 2.4 mm sand slurries flowing in a 263 mm pipe.

distributions (Figure B8) are not affected by the mean velocity nor by the temperature. The frictional headloss appears to be substantially reduced when the temperature is increased. This result is difficult to understand because it contradicts the other observations concerning the effect of temperature increases. It is possible that there was a problem with the pressure sensing device during this test.

5.2.3 Broad Particle Size Distributions

A sand sample with a particle size range of 0 to 1 mm (d = 0.29 mm) was tested in 53 and 263 mm pipes. Two other samples, a 0 to 6 mm sand sample (d = 0.38 mm) and a 0 to 10 mm coal sample, were tested in the 263 mm pipe. The particle size distributions are given in Figure 5.8.

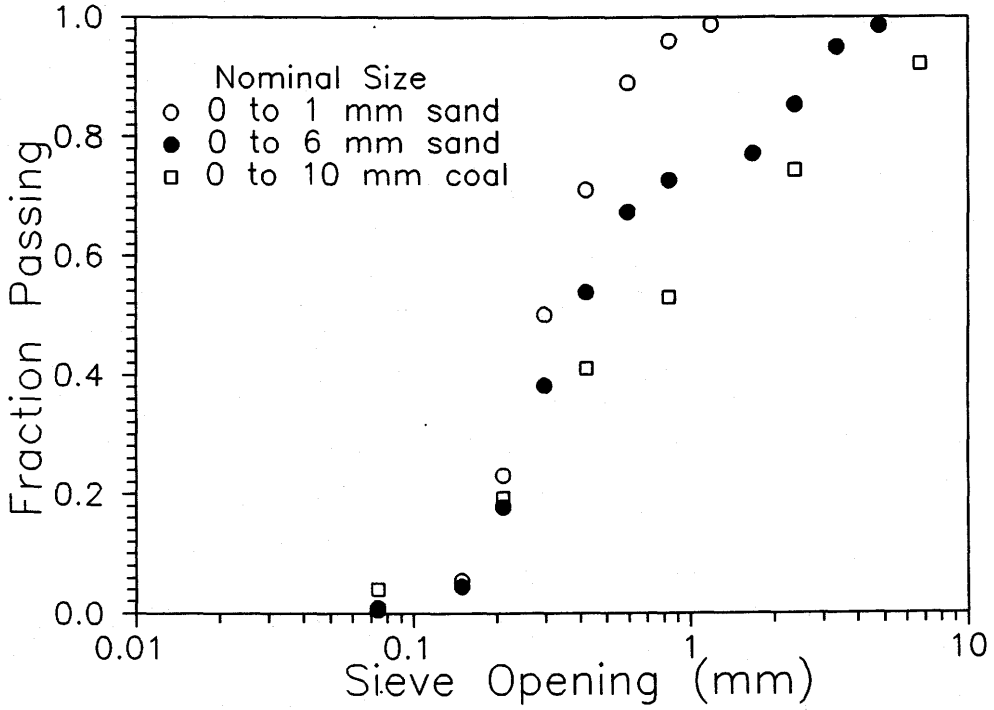

Figure 5.8: Particle size distributions for broadly sized solids.

The test results for the 0.29 mm sand slurry in the 53 mm pipe are shown in Figure 5.9. The concentration distribution (Figure B9) is strongly dependent on the mean velocity with substantially higher concentration gradients at 1.8 m/s than at 3.1 m/s.

Figure 5.10 shows the test results for the 0.29 mm sand slurry in the 263 mm pipe. There is a small temperature effect with somewhat higher headlosses at 40°C than at 15°C. The effect of temperature is also apparent when examining the velocity distributions (Figure C7). The flow is considerably more segregated at 40°C than at 15°C.

Figure 5.11 shows the experimental results for the 0.38 mm sand slurry in the 263 mm pipe. Analysis of the results is complicated somewhat because fines were generated over the course of this test. The density of the carrier fluid increased from 1004 kg/m^3 for C_t = 0.15 to 1045 kg/m^3 for C_t = 0.34. The headlosses are slightly higher than those for the 0.29 mm sand. The concentrations near the bottom of the pipe are considerably higher for the 0.38 mm sand (Figure B11) than for the 0.29 mm sand (Figure B10). The 0.38 mm sand has a broader size distribution than the 0.29 mm sand and therefore the maximum loosely packed bed concentration is also higher.

The frictional headlosses for the coal slurry are shown in Figure 5.12. The concentration distribution plots (Figure B12) show that the coal particles with an average density of 1374 kg/m^3 are much more uniformly distributed in the pipe than sand particles with a density of 2650 kg/m^3. The anomalously high concentrations in the bottom portion of the pipe are probably due to a small amount of rock material in the

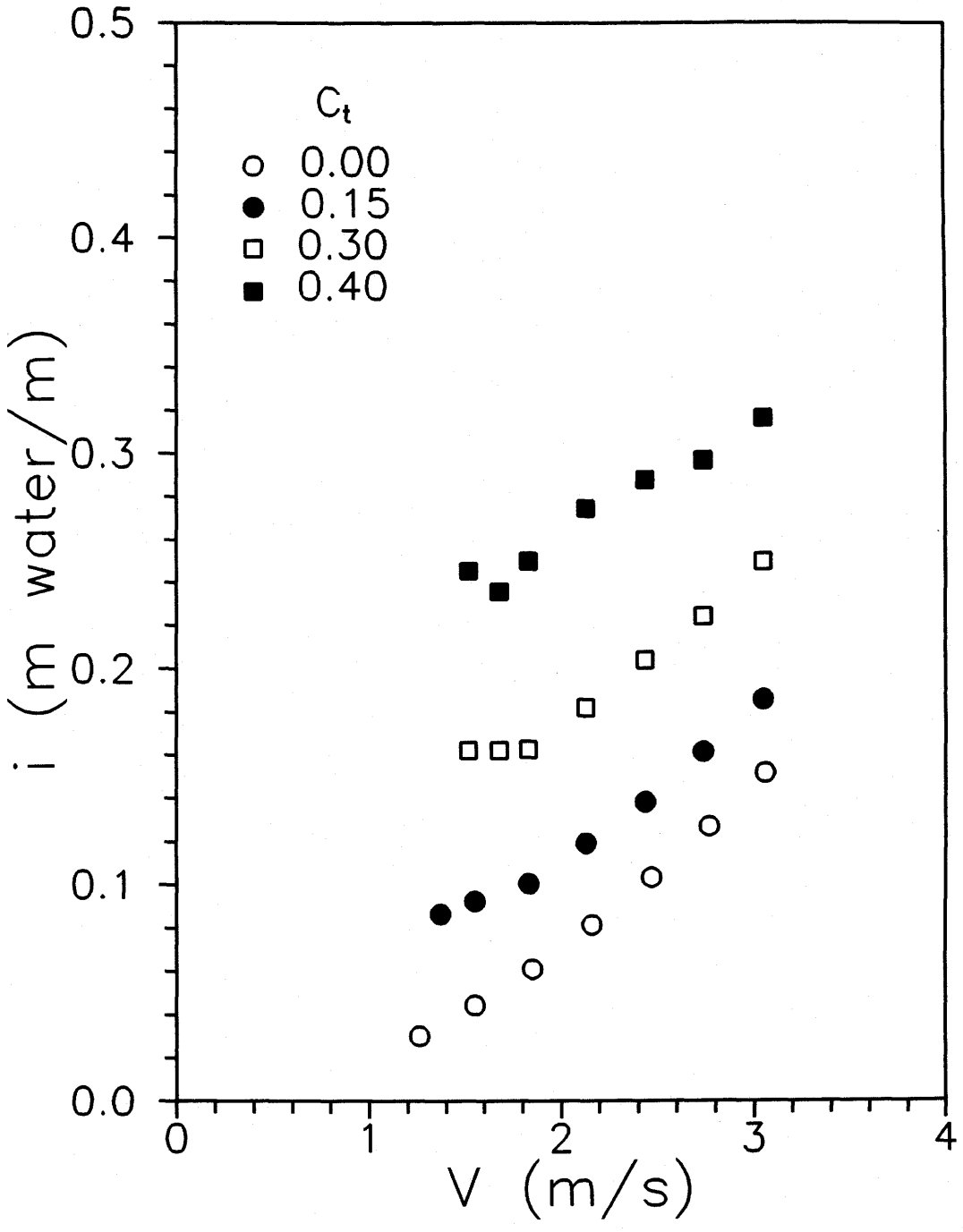

Figure 5.9: Frictional headlosses for 0.29 mm sand slurries flowing in a 53.2 mm pipe. T = 15°C.

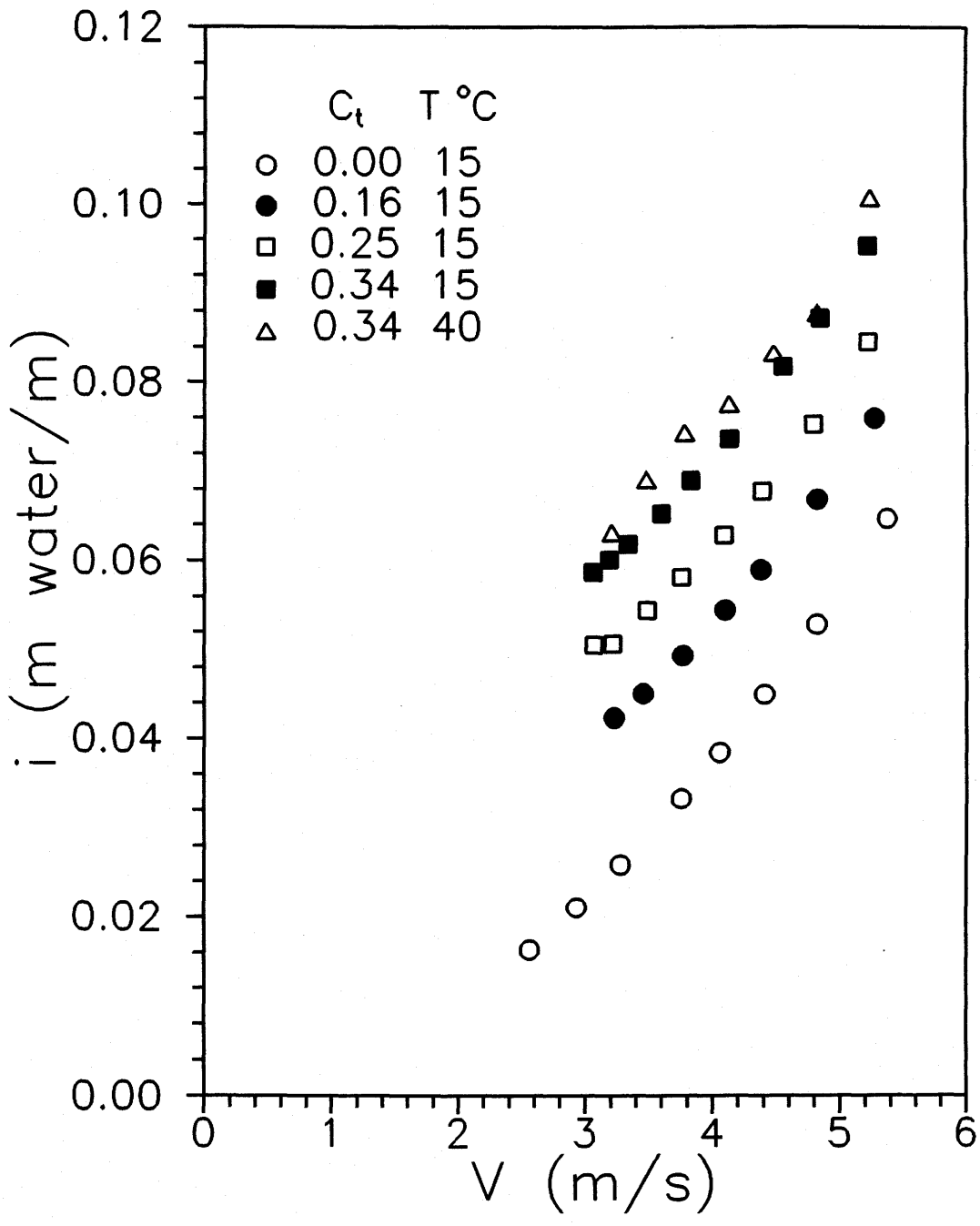

Figure 5.10: Frictional headlosses for 0.29 mm sand slurries flowing in a 263 mm pipe.

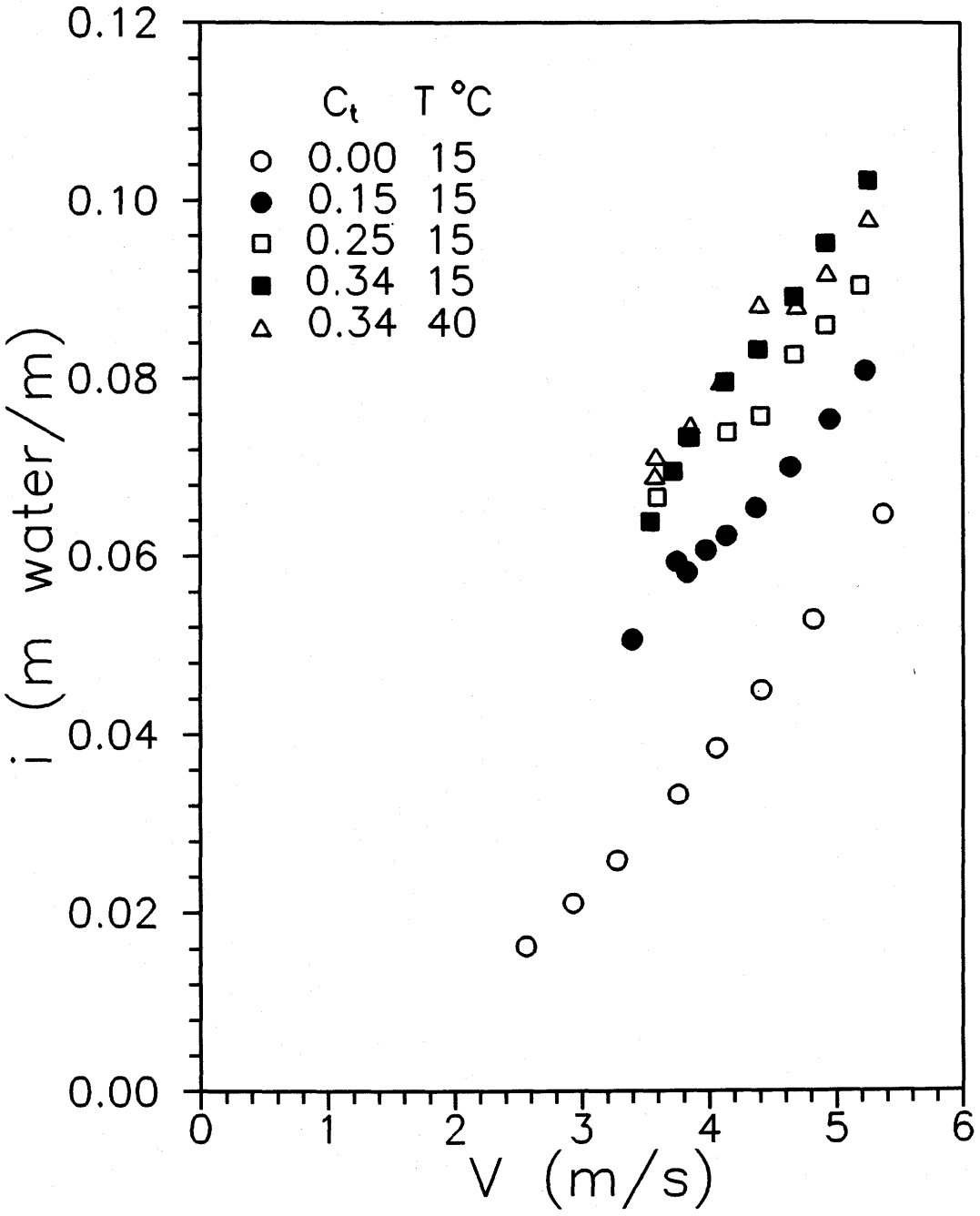

Figure 5.11: Frictional headlosses for 0.38 mm sand slurries flowing in a 263 mm pipe.

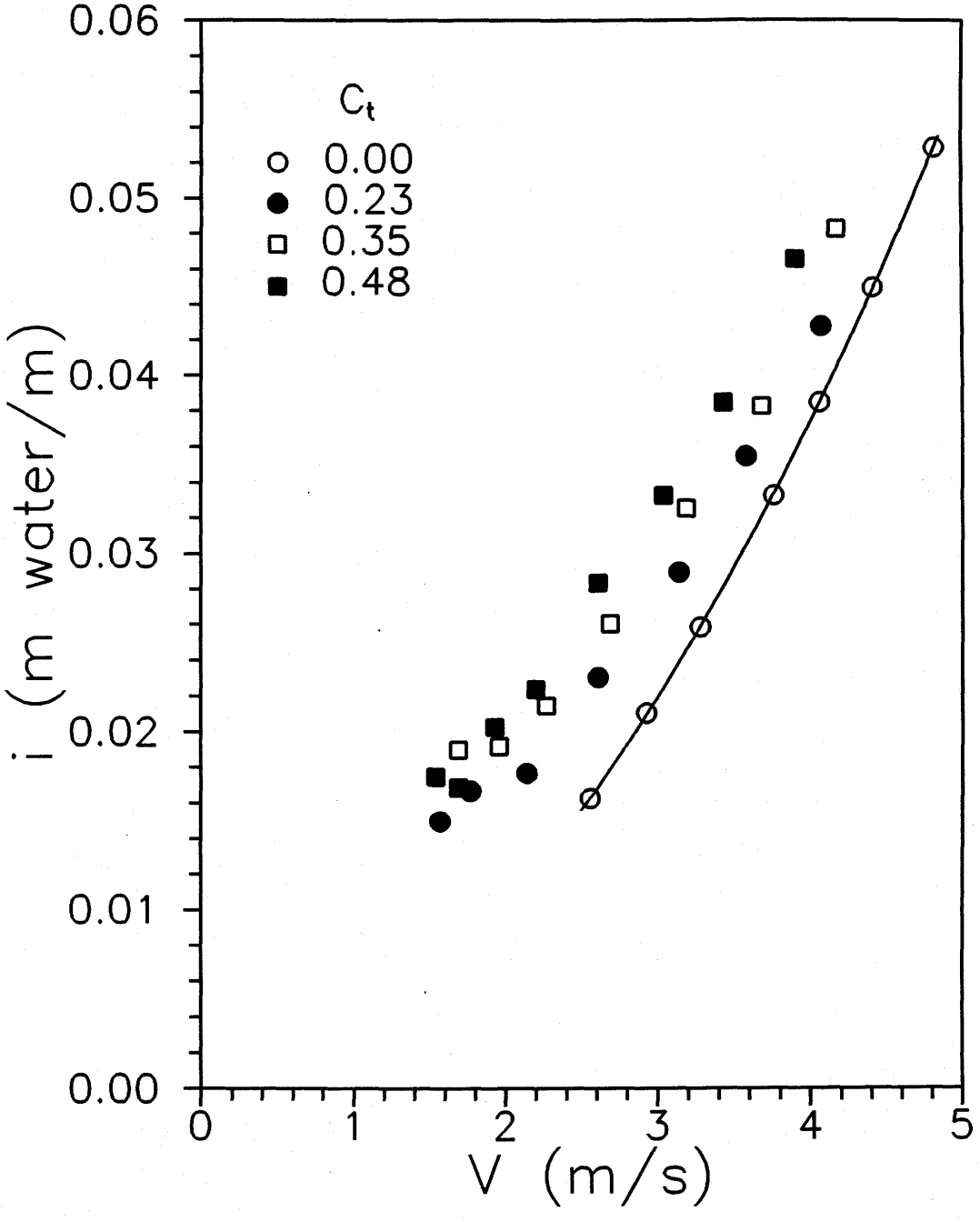

Figure 5.12: Frictional headlosses for 0 to 10 mm coal slurries flowing in a 263 mm pipe. T = 23°C.

coal sample. This dense rock travels preferentially near the bottom of the pipe. Unrealistically high concentrations are obtained when the average coal particle gamma ray absorption coefficient is used to calculate the solids volume fractions when a significant quantity of rock is present.

There was a considerable amount of coal particle attrition during the test and, as a result, the fines content increased as the experiment proceeded. As shown in Table 5.2, the generation of fines resulted in significant increases in the carrier fluid density and viscosity.

5.3 Particle Properties

5.3.1 Particle Size

The mass average particle sizes (d's) are given in Tables 5.1 and 5.2 and the distributions are tabulated in Appendix A. The particle size distributions shown in Figures 5.1 and 5.8 are representative of the material contained in the pipeline flow loop at the start of a series of tests. The coarse sand particles tended to degrade somewhat and, as a result, the concentration of very fine material in the mixture tended to increase over the course of a series of experiments.

Figure 5.13 shows the particle size distributions for the coarse (+0.074 mm) coal fraction for each test. The particle size distribution of the coarse solids fraction changed only slightly during the tests although considerable amounts of fines were generated. This is due to the fact that abrasion removes sharp corners and projections from the surface of the particles without changing their mean diameters substantially.

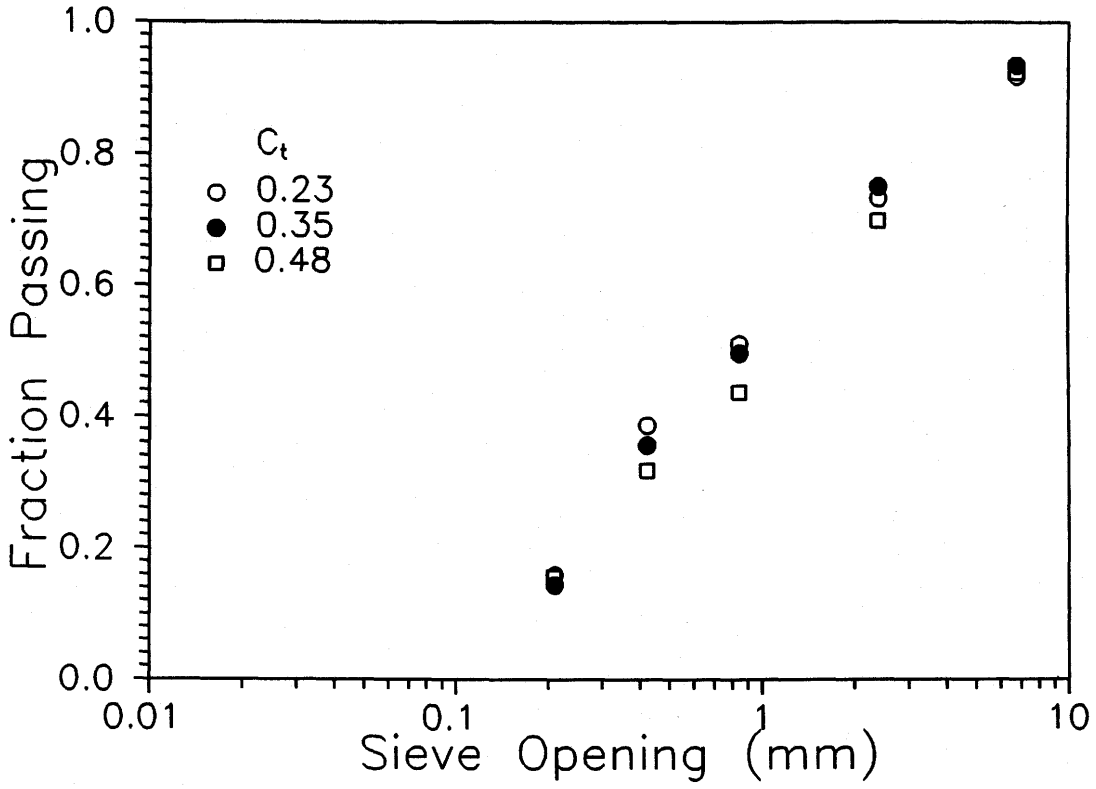

Figure 5.13: Particle size distributions for coarse fractions of 0 to 10 mm coal slurries.

5.3.2 Drag Coefficients

The particle drag coefficient data which were measured during this study, and other studies at the Saskatchewan Research Council and the University of Saskatchewan's Chemical Engineering Department, are reported by Shook and Roco (1990) and reproduced here (Table 5.4). The sand and coal particle drag coefficients were fitted to the following equation:

$$C_D = a\left(C_D Re_p^2\right)^b \qquad (5.1)$$

where the Archimedes Number, $C_D Re^2$, is given by Equation 4.11. Table 5.4 gives the correlating coefficients a and b for the particles. The drag coefficients show the importance of particle shape on the particle settling rates. The coal particle drag coefficients show substantial deviation from those for spheres. This was probably due to the fact that the coal particles were fractured by mining processes and had sharp edges. The sand particles were more rounded and had lower drag coefficients than the coal particles.

5.4 Carrier Fluid Properties

For the relatively low fines concentrations of these tests, the carrier fluids exhibited essentially Newtonian fluid behaviour. The carrier fluid viscosities and densities are reported in Tables 5.1 and 5.2.

Table 5.4: Particle drag coefficients for sand and western Canadian coals. (Reproduced from Shook and Roco, 1990.)

Particle	Range	a	b
Coal	Ar < 24	576	-1
	24 < Ar <4660	128	-0.482
	4660 < Ar	2.89	-0.0334
Sand	Ar < 24	576	-1
	24 < Ar < 2760	80.9	-0.475
	2760 < Ar < 46100	8.61	-0.193
	46100 < Ar	1.09	0

6 CORRELATIONS AND DISCUSSION

6.1 Turbulent Flow Considerations

For single phase fluid flows, it is known that the velocity fluctuations associated with turbulence tend to die in the region near the pipe wall. The viscous sublayer acts as a lubricating layer which suppresses direct transfer of eddy momentum to the pipe wall. For slurry flows, there are similar wall-repulsive effects which reduce the tendency for direct particle-wall interactions. However, the headloss data of Chapter 5 show that these wall-repulsive forces are not effective at preventing particle-wall contact under all circumstances. In terms of the contribution of the particles to frictional headloss, several factors may be important:

1. Particles which are small in comparison with the thickness of the viscous sublayer tend to be uniformly dispersed during flow. These fine particles add to the rate of momentum transfer by increasing the viscosity of the fluid in the sublayer.
2. The normal stresses which result from gravity may be strong enough to overcome the forces repelling the particles from the boundary, thus allowing the coarser particles to exchange momentum with the fluid in the sublayer or to make contact with the pipe wall directly.
3. If the mean solids concentration is high, the normal stresses resulting from particle interactions may also be strong enough to allow the coarser particles to penetrate into the wall region.

4. The particles may also affect the headloss by altering the nature of turbulence in the central core. However, this effect is likely to be relatively small in comparison with wall region effects.

6.2 Pseudohomogeneous Slurry Flows

The 0.18 mm sand slurry data of Figures 5.2 and 5.3 provide a test for particles of intermediate size between those which are so small that the solids and carrier liquid may be regarded as a continuum and those which are so large that coarse-particle effects dominate the frictional headloss. To begin our examination of these flows, we assume homogeneous fluid behaviour. For homogeneous mixtures, Equation 2.33 may be used to determine the headloss. The Fanning friction factor, f_m is a function of D, V, ρ_m, μ_m and the pipe wall roughness. The *in situ* solids concentration is used to determine the mixture density: $\rho_m = \rho_s C_t + \rho (1 - C_t)$. We assume that the wall-repulsive effects will be strong so we use the viscosity of water as an estimate of the mixture effective viscosity μ_m.

Figures 6.1 and 6.2 compare the actual frictional headlosses with the headloss values that might be expected if the slurries were truly homogeneous mixtures. In the small pipe there appears to be a significant coarse-particle component which contributes to the headlosses at low flowrates. At high flowrates the coarse-particle effects are reduced because the intensity of turbulent mixing increases and most of the immersed weight of the particles is suspended by fluid forces. In large pipes, although the

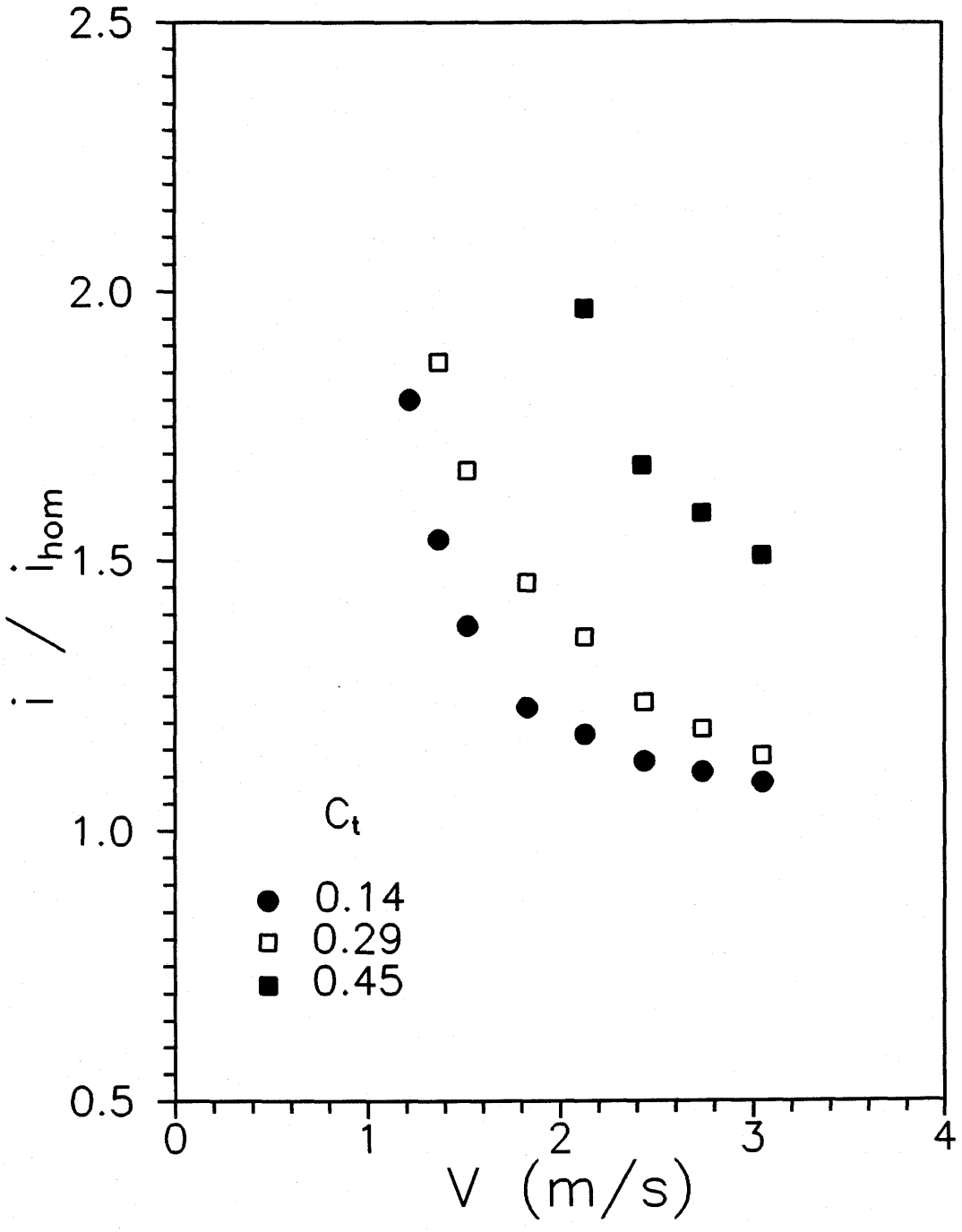

Figure 6.1: The ratio of actual to homogeneous mixture frictional headlosses for 0.18 mm sand slurries flowing in a 53.2 mm pipe.

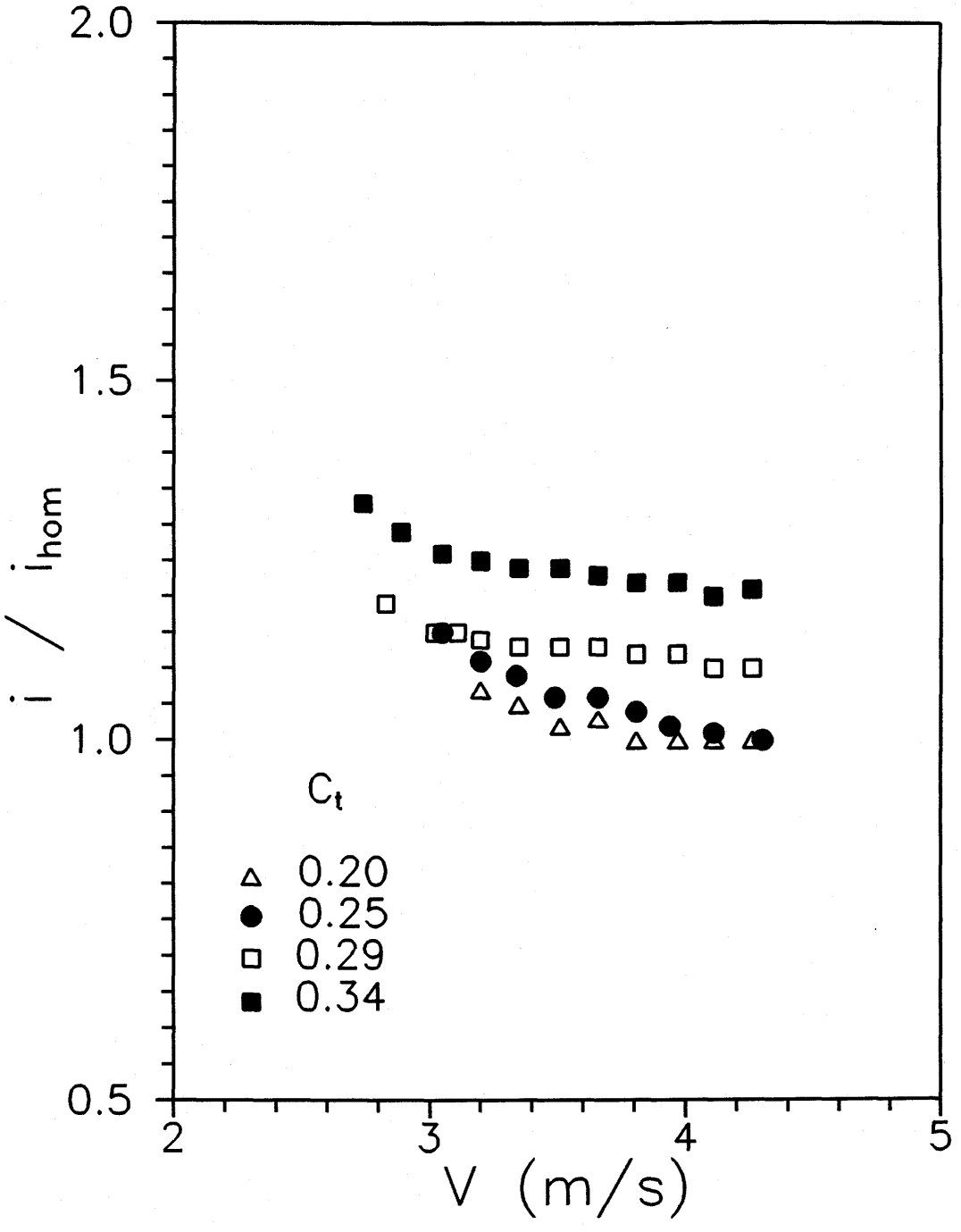

Figure 6.2: The ratio of actual to homogeneous mixture frictional headlosses for 0.18 mm sand slurries flowing in a 495 mm pipe.

concentration varies considerably with height (Figure B.4), the slurry headlosses differ only by small amounts from those that would be expected for homogeneous slurries. At high flowrates and at moderate solids concentrations the slurries behave, in terms of frictional headlosses, like Newtonian liquids with the viscosity of the carrier fluid and the density of the *in situ* mixture.

For $C_t = 0.34$ in the 495 mm pipe and $C_t = 0.45$ in the 53 mm pipe, the i/i_{hom} ratios approach values which are significantly greater than 1.0. The slurry has the headloss of a liquid with a viscosity greater than that of water when the solids concentration is high. It is likely that, with increased particle-particle interactions at the higher concentrations, the normal stresses are large enough to allow the solids to penetrate into the wall region. A similar result was reported by Shook (1985) for pipe flow of suspensions of nearly neutrally buoyant particles. Wall friction was shown to increase substantially at high concentrations. This phenomenon is often referred to as a "slurry viscosity" effect.

6.3 Coarse-Particle Slurry Model

The two-layer modelling concept developed by Wilson and co-workers was chosen as the basis for a model which would be useful for extending laboratory data to the design of industrial coarse-particle slurry pipelines. The two-layer approach was chosen because it provides a convenient method for analyzing experimental results and provides a mechanistic method for dealing with the wall stress contributions. While the model has the disadvantage of being oversimplified, it contains relatively few empirical

terms. This is a major advantage over more sophisticated models which require several empirical terms to be inferred from a limited amount of experimental data.

In the two-layer approach the solids are divided, conceptually, into "contact load" which contributes to particle-wall sliding friction and "suspended load" for which the immersed weight is transferred to the carrier fluid. The contact load fraction has a direct effect on the headloss and energy consumption making it an extremely important variable in the modelling process.

The model used here is different in several respects from that originally proposed by Wilson and co-workers during the 1970's. The major differences are outlined below:

1. For slurries containing a wide range of particle sizes, the unique contribution of the fine particles is recognized. The slurry is considered to be composed of two parts; a pseudo-continuous phase or carrier "fluid" which contains the carrier liquid and the fine solids, and a dispersed phase which contains only the coarse solids.

2. The lower layer was originally perceived to move as a sliding bed with a concentration equal to that of a loosely packed bed. Recent measurements of velocity distributions have shown that, with few exceptions, the mixture in the lower portion of the pipeline does not flow as a sliding bed. Instead, the mixture is sheared, with concentrations which are generally significantly less than the settled bed value. Therefore, the contact load stresses cannot be transferred by direct and continuous particle-particle contacts of the type that occurs in settled beds. An early version of the model (Section 6.3.1) was developed using a fixed

lower layer concentration. In an improved version (Section 6.3.2), the lower layer concentration is treated as a variable.

3. The new model recognizes that, during normal pipeline flows, suspended solids are present in both the upper and lower regions of the pipe. These solids increase the density of the suspension in the lower layer. Hence, there is a buoyancy effect which tends to reduce the immersed weight of the contact load solids.

4. Wilson and his earlier coworkers expressed the contact load concentration, C_c, as a fraction of the delivered solids concentration, C_v. The value of C_c / C_v can exceed unity for flows near deposition conditions. In the extreme case of very low flowrates, the delivered concentration will approach zero and the contact load concentration will approach the *in situ* solids concentration so the ratio C_c / C_v becomes infinitely large. Obviously, Equation 3.19 cannot be valid over the entire range of flow conditions encountered in pipeline operation. It seems better conceptually to express it as a fraction of the *in situ* solids concentration and this has been done in the new model.

6.3.1 Initial Headloss Modelling Effort

The total *in situ* solids concentration C_t is separated into fines and coarse fractions:

$$C_t = C_f + C_r \qquad (6.1)$$

The fines are defined as being the solids finer than 0.074 mm and this definition is essentially a practical one. Smaller particles are easily separated by wet screening so

that their volume fraction in the mixture (C_f) can be determined. The fines combine with the carrier liquid to form a mixture which is considered to act essentially as a carrier fluid of density ρ_f, where

$$\rho_f = \frac{\rho_L(1 - C_t) + \rho_s C_f}{1 - C_t + C_f} \tag{6.2}$$

The viscosity (μ_f) of the carrier fluid of density ρ_f may be measured or calculated. A slurry containing only fine particles can usually be tested with a viscometer. If measurements cannot be made, a reasonable estimate of the viscosity can be obtained from the correlations available in the literature for unflocculated slurries (e.g. Thomas, 1965).

The coarse particles are assumed to form two constant composition layers as shown in Figure 6.3. Particles suspended by fluid forces are distributed uniformly within the pipe with concentration C_1. The lower layer also contains particles whose immersed weight is transmitted to the pipe wall by particle-particle interactions. The latter are the contact load particles whose concentration, averaged over the whole pipe, is C_c. Thus,

$$C_r = C_1 + C_c \tag{6.3}$$

The lower layer concentration, C_{lim} is assumed to be the concentration of a loosely packed bed of solids. In terms of the total coarse-particle concentration of the lower layer (C_{lim}) the contact load particles produce the incremental concentration C_2:

$$C_2 A_2 = C_c A \tag{6.4}$$

where A and A_2 are the pipe and lower layer cross sectional areas and

$$C_{lim} = C_1 + C_2 \tag{6.5}$$

The ratio C_c / C_r is thus the fraction of the +0.074 mm particles which is not suspended by the fluid.

The density of the mixture in the upper layer is ρ_1:

$$\rho_1 = \rho_f(1-C_1) + \rho_s C_1 \tag{6.6}$$

In the lower layer the suspended particles combine with the fines and the liquid to form a mixture of density ρ_2.

$$\rho_2 = \frac{\rho_f(1-C_{lim}) + \rho_s C_1}{1 - C_{lim} + C_1} \tag{6.7}$$

The model employs volumetric balances for the mixture and the solid particles. Neglecting slip between the phases, the volumetric mixture flow is

$$AV = A_1V_1 + A_2V_2 \tag{6.8}$$

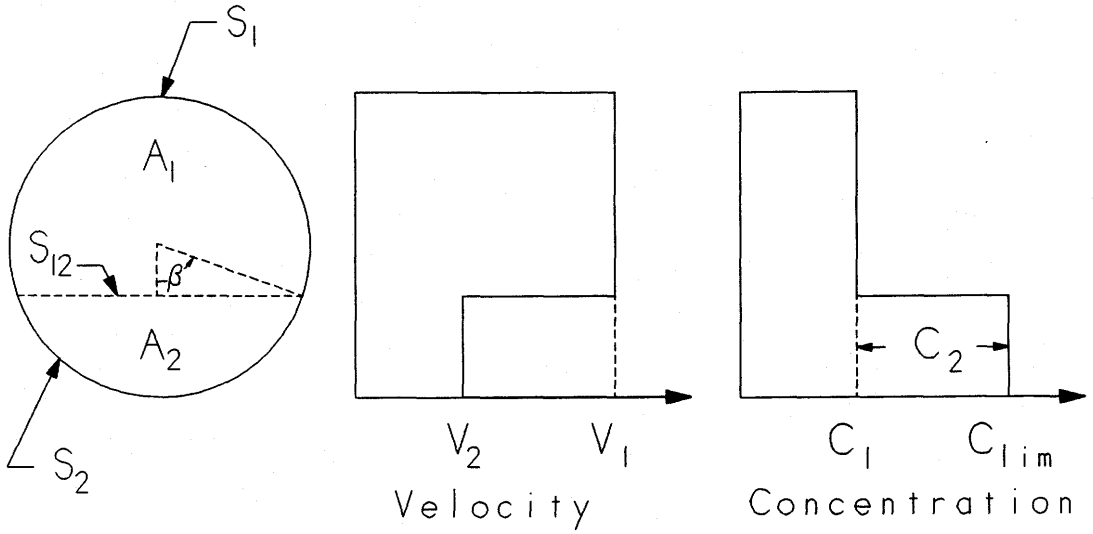

Figure 6.3: The version of the two layer model used in this study.

The delivered flowrate of solids, including fine (-0.074 mm) particles, is

$$C_v A V - C_1 A V + C_2 A_2 V_2 + Q_{fines} \qquad (6.9)$$

where Q_{fines} is the flux of fine particles. Q_{fines} is calculated from the expression

$$Q_{fines} = \frac{C_f}{1-C_r}\left[(1-C_1)A_1 V + (1-C_{lim})A_2 V_2\right] \qquad (6.10)$$

Forces balances are written for each layer in terms of the axial pressure gradient i ρ_L g. For horizontal flow, equations 3.12 and 3.13 apply. The sign of the interlayer stress τ_{12} is positive for $V_1 > V_2$.

The stress τ_1 is computed using a Fanning friction factor f_1 as

$$\tau_1 = f_1 V_1 |V_1| \rho_1 / 2 \qquad (6.11)$$

f_1 is calculated from the pipe wall roughness k and a Reynolds number which employs the mean velocity V:

$$f_1 = f_1[(DV\rho_1/\mu_1), (k/D)] \qquad (6.12)$$

It was found that for $C_r < 0.35$, good results are obtained using $\mu_1 = \mu_f$. Churchill's correlation (Equation 2.32) may be used to determine values for f_1.

The force $\tau_2 S_2$ results from the fluid-like resistance to flow of the mixture of density ρ_2 and the Coulombic friction associated with the contact load. Equation 3.16 needs modification to account for the buoyancy effect associated with the presence of suspended solids in the lower layer. With y measured downward, the normal stress resulting from the immersed weight of the contact load particles is

$$\frac{d\sigma}{dy} = (\rho_s - \rho_2)\, g\, (C_{lim} - C_1) \qquad (6.13)$$

The concept that the interfacial stress is transmitted through the solids to the pipe wall is difficult to justify if the lower layer is not actually a sliding bed and the interface is a hypothetical one. Equation 3.17, with the buoyancy effect added and the interfacial stress transmission term dropped, becomes

$$\tau_2 S_2 = \frac{f_1 V_2^2 \rho_2 S_2}{2} + \frac{(\rho_s - \rho_f) C_2 (1 - C_{lim}) g D^2 (\sin\beta - \beta\cos\beta) \eta_s}{2(1 - C_2)} \qquad (6.14)$$

As shown in Figure 6.3, β is the angle defining the lower layer.

The interfacial shear stress τ_{12} is calculated from the velocity difference (V_1 - V_2), the density of the upper layer and a Fanning friction factor f_{12}.

$$\tau_{12} = f_{12}(V_1 - V_2)\,|V_1 - V_2|\,\rho_1 / 2 \qquad (6.15)$$

The interfacial shear stress is associated with the velocity gradient in the slurry and does not affect the pressure gradient. This can be seen by eliminating τ_{12} between Equations 3.12 and 3.13. The volumetric flowrate relationships (Equations 6.8 and 6.9) show that the interfacial friction has a strong influence on the relationship between C_t and C_v. Thus the interfacial friction factor f_{12} used in the model influences the prediction of the delivered solids concentration. The usual practice of evaluating f_{12} based on a rough boundary friction condition (Equation 3.15) was used in this initial modelling effort.

Table D.1 (Appendix D) summarizes the data base which was used to establish the correlation for C_c / C_r. The first correlation was obtained before some of the 50 mm pipeline experiments of Chapter 5 had been completed. Data from previous Saskatchewan Research Council studies were used instead and the substituted data may

have been of somewhat inferior quality because the test conditions were not controlled so closely in earlier studies. In selecting the data a number of arbitrary decisions were made.

1. To allow the "slurry viscosity" effects to be estimated, only isothermal (constant μ_L) runs with $C_r \leq 0.38$ were considered. Section 6.2 shows that these effects become significant at concentrations which are somewhat lower than $C_r = 0.38$ for fine sand and that perhaps a lower maximum concentration restriction should have been imposed.
2. Three experimental i-V pairs were chosen for each run, spanning the range between the lowest deposit-free velocity and the maximum velocity.
3. Only washed (clay-free) sand and gravel with unimodal size distributions were considered. η_s was known to be 0.5 for these materials in the pipes which were used.
4. Only coals for which μ_f had been measured were considered. η_s was taken as 0.4 for the coal since this was the mean of the values which had been measured.

The correlation can be expressed in a variety of ways, depending upon the choice of dimensionless groups. Its form was chosen to reflect the fact that C_c / C_r should approach zero when the suspending power of the flow is high and unity at the other limit. In terms of the Archimedes number for particles in the carrier fluid, the correlation is:

$$\frac{C_c}{C_r} = \exp\left[-0.124 Ar^{-0.061} Fr_p^{-0.028} \left(\frac{D}{d}\right)^{0.43} \left(\frac{\rho_s}{\rho_f} - 1\right)^{-0.27}\right] \qquad (6.16)$$

Fr_p is the Froude number for the particles, V^2 / g d.

This expression provided a reasonable fit for a wide range of experimental conditions. This can be seen in the comparisons of Figures 6.4 and 6.5 where values of C_c / C_r inferred from the experimentally determined headlosses are compared with Equation 6.16. There is evidence of a residual velocity effect not taken into account by Equation 6.16 since the data for any one set of experiments (when all other factors are fixed) show considerable spread in some cases.

Figure 6.6 shows that the model predicted delivered concentrations which were lower than the experimental values and the deviation is largest when the pipe to particle diameter ratio is low. The interfacial friction factor f_{12} thus needs to be increased, particularly for very coarse particles.

6.3.2 Improved Headloss Model

As mentioned previously, early modelling efforts used a fixed value of C_{lim}. Appropriate for extremely coarse particles, this simplification departs from measured concentrations as C_r is reduced or as the particle settling velocity decreases. Using the settled bed value for C_{lim} results in a systematic distortion of C_c/C_r values inferred from experimental results. The improved headloss model used the following correlation to estimate C_{lim}:

$$\frac{C_{max} - C_{lim}}{C_{max} - C_r} = 0.074\left(\frac{V}{V_\infty}\right)^{0.44}(1 - C_r)^{0.189} \qquad (6.17)$$

where V_∞ is the terminal falling velocity, in water and fines, of the mass median diameter of the coarse (+0.074 mm) particles. C_{max} , the loosely packed bed

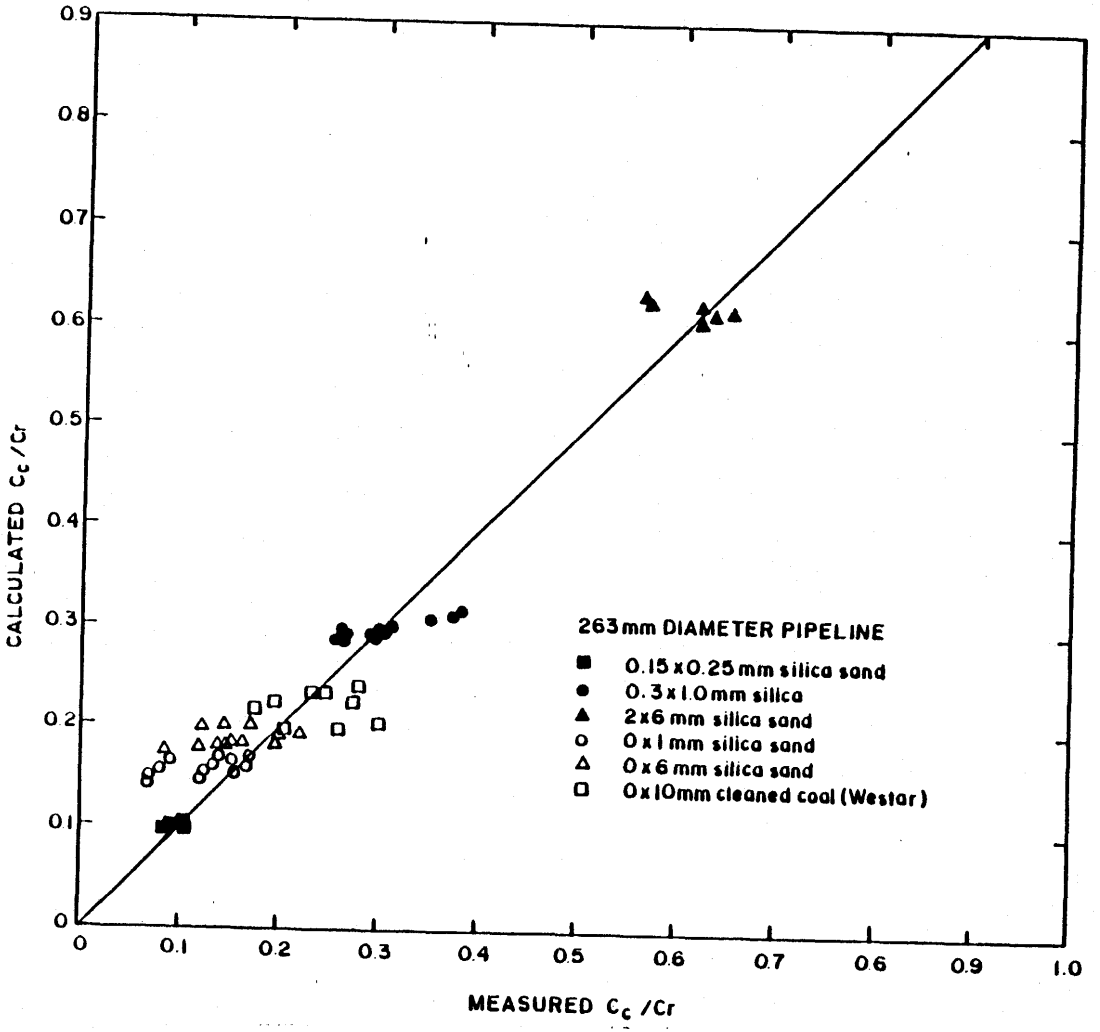

Figure 6.4: Contact load correlation for slurries flowing in a 263 mm pipeline.

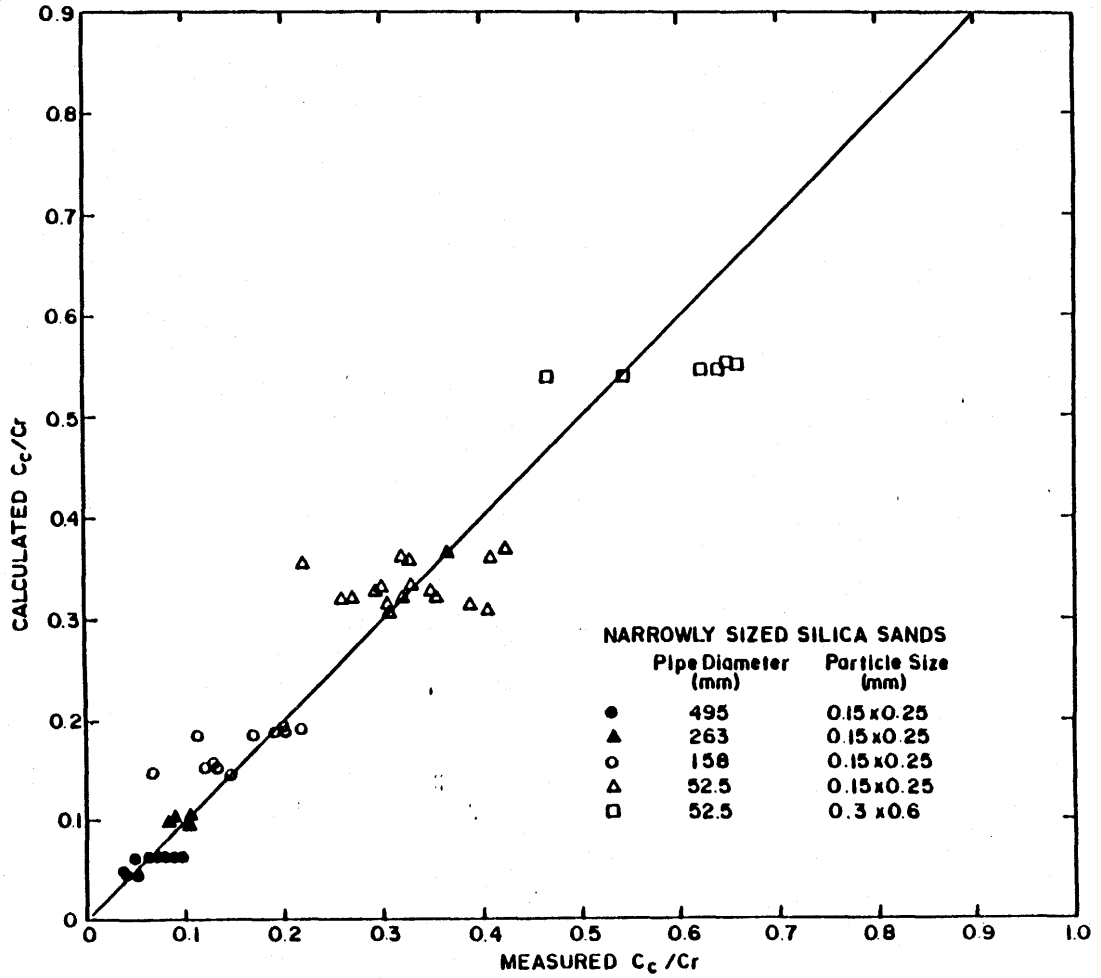

Figure 6.5: Contact load correlation for narrowly sized sand slurries in pipes of various sizes.

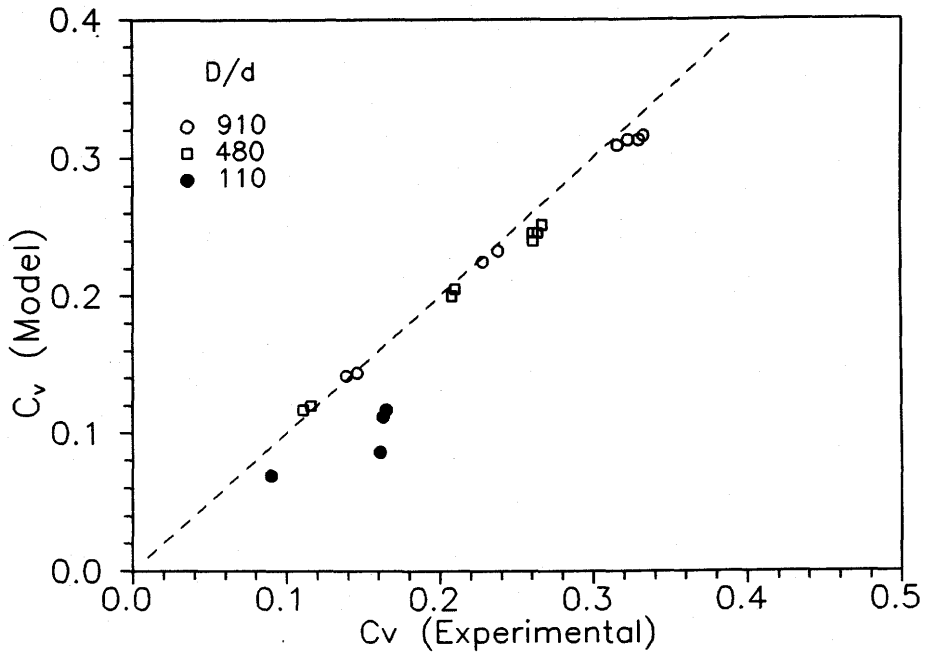

Figure 6.6: A comparison of experimentally determined delivered concentrations with estimates obtained using the two layer model and Equation 3.15 to estimate f_{12}.

concentration, depends on the breadth of the particle size distribution and may be determined by measuring the density (mass / volume) of a settled bed.

Figure 6.7 compares the values of C_{lim} computed from Equation 6.17 with local concentrations measured by gamma ray absorption at a location y = 0.15 D from the bottom of the pipe. Figure 6.7 shows that Equation 6.17 still provides only a rough estimate of C_{lim} so that an improved method would be desirable. The modelling of concentration distributions is addressed in Section 6.3 and a new method for predicting C_{lim} is presented.

Figure 6.8 compares the distribution measured by gamma ray absorption for a slurry of fine sand with $C_r = 0.15$ with its approximation in the first version of the

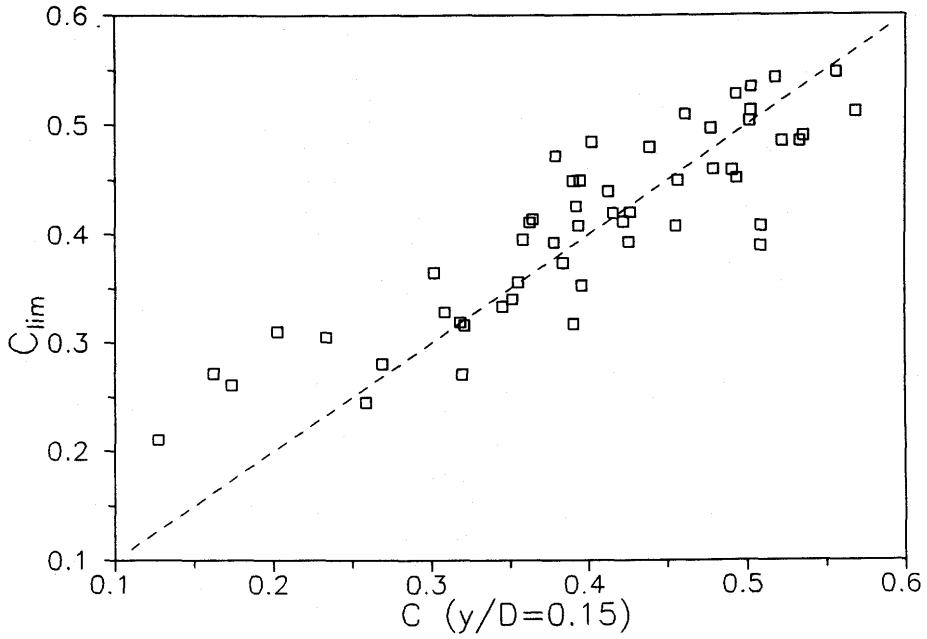

Figure 6.7: C_{lim} values computed from Equation 6.17 and concentrations measured by gamma ray absorption at y/D = 0.15 for sand and gravel slurries.

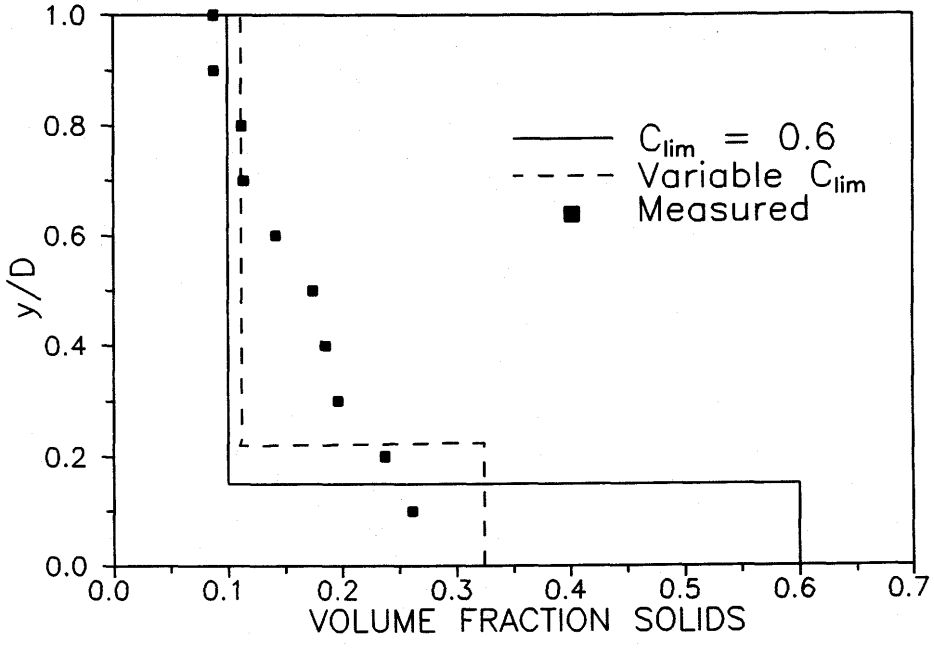

Figure 6.8: Model representations of concentration distribution and measured chord average concentration as a function of height for 0.18 mm sand in a 53 mm pipeline.

two layer model (solid lines) and its approximation using Equation 6.17 (dashed lines). The effect of Equation 6.17 is most pronounced at low concentrations and high velocities where C_{lim} tends to be lowest. The effect is shown in Figure 6.9 which compares inferred values of C_c / C_r to those obtained using C_{lim} = 0.60, using the fine sand slurry of Figure 6.7. The tendency of C_c / C_r to display a minimum is reduced by use of the correlation. As a result, the problems of the earlier correlation in dealing with the velocity variation are reduced. It is seen that the C_{lim} value in Figure 6.8 is still somewhat higher than the experimental measurements would suggest. Had Equation 6.17 predicted lower C_{lim} values at high velocities, the minimum in Figure 6.9 would have been removed completely.

To improve the model's ability to estimate delivered concentrations, a modified method for estimating the interfacial friction factor was used:

$$f_{12} = \frac{1 + 2Y}{(4\log_{10}(D/d_{12}) + 3.36)^2} \qquad (6.18)$$

where $Y = 5 + 1.86 \log_{10} (d_{12}/D)$ for $d_{12}/D > 0.002$ and $Y = 0$ otherwise.

In Equation 6.18, d_{12} is the particle diameter at the hypothetical interface, determined by assuming that all the +0.074 mm particles of diameter greater than d_{12} are in the lower layer as shown in Figure 6.10.

Table D.2 summarizes the data base which was used to establish the improved correlation for C_c / C_r. In this case, the criterion $C_r < 0.35$ was imposed and the new experimental data from this study were used instead of some of the experimental data from earlier experiments.

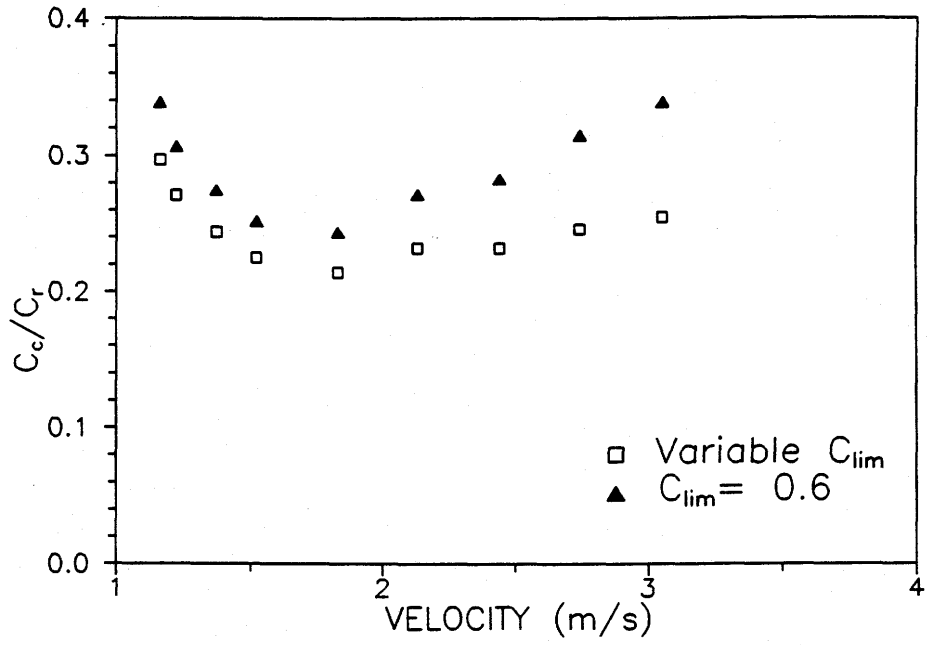

Figure 6.9: Effect of C_{lim} and mean flow velocity on C_c/C_r values inferred from experimental headlosses. These results refer to the slurry of Figure 6.8.

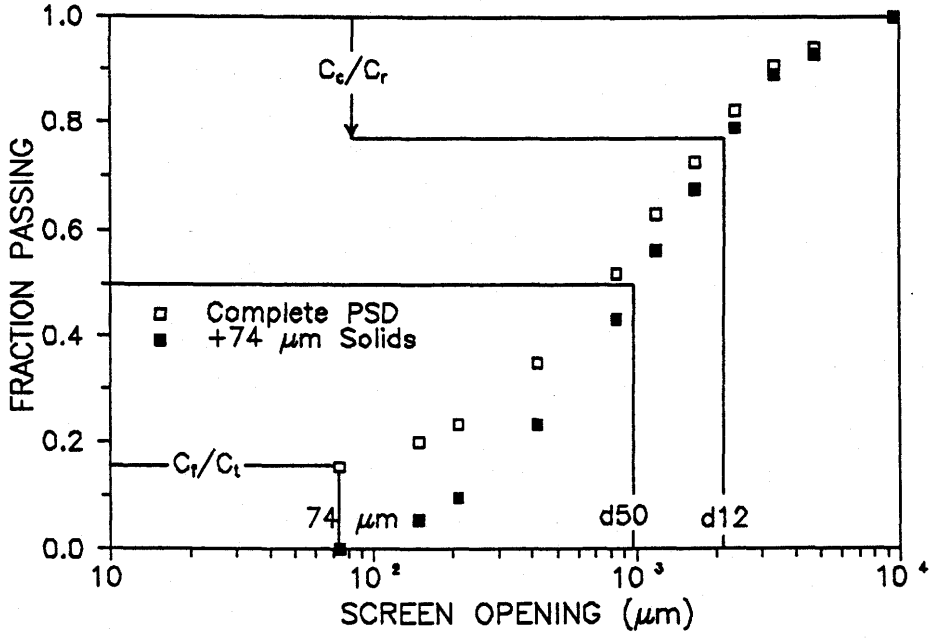

Figure 6.10: Particle size distribution illustrating definitions of C_f, d_{50} and d_{12}.

Figure 6.11 presents the inferred C_c / C_r values as a function of the ratio of the mean velocity to the terminal settling velocity of the mass median particle. Considering the range of experimental conditions shown in Table D.2, the agreement is encouraging. The correlation is

$$C_c/C_r = \exp(-0.0184\,V/V_\infty) \qquad (6.19)$$

and the standard error of estimate for C_c/C_r is 0.078.

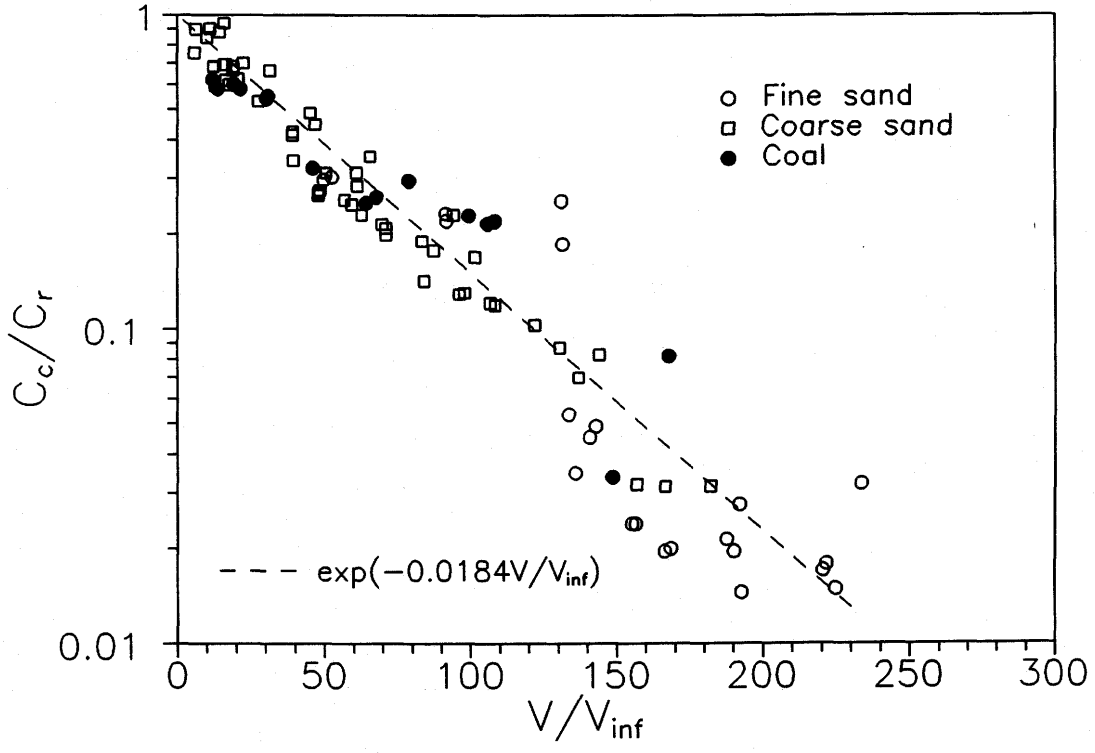

Figure 6.11: Effect of velocity ratio on the contact load fraction for pipeline flow of coarse-particle slurries.

The headloss model of Section 6.3.2 is superior to that of Section 6.3.1 in that most of the systematic deviation with mean velocity has been eliminated. A systematic deviation was observed for the fine sand data and this deviation increases substantially for $C_r > 0.35$. The assumption that μ_f can be used to estimate μ_1 appears to fail at relatively low concentrations for fine sand slurries. Experience in testing industrial slurries confirms these observations, suggesting that the model is least reliable for high concentrations of slowly settling particles flowing in small pipes.

The correlation of Equation 6.19 incorporates a very wide data base and its simplicity is encouraging. The model remains untested in some conditions which are of industrial importance. These include non-Newtonian carrier fluids and transport at high concentrations of coarse particles ($C_r > 0.35$). The selection of V and V_∞ as independent variables for the correlation reflects the fact that the magnitude of C_c / C_r is determined mainly by the relative magnitudes of turbulent mixing forces and gravitational forces. The mean velocity, V, is a good indication of the intensity of turbulence, and the terminal settling velocity provides a measure of the net gravitational effect acting on the particles.

6.3.3 Using the Improved Headloss Model

Before the model can be used, the pipeline designer will have to specify values for V, C_t, D, C_{max}, μ_L, ρ_s, ρ_L, and k. Also the particle size distribution, the viscosity-concentration relationship for the fines and the particle drag coefficients have to be known. The steps to be followed in calculating i and C_v are given below:

1. C_f and d are determined from C_t and the particle size distribution. ρ_f is calculated from Equation 6.2 and μ_f is determined experimentally.

2. V_∞ is calculated from ρ_s, ρ_f, μ_f, d and the particle drag coefficient using Equation 4.10.

3. From C_r, V, C_{max} and V_∞, C_{lim} and C_c / C_r values are calculated using Equations 6.17 and 6.19. Alternatively, the method suggested in Section 6.4 may be used to determine C_{lim}.

4. Equation 6.3 provides C_1 and this is used to calculate ρ_1 from Equation 6.6 and ρ_{2f} from Equation 6.7. C_2 is calculated from Equation 6.5.

5. The ratio A_2 / A is given by C_c / C_2 according to Equation 6.4. This allows β, the angle defining the lower layer to be determined.

6. Using the fact that $A_1 = A - A_2$, the two force balances and the total volumetric flow equation (Equations 3.12, 3.13 and 6.8) are solved iteratively to obtain i, V_1 and V_2. The stresses are calculated from Equations 6.11, 6.14 and 6.15 and the friction factors are given by Equations 6.12 and 6.18.

7. The delivered concentration C_v is calculated from Equation 6.9. If C_v is specified, iteration will be required. A value of C_t (greater than C_v) is first selected and steps 1 to 7 are performed until the assumed C_t value satisfies the C_v constraint.

The improved model was tested by using the method which will be outlined in Section 6.4 to estimate C_{lim}, Equation 6.18 for f_{12} and Equation 6.19 for C_c. Figures 6.12 and 6.13 show that the improved model provides good estimates of the delivered

concentration over the entire range of experimental conditions. The improved model also provides good estimates for the frictional headloss for most of the experimental conditions but somewhat underestimates the headloss for the flow of very coarse particle mixtures in the 53 mm pipeline. The standard error of estimate is 0.013 for C_v and 0.015 m water / m for i.

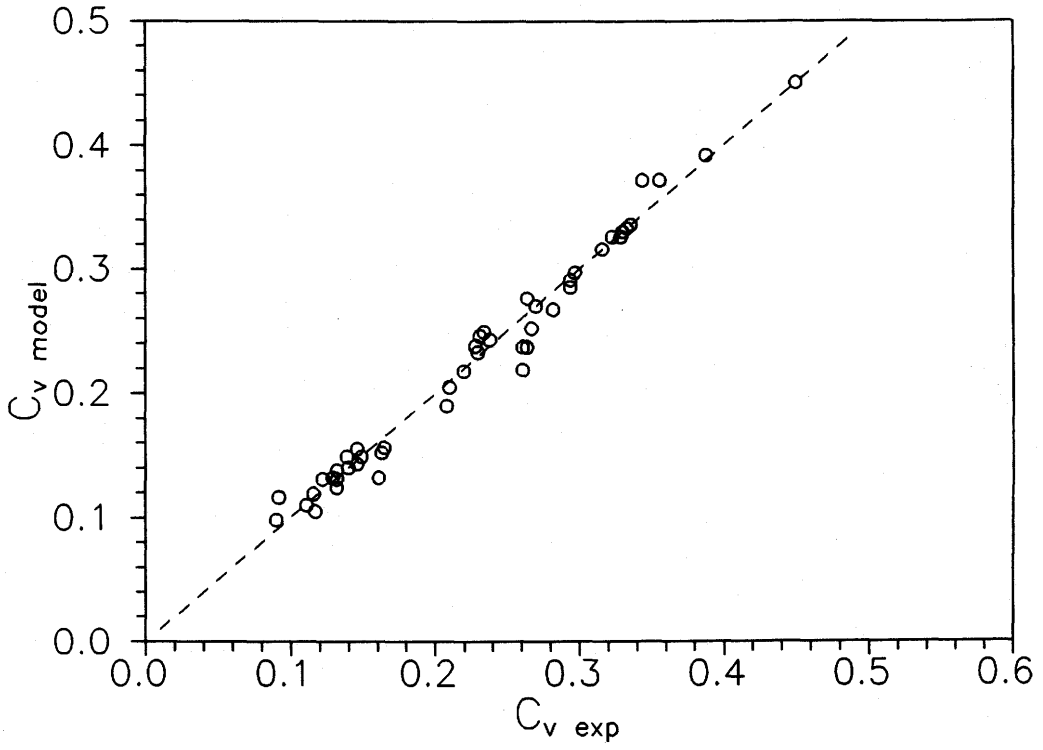

Figure 6.12: A comparison of experimentally determined delivered concentrations with estimates obtained using Equation 6.18 to determine f_{12}.

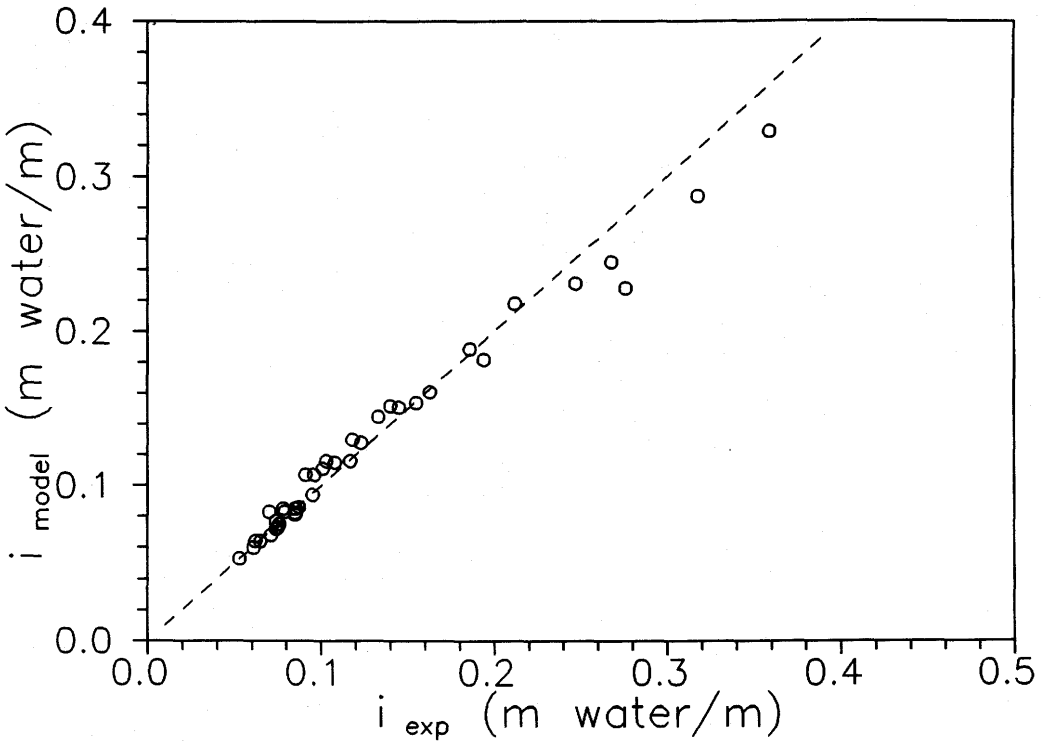

Figure 6.13: A comparison of experimentally determined frictional headlosses with estimates obtained using the improved two layer model.

6.4 Concentration Distributions

With a wide range of particle and pipe sizes, the experimental results of this study provide a good test for concentration distribution modelling techniques. A one dimensional modelling approach was used because the gamma ray density gauge provides measurements of the solids concentration as a function of elevation only, c = c(y). To minimize the effects of scatter in the data, the concentration distributions of Appendix A were fitted to fourth order polynomial equations of the form

$$c = a_0 + a_1(y/R) + a_2(y/R)^2 + a_3(y/R)^3 + a_4(y/R)^4 \qquad (6.20)$$

where c is the chord-average concentration.

The polynomial equations were differentiated to obtain smoothed values for the experimental concentration gradients dc / d(y/R).

$$\frac{dc}{d(y/R)} = a_1 + 2a_2(y/R) + 3a_3(y/R)^2 + 4a_4(y/R)^3 \qquad (6.21)$$

The vertical concentration distribution has to reflect a balance of the forces identified in the momentum conservation equations. Momentum is conserved in the y (upward) direction for the solids when

$$\rho_s \frac{Dv_{sy}}{Dt} = f_{sw} + f_{sL} + \rho_s g - \frac{\partial P}{\partial y} \qquad (6.22)$$

and for the liquid when

$$\rho_L \frac{Dv_{Ly}}{Dt} = f_{Ls} + \rho_L g - \frac{\partial P}{\partial y} \qquad (6.23)$$

Subtracting Equation 6.23 from 6.22 to eliminate the pressure term we obtain

$$\rho_s \frac{Dv_{sy}}{Dt} - \rho_f \frac{Dv_{Ly}}{Dt} - f_{sL} + f_{Ls} = (\rho_s - \rho_L)g + f_{sw} \qquad (6.24)$$

The left hand side of Equation 6.24 represents the forces experienced by particles due to turbulence while the two terms on the right hand side of the equation represent the gravitational and wall interaction effects. The latter effect is transmitted from the wall to the bulk of the flow through particle-particle interactions.

Following Shook and Roco (1990), the steady state force per unit volume of particles due to turbulence is assumed to be

$$F_t = -\frac{3\rho_f C_D (\epsilon_s/R)^2}{4dc^2(1-c)^{2m}} \left(\frac{dc}{dy_0}\right) \left|\frac{dc}{dy_0}\right| \qquad (6.25)$$

Here y_0 = -y/R so y_0 is zero at the centre of the pipe and is positive in the downward direction. Therefore, dc/dy_0 is positive for the usual situation where the concentration increases toward the bottom of the pipe. The turbulent mixing effects act in the negative y_0 direction, moving particles from the region of high concentration near the bottom of the pipe to the region of lower concentration in the upper portion of the pipe.

The correlating coefficient on the term (1 - c) has been increased from m-1 to m to reflect more precisely the concentration dependence of the dc/dy observed in the experiments here and those of Daniel (1965).

The friction velocity, $u_* = (\tau_w / \rho)^{0.5}$, is commonly used to provide an indication of the intensity of turbulence for liquid flows and τ_w = D i ρ g / 4. For coarse-particle mixtures, the mean wall shear stress, τ_w, is composed of a fluid friction term and a contact load component. Since we are attempting to quantify turbulent mixing effects, it was decided that a homogeneous fluid wall stress, τ_{wf}, should be used rather than τ_w to determine values of u_* for use in attempting to model the concentration gradient. τ_{wf} is computed using the method described in Section 6.2.

In Equation 3.25, Roco and Shook divide the particle interaction effects into a strain rate dependent interparticle stress arising as a result of collisions between particles moving in layers at different velocities and a strain rate independent stress resulting from the transmission of the contact load fraction to the pipe wall. Unfortunately, it was not possible to obtain concentration distribution data over a wide range of velocities

in this study. As a result, it is difficult to separate the strain rate independent effects from the rate dependent effects. In terms of the two-layer model, the combined contribution of the two effects would be included in the C_c / C_r correlation (Equation 6.19).

Shook and Roco (1990) suggest that particle interaction effects could be regarded as a reduction in the settling tendency of the particles:

$$F_p = -\kappa g(\rho_s - \rho_f) \tag{6.26}$$

The parameter κ will approach zero for flows where particle interaction effects are negligible and unity for flows where the particle interactions are so large as to result in a uniform bed of solids.

Neglecting the residual effects which result in a reduced particle concentration near the wall, the force balance is

$$\frac{3\rho_f C_D(\epsilon_s/R)^2}{4dc^2(1-c)^{2m}}\left(\frac{dc}{dy_0}\right)\left|\frac{dc}{dy_0}\right| = g(\rho_s-\rho_f) - \kappa g(\rho_s-\rho_f) \tag{6.27}$$

By combining Equations 4.10 and 6.27 and by assuming that, for horizontal pipe flows, dc/dy_0 will always be a non-negative quantity in the central region of the pipe, the force balance can be simplified as follows:

$$\frac{dc}{dy_0} = \frac{(1-\kappa)^{0.5} V_\infty c(1-c)^m}{\epsilon_s/R} \tag{6.28}$$

To model the experimentally determined concentration distributions, we start by limiting the examination to flow of fine sand slurries for which particle interactions should be small. For this reason, all data points where the contact load fraction C_c / C_r

> 0.2 were excluded. The examination was further limited to the central region of the pipe ($-0.75 < y_0 < 0.75$) where wall repulsion effects are likely to be small. For these fine sand slurry flows, the turbulent mixing effects and gravitational effects are the major contributors to the force balance for the particles.

Roco and Frasineanu (1977) suggested the following correlation for the eddy kinematic viscosity for fully turbulent pipe flow for a Newtonian liquid:

$$\nu_t = 0.146 u_* R[1-(r/R)^2][(r/R)^2 + 0.54] \qquad (6.29)$$

so, in the central core, ν_t is approximately 0.08 u_* R. Figure 6.14 shows that for fine sand slurry flows in the 50 mm pipe, ϵ_s varies approximately as ν_t for liquid flows. An analogy is often drawn among the processes of turbulent transport of momentum, energy and mass. This result would appear to extend the analogy to the turbulent transport of fine solid particles as well.

Figure 6.15 shows that the situation is not so simple for the fine sand slurries in larger pipes, however. Here, the mixtures are not so well dispersed as in the smaller pipe. This is particularly evident when the concentration gradient is relatively high. It would appear that the dispersive effects of turbulence are reduced for flows in large pipes. The Richardson number is known to provide an indication of the tendency for turbulence suppression in the presence of a density gradient. The Richardson number is

$$Ri = -\frac{g(d\rho/dy)}{\rho(dv/dy)^2} \qquad (6.30)$$

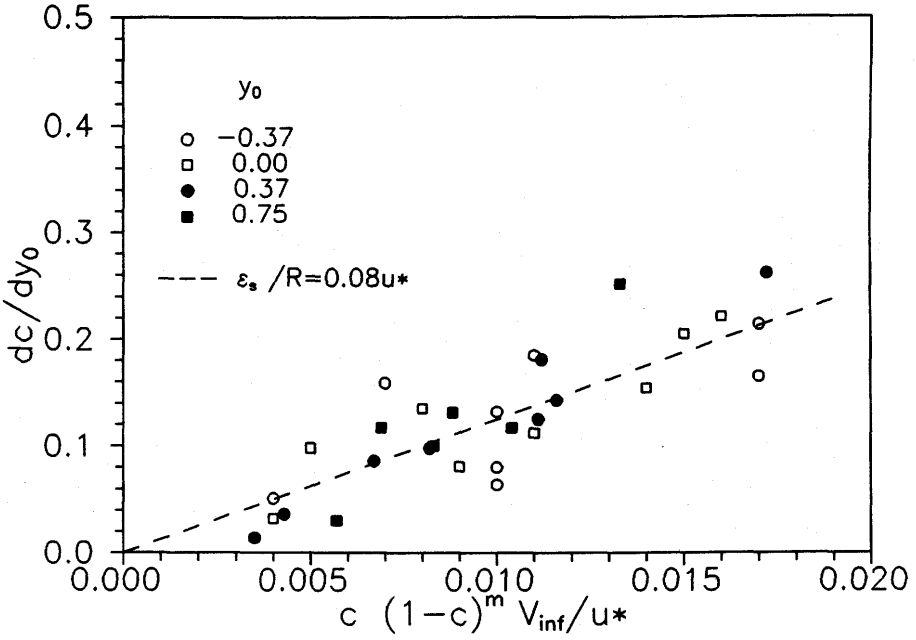

Figure 6.14: Concentration distribution correlation for fine sand slurries ($C_c/C_r < 0.2$) in a 53.2 mm pipe.

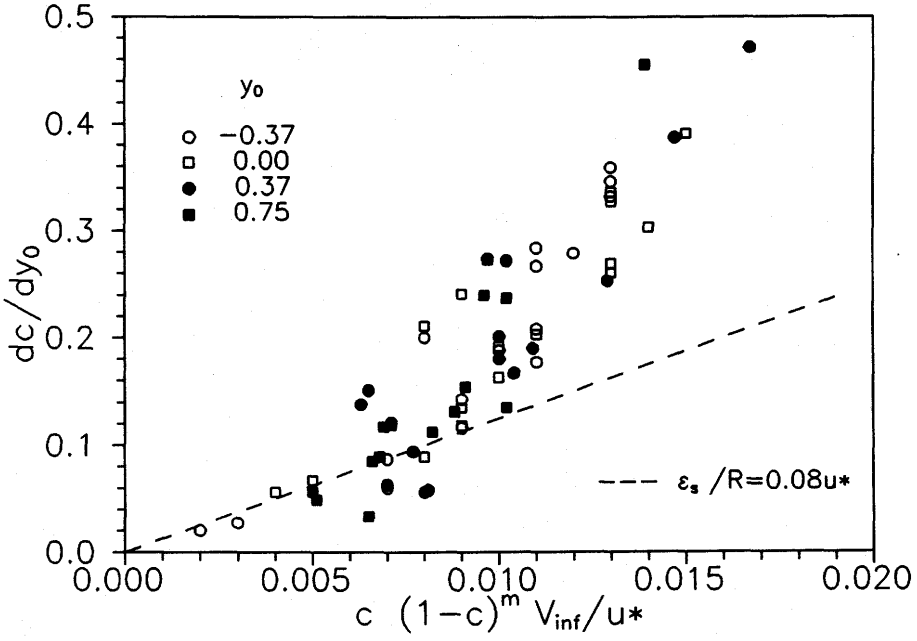

Figure 6.15: Concentration distribution correlation for fine sand slurries ($C_c/Cr < 0.2$) flowing in large pipes ($D \geq 150$ mm).

Schlichting (1978) showed that single phase flows with Ri > 0.042 are nonturbulent.

For pipe flows we see a problem in that local values of the Richardson number become very large in the region of the pipe where time-average values of dv/dy are small. If one assumes that the tendency for turbulence suppression depends on some average value of dv/dy in the whole pipe, then we can use the fact that dv/dy scales approximately with V/D to study the effect. Since the mixture density ρ is c (ρ_s - ρ_f) + ρ_f and y_0 = - y/R, the density gradient can be written in terms of the concentration gradient as follows:

$$\frac{1}{\rho}\frac{d\rho}{dy} = -\frac{2}{D}\frac{\rho_s-\rho_f}{\rho}\frac{dc}{dy_0} \qquad (6.31)$$

The Richardson number is approximately

$$Ri \sim B\frac{g D(\rho_s-\rho_f)}{\rho V^2}\frac{dc}{dy_0} \qquad (6.32)$$

where B is a constant.

For conditions where Equation 6.28 is applicable and κ is likely to be small, the experimentally determined concentration distributions can be used to obtain estimates of ϵ_s / R u_*. Figure 6.16 shows that there is a relationship between the Richardson number dependent parameter and the effectiveness of turbulence for dispersing the particles. At high values of the Richardson number dependent parameter, ϵ_s / R u_* is considerably less than 0.08. At low values of the parameter, there is a large spread in the values of ϵ_s / R u_* and the Richardson number parameter does not help to identify

those situations where turbulence suppression occurs. For some of the large pipe data, there appears to be a turbulence suppression effect over the entire range of the Richardson number dependent parameter while in the 50 mm pipe, the suppression effect rarely occurs.

In the absence of a convincing general correlation, a piece-wise approach is suggested for estimating ϵ_s values for the fine sand slurries.

$$\frac{\epsilon_s}{R} = u_* \left(b_1 + \frac{b_2}{dc/dy_0} \right) \tag{6.33}$$

The values of the parameters b_1 and b_2 will be either ($b_1 = 0.08$, $b_2 = 0$) or ($b_1 = 0.027$, $b_2 = 0.005$). The first set of coefficients should be used for sand slurry flows in small pipes. For large pipe flows, the set of coefficients which gives the highest value of dc/dy_0 should be used.

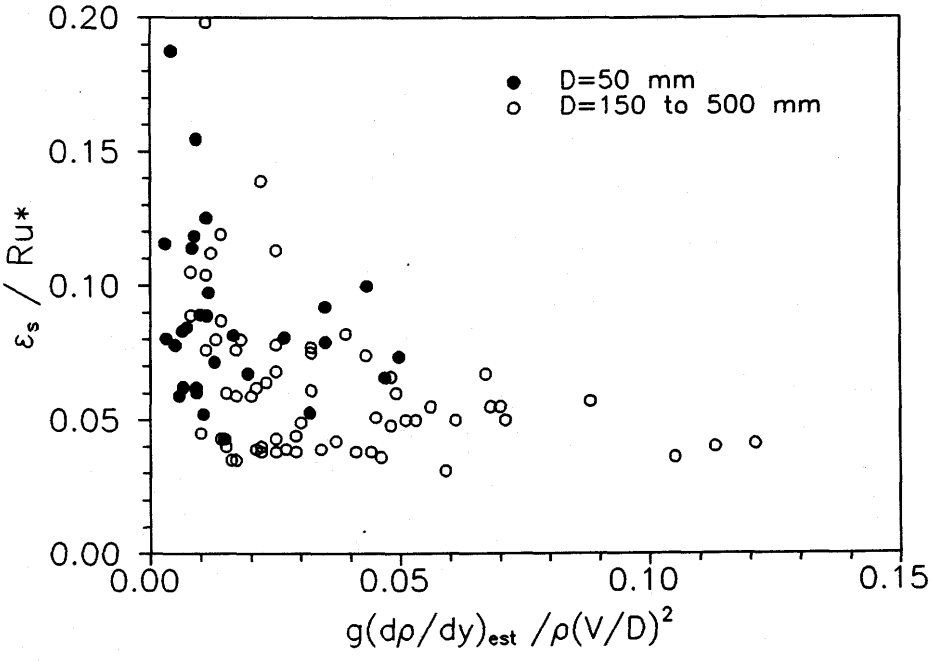

Figure 6.16: Particle diffusion coefficient versus Richardson number dependent parameter for pipeline flow of fine sand slurries ($C_c/C_r < 0.2$).

For coarser sand slurries, one might expect to find a correlation between the C_c/ C_r values used in the two-layer model and κ. Experimental values of κ can be obtained using Equation 6.27 as follows:

$$\kappa = 1 - \frac{(dc/dy_0)^2}{(dc/dy_0)_0^2} \tag{6.34}$$

where $(dc/dy_0)_0$ is the concentration gradient for $\kappa = 0$ and may be estimated using Equations 6.28 and 6.33. In Figure 6.17, experimental κ values are plotted against C_c / C_r values obtained from Equation 6.19. There is evidence of a correlation but the spread is disappointingly large. The concentration distribution is a reflection of the force balance in the central core while the contact load is affected by the conditions at the pipe wall as well. As the particle diameter increases, the contact load (which is inferred from headloss measurements) increases by an amount which is determined by the net effect of changes in the normal forces within the flow and the changes in wall repulsive forces.

Figure 6.18 shows that when the particles are coarse (C_c / C_r > 0.2), the concentration gradient does not depend strongly on the contact load fraction. Over the velocity range of the tests, dc/dy_0 reaches a limiting value such that any further increase in the settling tendency is offset by an increase in the particle dispersion tendency. The limiting value of dc/dy_0 depends on the concentration:

$$\left(\frac{dc}{dy_0}\right)_{max} = b_3 c(1-c)^m \tag{6.35}$$

The parameter b_3 has an average value of 5.8 for sand slurry flows.

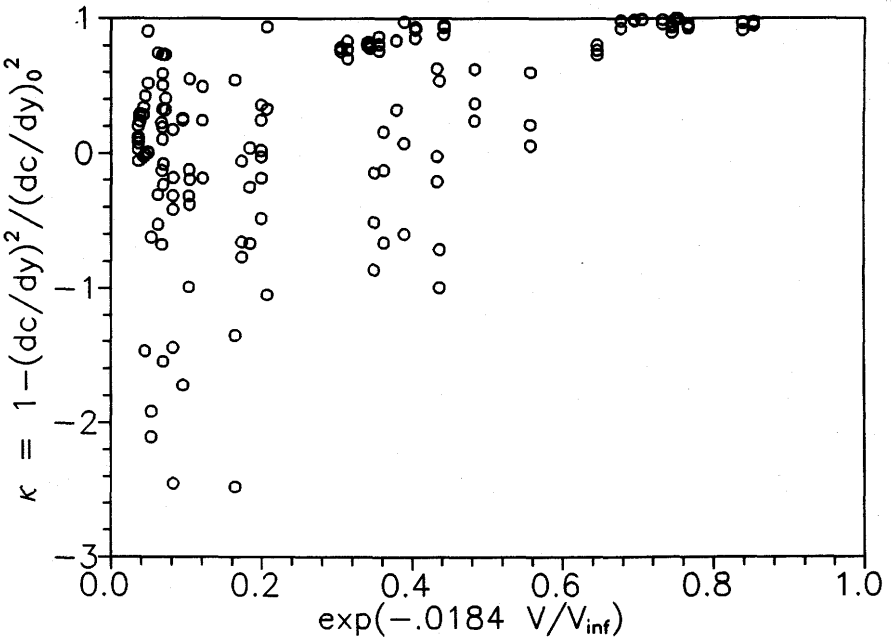

Figure 6.17: Particle interaction support fraction (κ) and estimated overall contact load fraction (Equation 6.19) for pipeline flow of sand slurries.

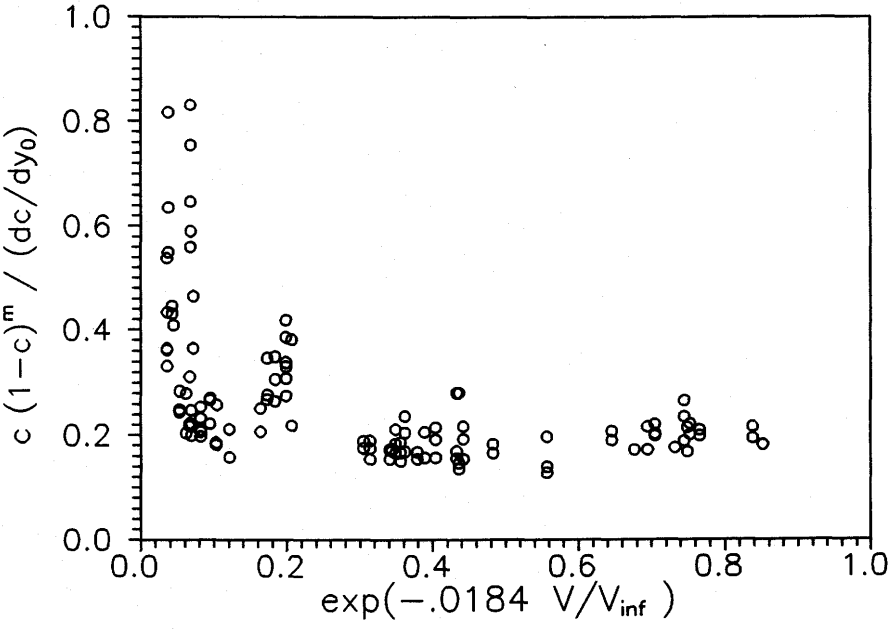

Figure 6.18: Concentration distribution versus estimated overall contact load fraction (Equation 6.19) for pipeline flow of coarse sand slurries.

With wall repulsive effects neglected, the concentration distribution for sand slurries can be estimated by using Equations 6.28, 6.33 and 6.35. A fourth order Runge-Kutta method is used to determine $c = c(y_0)$ from estimated values of dc/dy_0. The following steps are involved:

1. The actual mean *in situ* concentration C_t may be used as an initial estimate for $c(y_0=0)$.
2. Using Equation 6.28 (with ϵ_s/R from Equation 6.33) and Equation 6.35 to obtain estimates of dc/dy_0, the lesser of the two values is selected and used with the Runge-Kutta method to obtain $c = c(y_0)$ for $0 < y_0 < 1$ and for $-1 < y_0 < 0$.
3. The $c = c(y_0)$ values are integrated over the pipe cross section to obtain a value for C_t. This value is compared with the actual mean concentration.
4. Iteration will be required to obtain the correct mean concentration. A new value for $c(y_0=0)$ is selected and steps 2 through 4 are repeated until the integration provides a value of C_t which matches the actual value.

The dashed lines in the plots of Appendix B illustrate the effectiveness of the concentration distribution model. The model reproduces the experimental concentration distributions very well except when wall repulsive forces are significant. The concentration distribution plots show that the wall effect has a significant impact on the concentration at the bottom of the pipe for flows of coarse particles at high velocities. For a particular particle size, the effect is strongest in the small 50 mm pipe.

Even with the wall repulsive effects neglected, Figure 6.19 shows that the model provides good estimates of the concentration in the bottom portion of the pipe. Here,

experimental and predicted values of c are compared at y/D = 0.15 (y_0 = 0.7). The correlation is encouraging and it is recommended that the predicted value of c at y_0 = 0.7 be used to estimate C_{lim} values for the improved headloss model. Further refinement could be made to the estimate for C_{lim} by including a term to account for the wall-repulsive effect. However, the improvement would be small and, with the data available now, only a tentative correlation could be proposed.

Further experiments are required, with greater variation in ρ_s/ρ_f and V in intermediate sized pipes (50 mm $\leq$ D $\leq$ 150 mm), to establish a broadly applicable correlation for ϵ_s. To study the wall repulsive effect systematically, experiments of the type reported by Shook (1985), using neutrally buoyant mixtures, are required in larger pipes.

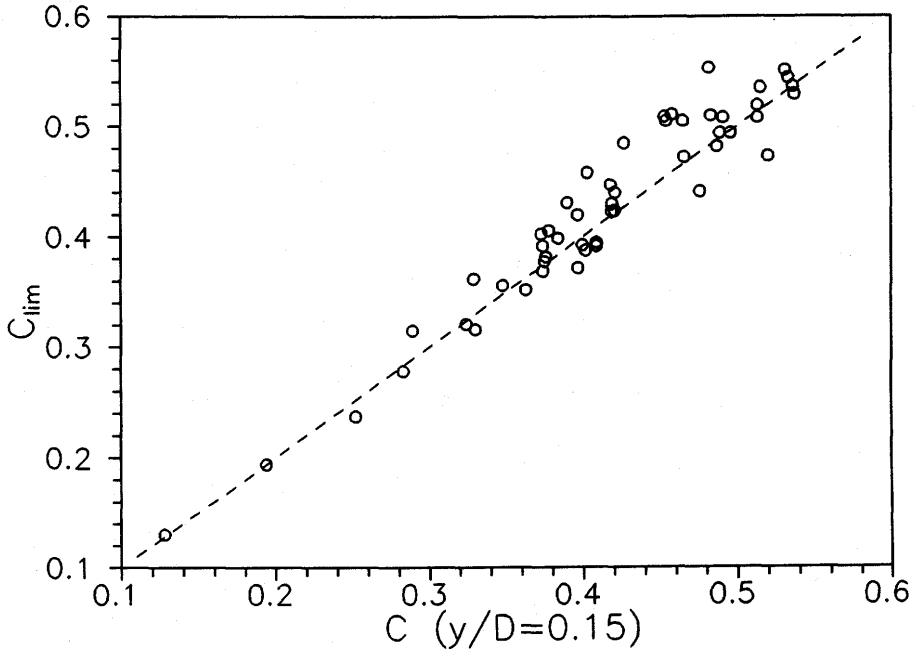

Figure 6.19: C_{lim} values computed using the concentration distribution model versus concentrations measured by gamma ray absorption at y/D = 0.15 for sand and gravel slurries.

6.5 Deposition Velocities

The tests of Tables 5.1 and 5.2 provide a deposition velocity database for a wide range of pipe and particle diameters. The deposition velocities were determined visually by inspecting the flows through glass or plexiglass pipe sections. In each case, the flows were isothermal and the coarse solids *in situ* concentration (C_r), particle density (ρ_s) and mass median particle diameter (d_{50}) were measured. The carrier fluid density (ρ_f) and viscosity (μ_f) were measured if the water contained a significant amount of fines.

The data of Tables 5.1 and 5.2 and a few industrial slurry test results obtained at the Saskatchewan Research Council were used to examine deposition. A force balance analysis of the deposition phenomenon was adopted in an attempt to obtain a correlation for deposition velocities. The effort is described in the remainder of this section.

The layer force balance model described in Section 6.3.2 has been shown to be useful for estimating wall shear stresses for coarse-particle slurry pipeline flows. The deposition condition occurs when the stresses near the wall of the pipe are not large enough to sustain particle motion so the layer model should be useful for interpreting the solids deposition phenomenon.

Figure 6.20 shows an idealization of the flow of a settling slurry before a deposit is present. There are two constant composition regions and the upper layer contains only particles whose immersed weight is borne by fluid lift forces. The density of this mixture determines the gradient of hydrostatic pressure.

The total concentration in the lower layer, C_{lim}, is known to be a function of the mean in-situ concentration C_r and the ratio of the mean flow velocity V to the terminal velocity V_∞ of the mass median particle (Equation 6.19). V_∞ is computed for settling in a hypothetical mixture consisting of the carrier liquid and the finest (-0.074 mm) particles. The difference (C_{lim} - C_1) represents particles which are not supported by fluid lift forces. These particles experience a buoyant force which depends on the density of the mixture of fluid and turbulently suspended particles. The particles which are not suspended generate an interparticle stress which increases with depth according to the relationship

$$\frac{d\sigma_n}{dy} = (\rho_s - \rho_2)\, g\, (C_{lim} - C_1) \qquad (6.36)$$

where ρ_2 is the density of the mixture of fluid and suspended solids in the lower layer. The interparticle stress σ_n is zero at the interface between layers 1 and 2.

Stress σ_n contributes a velocity independent frictional resistance to flow, which increases as β_2 increases. From pressure drop measurements we know that β_2 depends upon the factors which determine C_{lim}. If we now consider flow with a deposit (Figure 6.21), Equation 6.36 applies within the middle layer. Within the stationary deposit, the buoyant force is produced only by the fluid. In terms of the concentration C_{bed} in the deposit, the stress gradient in this region is:

$$\frac{d\sigma_n}{dy} = (\rho_s - \rho_L)\, g\, C_{bed} \qquad (6.37)$$

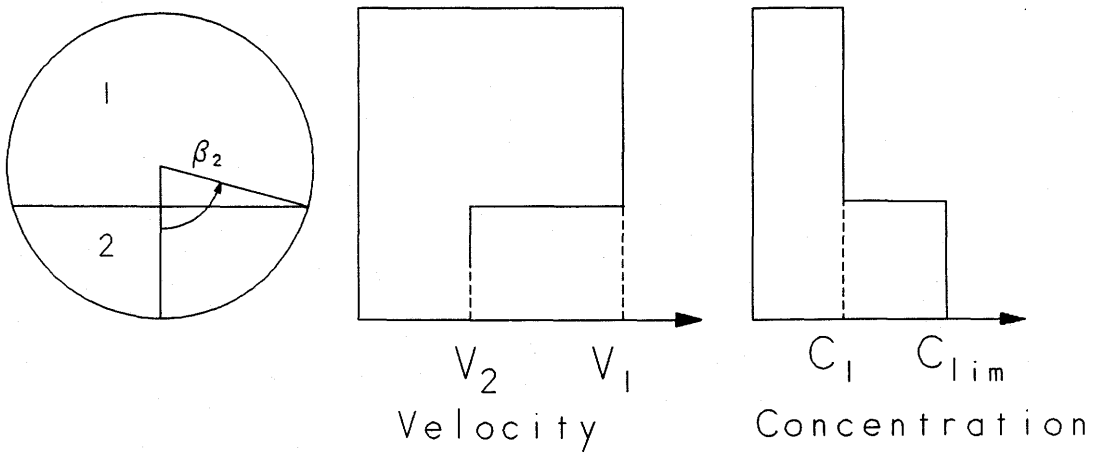

Figure 6.20: Idealized velocity and concentration distributions in a slurry before deposition.

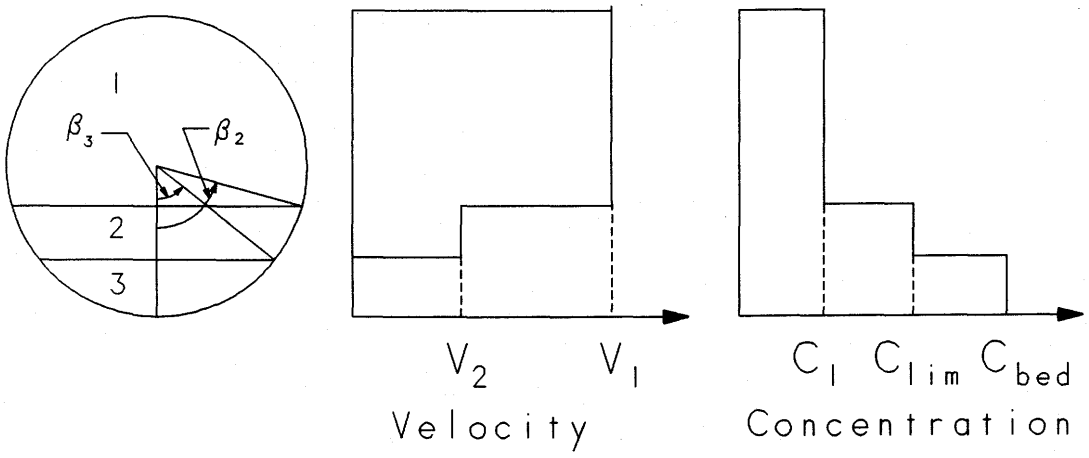

Figure 6.21: Idealized velocity and concentration distributions in a slurry after a stationary deposit forms.

The stress gradient in the stationary layer is usually much greater than that in the flowing mixture above it. Deposition can therefore be considered to reflect the inability of a flowing mixture to support all the available solid particles in the pipe cross-section.

At the interface between moving solids (layer 2) and stationary solids (layer 3) the normal stress obtained from integrating Equation 6.36 is in equilibrium with the shear stress derived from the flow τ_{23}. The coefficient of proportionality between the stresses is tan α, where α is the angle of internal friction of the solid particles.

$$\tau_{23} = 0.5\,(\rho_s - \rho_2)\,g\,D\,(\cos\beta_3 - \cos\beta_2)\,(C_{lim} - C_1)\tan\alpha \qquad (6.38)$$

where β_2 and β_3 define the boundaries of layer 2 (Figure 6.21). If the stress τ_{23} is expressed in terms of a friction factor f_{23} for the flow as a whole then

$$\tau_{23} = f_{23} V^2 \rho_m / 2 \qquad (6.39)$$

We have an expression for V_c in the limiting case where the deposit is infinitesimal and V becomes V_c:

$$V_c^2 = \frac{(\rho_s - \rho_2)\,(1 - \cos\beta_2)\,(C_{lim} - C_1)\,g\,D\tan\alpha}{f_{23}\,\rho_m} \qquad (6.40)$$

Equation 6.40 shows that to a first approximation V_c varies as $(g\ D)^{0.5}$. However, C_{lim}, β_2 and the ratio C_1/C_r depend upon the ratio V / V_∞ so that the relationship between V_c and D is rather complex. The interfacial friction factor f_{23} is unknown but presumably varies with the ratio of particle diameter to pipe diameter, and possibly the pipe flow Reynolds number.

Although it has a mechanistic origin, Equation 6.40 is based upon several simplifying assumptions and contains a number of unknown parameters. In the absence

of information concerning tan α and f_{23}, a correlation is proposed as an alternative for pipeline design. The dimensionless deposit velocity F_L has been used by many workers since Durand (1953).

$$F_L = \frac{V_c}{[g D (S_s - 1)]^{0.5}} \tag{6.41}$$

F_L depends upon the drag coefficient of the particles settling in an equivalent fluid of density ρ_f and viscosity μ_f. Experimental drag coefficients can be determined by measuring single particle terminal falling velocities using the procedure described in Section 4.3.3.

The correlation for F_L is:

$$F_L = \exp\left[0.51 - 0.0073 C_D - 12.5 (K_1 - 0.14)^2\right] \tag{6.42}$$

where the factor K_1 contains the viscosity and density of the carrier liquid.

$$K_1 = \frac{(\mu_L / \rho_L)^{2/3}}{g^{1/3} d_{50}}$$

The correlation predicts that the deposition velocity reaches a maximum at some particle size and then decreases for coarse particles. This maximum in the V_c - d_{50} relationship is consistent with Wilson's (1979) nomogram. The coarse particles tend to roll along the bottom of the pipe at mean velocities which are less than the deposition velocity of somewhat smaller particles.

Figure 6.22 compares the values of V_c predicted by the correlation with those observed experimentally when testing water slurries. Equation 6.42 predicts the deposition velocities with a correlation coefficient, $R^2 = 0.96$, for the broad range of

experimental values (1.1 m/s $\leq V_c \leq$ 4.5 m/s). With only a few exceptions, the predicted values are well within the $\pm$ 20% error band. The correlation should not be used outside the range of experimental conditions defined in Table 6.1.

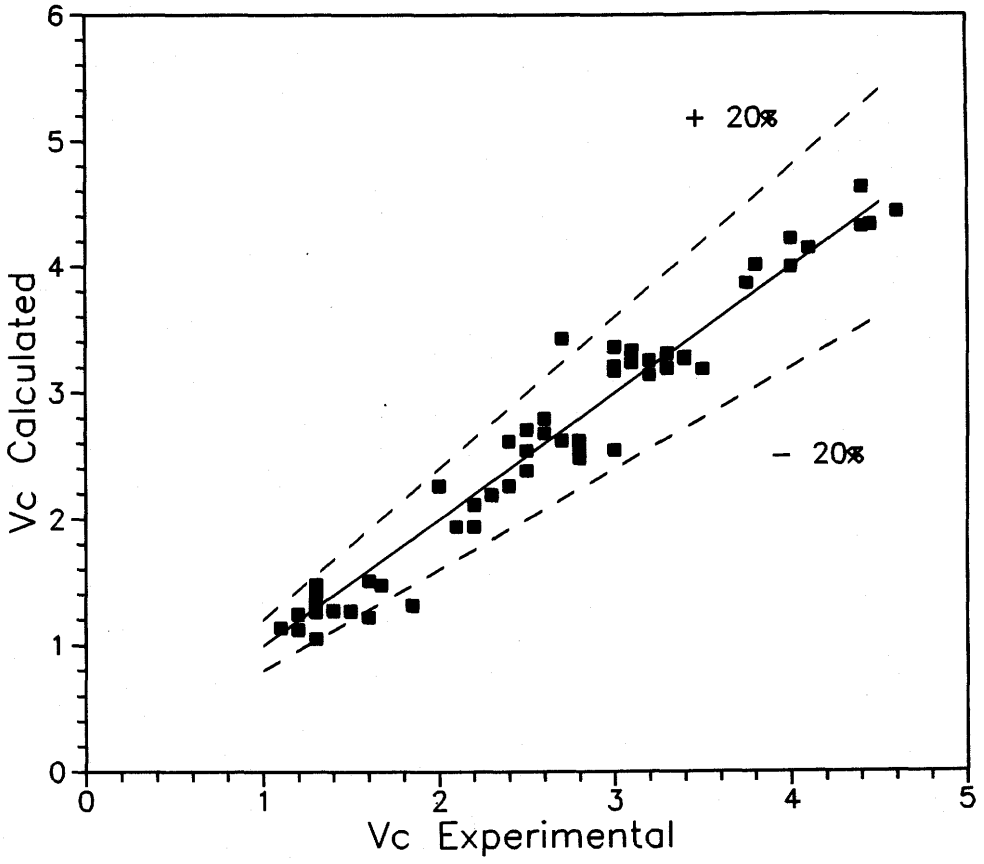

Figure 6.22: Comparison of measured deposition velocities with those predicted by the correlation of Equation 6.42.

Table 6.1: Parameter Range for Coarse-Particle Slurry Pipeline Deposition Velocity Correlation

Parameter	Minimum Value	Maximum Value
Pipe Diameter, D (mm)	53	495
Particle Diameter, d (mm)	0.15	4.0
Carrier Fluid Viscosity, μ_f (mPa.s)	0.5	3.4
Solids Concentration, C_t	0.14	0.44
Solids Density, ρ_s (kg/m^3)	1374	2650

7 CONCLUSIONS AND RECOMMENDATIONS

1. This study has added significantly to the database for coarse-particle slurry flows by providing headloss versus flowrate data, concentration distributions, and velocity distributions for a wide range of pipe sizes, particle sizes, and solids concentrations and over a limited range of particle to carrier fluid density ratios and carrier fluid viscosities.

2. For the flow of mixtures containing solids with broad size distributions, the analysis may be simplified by dividing the solids arbitrarily into a coarse particle fraction and a fines fraction. The fines are considered to contribute to the volume fraction, density and viscosity of the carrier fluid. Dividing the solids at d=0.074 mm is a practical approach. These solids are easily separable by sieving and the settling velocity of -0.074 mm fine particles is usually low enough to allow testing of the (carrier liquid + fines) mixture in a laboratory viscometer.

3. For coarse-particle slurry flows in horizontal pipelines, particle-wall friction is the dominant mechanism determining the headloss. In determining the magnitude of the particle-wall friction component, the ratio of the pipeline mean velocity to the particle settling velocity (V/ V_{∞}) is the parameter of greatest importance.

4. A modified two-layer model, which uses a variable lower layer concentration, provides a relatively simple and effective means for estimating coarse-particle

slurry frictional headlosses. The range of validity of the model is determined by the data base it incorporates. The performance of the model has been verified for the following conditions:

a. $C_r \leq 0.35$

b. Essentially Newtonian carrier fluids with $\mu_f < 4$ mPa.s.

5. The factors which determine the concentration distributions for coarse-particle slurries are more complex than indicated by previous studies.

a. For situations where the dominant forces are due to turbulent mixing and gravity, there is strong evidence of a reduction in the effectiveness of turbulence in large pipes but there is no evidence of any reduction in the dispersive tendency for flows in small pipes. A transition must occur in pipes of intermediate size (50 mm $\leq$ D $\leq$ 150 mm).

b. Over the velocity range of considerable industrial importance, where $V_c < V < 2\ V_c$, the concentration gradient approaches a maximum value which depends on the local concentration but does not depend on the mean velocity nor on the settling velocity of the particles.

c. Additional experiments are required with fine sand slurries in intermediate sized pipes to investigate the particle diffusion phenomenon in greater detail. Also, the range of S_s should be extended to 1.0 (neutral buoyancy) to study wall repulsive forces in the absence of gravitational effects.

6. When the carrier fluid is essentially Newtonian and $\mu_f < 4$ mPa.s, satisfactory estimates of the coarse particle slurry solids deposition velocity can be obtained by using a correlation which incorporates the solids to carrier fluid density ratio (S_s), the particle drag coefficient (C_D), the pipe diameter (D), the particle mass median diameter (d_{50}), and the kinematic viscosity of the carrier (μ_L / ρ_L).

7. For many coarse-particle slurries of industrial importance, the carrier fluid viscosity is outside the range studied here. Experiments are required with higher viscosity Newtonian carrier fluids and non-Newtonian fluids to determine how particle-wall friction and solids deposition velocities are affected.

REFERENCES

Bagnold, R.A. 1954. "Experiments on a gravity-free dispersion of large solid spheres in a Newtonian fluid under shear." Proc. Roy. Soc., Ser. A. **225**: 40-63.

Bagnold, R.A. 1956. "The flow of cohesionless grains in fluids." Philosophical Transactions, Royal Society, London. **249**.

Bird, R.B., Stewart, W.E., and Lightfoot, E.N. 1960. Transport Phenomena, Wiley, New York.

Brown, N.P., Shook, C.A., Peters, J., and Eyre, D. 1983. "A probe for point velocities in slurry flows." Can. J. Chem. Eng. **61:** 597-602.

Carleton, A.J. and Cheng, D.C. 1974. "Design velocities for hydraulic conveying of settling suspensions." Proc. Hydrotransport Conf., BHRA, Cranfield, UK, Paper E5, pp. 57-74.

Charles, M.E. 1970. "Transport of solids by pipelines." Proc. Hydrotransport 1 Conf., BHRA, Cranfield, UK, Paper A3, pp. 25-36.

Churchill, S.W. 1977. "Friction factor spans all fluid regimes." Chem. Eng. **84**(24): 91-92.

Daniel, S.M. 1965. "Flow of suspensions in a rectangular channel." Ph.D. Thesis. University of Saskatchewan.

Dodge, D.W. and Metzner, A.B. 1959. "Turbulent flow of non-Newtonian systems." AIChE J. **5:** 189-204.

Durand, R. 1953. "Basic relationships of the transportation of solids in pipes experimental research." Proc. Minn. Int. Hyd. Conv., Univ. of Minnesota, pp. 89-103.

Durand, R. and Condolios, E. 1952. "Experimental study of the hydraulic transport of coal and solids materials in pipes." Proc. Colloq. on the Hydraulic Transport of Coal, National Coal Board (UK), Paper IV, pp. 39-55.

Faddick, R.R. 1982. Lecture Notes for Short Course. Proc. Hydrotransport 8 Conf., BHRA, Cranfield, UK.

Gillies, R.G., Husband, W.H.W. and Small, M. 1985. "A study of flow conditions arising in horizontal coarse slurry short distance pipelining practice. Phase 1: Sand-slurry tests in a 250 mm pipeline." Saskatchewan Research Council, Saskatoon, Canada. SRC Publication R-833-2-C-85.

Gillies, R.G. and Shook, C.A. 1992. "Emulsions for short distance transportation of heavy crude oil: pipeloop test results." J. Can. Pet. Tech. **31**(9): 41-47.

Hanes, D.M. and Inman, D.L. 1985. "Observations of rapidly flowing granular-fluid materials." J. Fluid Mech. **150:** 357-380.

Hsu, F.-L., Turian, R. and Ma, T.-W. 1989. "Flow of noncolloidal slurries in pipelines." AIChE J. **35**(3): 429-442.

Laufer, J. 1954. National Advisory Committee on Aeronautics. Report 1174.

Longwell, P.A. 1966. Mechanics of Fluid Flow. McGraw-Hill, New York.

Maxwell, J.C. 1892. A Treatise on Electricity and Magnetism. 3rd ed. Clarendon Press, Oxford.

Metzner, A.B. and Reed, J.C. 1955. "Flow of non-Newtonian fluids - correlation of the laminar, transition and turbulent flow regions." AIChE. J. **1:** 434-440.

Nasr-El-Din, H., Shook, C.A. and Colwell, J. 1987. "A conductivity probe for local concentration measurement in slurry flows." Int. J. Multiphase Flow **13:** 365-378.

Newitt, D.M., Richardson, J.F., Abbott, M. and Turtle, R.B. 1955. "Hydraulic conveying of solids in horizontal pipes." Trans. Inst. Chem. Engrs. **33**(2): 93-113.

Rasteiro, M.G., Rebola, M.M. and Scarlett, B. 1988. "Simulation of solid/liquid transport in pipes." Proc. Hydrotransport 10 Conf., BHRA, Cranfield, UK, Paper B1, pp. 49-61.

Richardson, J.F. and Zaki, W.N. 1954. "Sedimentation and fluidization." Trans. Inst. Chem. Engrs. **32:** 35-52.

Roco, M.C. and Balakrishnam, N. 1983. "Multi-dimensional flow analysis of solid-liquid mixtures." J. Rheology **29**(4): 431-456.

Roco, M.C. and Frasineanu, G. 1977. "Computational method for two-phase liquid-solid flow in pipes and channels.". St. Cerc. Mec. Appl. **36:** 311-324.

Roco, M.C. and Mahadevan, S. 1986. "Scale-up technique of slurry pipelines. Part I: Turbulence Modeling. Part II: Numerical Simulation." J. Energy Resources Technol. **108:** 269-283.

Roco, M.C. and Shook, C.A. 1983. "Modeling of slurry flow: the effect particle size." Can. J. Chem. Eng. **61:** 494-503.

Rouse, H. 1937. "Modern conceptions of the mechanics of fluid turbulence." Tran. ASCE **102:** 463-505.

Saffman, P.G. 1965. "The lift on a small sphere in shear flow." J. Fluid Mech. **22:** 385-400.

Schlichting, H. 1978. Boundary Layer Theory. 7th ed. McGraw-Hill, New York. p. 513.

Schmidt, W. 1925. "Der Massenaustausch in Freien Luft und Verwandte Erscheinungen." Probleme der Kosmischen Physik 7.

Shook, C.A. 1985. "Experiments with concentrated suspensions of particles with densities slightly greater than the carrier fluid." Can. J. Chem Eng. **63:** 861-869.

Shook, C.A., Gillies, R.G., Haas, D.B., Husband, W.H.W. and Small, M. 1982. "Flow of coarse and fine sand slurries in pipelines." J. Pipelines **3:** 13-21.

Shook, C.A., Gillies, R.G., Small, M. and Husband, W.H.W. 1982a. "Sliding coefficient of friction experimental measurements." Saskatchewan Research Council, Saskatoon, Canada. SRC Publication E-725-9-C-82.

Shook, C.A. and Roco, M.C. 1990. Slurry Flow Principles and Practice. Butterworth-Heinemann, Boston.

Sumner, R.J., McKibben, M.J. and Shook, C.A. 1989. "Concentration measurements in pipelines containing flowing two-phase mixtures." Southern Saskatchewan (Canada) Technical Meeting, CIM Petroleum Society.

Televantos, Y., Shook, C. Carleton, A. and Streat, M. 1979. "Flow of slurries of coarse particles at high solids concentrations". Can. J. Chem. Eng. **57:** 255-262.

Thomas, D.G. 1965. "Transport characteristics of suspensions: VIII. A note on the viscosity of Newtonian suspensions of uniform spherical particles." J. Colloid Sci. **20:** 267-277.

Turian, R.M, Hsu, F.-L. and Ma, T.-W. 1987. "Estimation of the critical velocity in pipeline flow of slurries." Powder Technology **51:** 35-47.

Wallis, G.B. 1969. One Dimensional Two Phase Flow. McGraw-Hill, New York.

Wasp, E.J., Aude, T.C., Kenny, J.P, Seiter, R.H. and Jacques, R.B. 1970. "Deposition velocities, transition velocities and spatial distributions of solids in slurry pipelines." Proc. Hydrotransport 1 Conf. BHRA, Cranfield, UK, Paper H4, pp. 53-76.

Wilson, K.C. 1970. "Slip point of beds in solid-liquid pipeline flow." ASCE. J. Hyd. Div. **96:** 1-12.

Wilson, K.C. 1976. "A unified physically based analysis of solid-liquid pipeline flow." Proc. Hydrotransport 4 Conf., BHRA, Cranfield, UK, Paper A1, pp. 1-16.

Wilson, K.C., 1979. "Deposition limit nomograms for particles of various densities in pipeline flow." Proc. Hydrotransport 6 Conf., BHRA, Cranfield, UK, Paper A1, pp. 1-12.

Wilson, K.C. and Pugh, F.J. 1988. "Dispersive-force modelling of turbulent suspension in heterogeneous flow". Can. J. Chem. Eng. **66:** 721-727.

Wilson, K.C., Streat, M. and Bantin, R.A. 1972. "Slip-model correlation of dense two-phase flow." Proc. Hydrotransport 2 Conf., BHRA, Cranfield, UK, Paper B1, pp. 1-10.

Wilson, K.C. and Thomas, A.D. 1985. "A new analysis of the turbulent flow of non-Newtonian fluids." Can. J. Chem. Eng. **63:** 539-546.

Wysoluzil, B., Kessick, M.A. and Masliyah, J.H., 1987. "Flow behaviour of heavy crude oil emulsions" Can. J. Chem. Eng. **65:** 353-360.

APPENDIX A

PIPELINE FLOW DATA

PIPELINE FLOW DATA FOR CLEAR WATER

RUN NUMBER: S8605030
DATE: 07/86
TEMP. (C): 15
PIPE DIA. (m) 0.0532

VELOCITY (m/s)	HEADLOSS (m/m)	ROUGHNESS (mm)
3.06	0.1521	0.002
2.77	0.1273	0.002
2.47	0.1035	0.002
2.16	0.0816	0.003
1.85	0.0612	0.001
1.55	0.0445	0.001
1.26	0.0304	

RUN NUMBER:	S8215010	S8205020
DATE:	12/82	12/82
TEMP. (C):	10	57
PIPE DIA. (m)	0.159	0.159

VELOCITY (m/s)	HEADLOSS (m/m)	ROUGHNESS (mm)	VELOCITY (m/s)	HEADLOSS (m/m)	ROUGHNESS (mm)
4.11	0.0869	0.042	4.24	0.0802	0.009
3.86	0.0770	0.042	3.93	0.0697	0.010
3.58	0.0668	0.044	3.64	0.0604	0.010
3.28	0.0569	0.046	3.24	0.0487	0.010
3.03	0.0489	0.046	3.04	0.0433	0.010
2.63	0.0378	0.051	2.67	0.0340	0.009
2.31	0.0291	0.045	2.30	0.0258	0.008
2.01	0.0229	0.054	1.93	0.0185	0.006
1.76	0.0178	0.059			

PIPELINE FLOW DATA FOR CLEAR WATER

RUN NUMBER: S8525050
DATE: 04/85
TEMP. (C): 15
PIPE DIA. (m) 0.2631

VELOCITY (m/s)	HEADLOSS (m/m)	ROUGHNESS (mm)
5.37	0.0647	0.004
4.82	0.0529	0.003
4.41	0.0450	0.004
4.06	0.0385	0.003
3.76	0.0333	0.003
3.28	0.0259	0.003
2.93	0.0211	0.003
2.56	0.0163	

RUN NUMBER: S795010
DATE: 04/79
TEMP. (C): 10
PIPE DIA. (m) 0.4953

VELOCITY (m/s)	HEADLOSS (m/m)	ROUGHNESS (mm)
4.11	0.0203	0.015
3.97	0.0187	0.012
3.66	0.0164	0.017
3.35	0.0138	0.015
3.05	0.0116	0.016
2.74	0.0098	
2.44	0.0079	
2.14	0.0063	
1.83	0.0050	

PIPELINE FLOW DATA FOR 0.1 x 0.3 mm SAND-IN-WATER SLURRIES

RUN #: S8605031
DATE: 07/86
TEMP (C): 15
CARRIER: Water
SOLIDS: 0.1x0.3 mm silica sand

PIPE DIAMETER (m): 0.0532
SOLIDS DENSITY (g/cc): 2.65
SOLIDS VOL. FRACTION: 0.15

PARTICLE SIZE:

SIEVE SIZE (microns)	WEIGHT% PASSING
74	0.5
149	14.7
210	57.1
297	95.3
420	99.8
595	100.0

PIPELINE PERFORMANCE:

VELOCITY (m/s)	HEADLOSS (m/m)	DEPOSIT
3.05	0.1939	
2.74	0.1628	
2.44	0.1346	
2.13	0.1101	
1.83	0.0872	
1.52	0.0700	
1.37	0.0649	INT
1.22	0.0615	INT
1.16	0.0624	INT
1.10	0.0561	

VELOCITY DISTRIBUTIONS:

POSITION r/R	y/R	V (m/s)	V (m/s)
0.8	0.785	1.88	2.82
0.8	0.665	1.81	2.82
0.8	0.444	1.78	2.82
0.8	0.156	1.71	2.74
0.8	-0.156	1.66	2.74
0.8	-0.444	1.55	2.67
0.8	-0.665	1.43	2.59
0.8	-0.785	1.30	2.53
0.4	0.370	2.18	3.35
0.4	0.153	2.04	3.35
0.4	-0.153	1.96	3.28
0.4	-0.370	1.85	3.20
0.0	0.000	2.09	3.56
Average:		1.78	2.94
MFM:		1.83	3.05

CHORD AVERAGE CONCENTRATIONS:

POSITION y/R	C	C
0.90	0.042	0.099
0.70	0.024	0.078
0.50	0.049	0.112
0.30	0.065	0.114
0.10	0.096	0.142
-0.10	0.163	0.174
-0.30	0.190	0.185
-0.50	0.235	0.196
-0.70	0.315	0.237
-0.90	0.348	0.261
V (m/s):	1.83	3.05

PIPELINE FLOW DATA FOR 0.1 x 0.3 mm SAND-IN-WATER SLURRIES

RUN #:	S8605032	PIPE DIAMETER (m):	0.0532
DATE:	07/86	SOLIDS DENSITY (g/cc):	2.65
TEMP (C):	15	SOLIDS VOL. FRACTION:	0.30
CARRIER:	Water		
SOLIDS:	0.1x0.3 mm silica sand		

PARTICLE SIZE:		PIPELINE PERFORMANCE:		
SIEVE SIZE (microns)	WEIGHT% PASSING	VELOCITY (m/s)	HEADLOSS (m/m)	DEPOSIT
74	0.5	3.05	0.2365	
149	14.7	2.74	0.2030	
210	57.1	2.44	0.1719	
297	95.3	2.13	0.1468	
420	99.8	1.83	0.1201	
595	100.0	1.52	0.0979	INT
		1.37	0.0910	INT
		1.22	0.1032	INT
		1.10	0.1016	STA

VELOCITY DISTRIBUTIONS:

POSITION r/R	y/R	V (m/s)	V (m/s)
0.8	0.785	1.76	2.67
0.8	0.665	1.76	2.67
0.8	0.444	1.73	2.63
0.8	0.156	1.66	2.56
0.8	-0.156	1.60	2.26
0.8	-0.444	1.48	2.18
0.8	-0.665	1.39	2.09
0.8	-0.785	1.33	2.06
0.4	0.370	2.11	3.37
0.4	0.153	2.04	3.31
0.4	-0.153	1.96	3.25
0.4	-0.370	1.81	3.15
0.0	0.000	2.16	3.49
Average:		1.74	2.72
MFM:		1.83	3.05

CHORD AVERAGE CONCENTRATIONS:

POSITION y/R	C	C
0.90	0.152	0.238
0.70	0.176	0.249
0.50	0.233	0.269
0.30	0.256	0.271
0.10	0.297	0.285
-0.10	0.336	0.317
-0.30	0.336	0.311
-0.50	0.356	0.325
-0.70	0.395	0.382
-0.90	0.448	0.383
V (m/s):	1.83	3.05

PIPELINE FLOW DATA FOR 0.1 x 0.3 mm SAND-IN-WATER SLURRIES

RUN #: S8605033
DATE: 07/86
TEMP (C): 15
CARRIER: Water
SOLIDS: 0.1x0.3 mm silica sand

PIPE DIAMETER (m): 0.0532
SOLIDS DENSITY (g/cc): 2.65
SOLIDS VOL. FRACTION: 0.45

PARTICLE SIZE:		PIPELINE PERFORMANCE:		
SIEVE SIZE (microns)	WEIGHT% PASSING	VELOCITY (m/s)	HEADLOSS (m/m)	DEPOSIT
74	0.5	3.05	0.3586	
149	14.7	2.74	0.3099	
210	57.1	2.43	0.2636	
297	95.3	2.13	0.2434	
420	99.8	1.83	0.2510	INT
595	100.0	1.52	0.2657	INT
		1.34	0.2880	INT
		1.19	0.2873	STA

VELOCITY DISTRIBUTIONS:

POSITION r/R	y/R	V (m/s)	V (m/s)
0.8	0.785	2.46	3.47
0.8	0.665	2.46	3.47
0.8	0.444	2.34	3.43
0.8	0.156		3.00
0.8	-0.156	1.28	2.82
0.8	-0.444		2.53
0.8	-0.665		2.29
0.8	-0.785		2.29
0.4	0.370	2.13	3.35
0.4	0.153	1.60	3.20
0.4	-0.153	1.11	2.67
0.4	-0.370	0.72	2.59
0.0	0.000	1.28	2.82
Average:			2.92
MFM:		1.83	3.05

CHORD AVERAGE CONCENTRATIONS:

POSITION y/R	C	C
0.90	0.321	0.400
0.70	0.326	0.402
0.50	0.441	0.449
0.30	0.441	0.434
0.10	0.468	0.452
-0.10	0.494	0.473
-0.30	0.480	0.439
-0.50	0.474	0.457
-0.70	0.494	0.441
-0.90	0.514	0.479
V (m/s):	1.83	3.05

PIPELINE FLOW DATA FOR 0.1 x 0.3 mm SAND-IN-WATER SLURRIES

RUN #:	S8215011	PIPE DIAMETER (m):	0.159
DATE:	12/82	SOLIDS DENSITY (g/cc):	2.65
TEMP (C):	11	SOLIDS VOL. FRACTION:	0.06
CARRIER:	Water		
SOLIDS:	0.1x0.3 mm silica sand		

PARTICLE SIZE:		PIPELINE PERFORMANCE:		
SIEVE SIZE (microns)	WEIGHT% PASSING	VELOCITY (m/s)	HEADLOSS (m/m)	DEPOSIT
74	0.8	2.61		
105	4.5	2.44		INT
149	24.6	2.30		INT
177	43.4	2.18		INT
210	55.8	2.11		STA
297	93.7			
420	100.0			

VELOCITY DISTRIBUTIONS:

POSITION r/R	y/R	V (m/s)	V (m/s)
0.8	0.785		
0.8	0.665		
0.8	0.444		
0.8	0.156		
0.8	-0.156		
0.8	-0.444		
0.8	-0.665		
0.8	-0.785		
0.4	0.370		
0.4	0.153		
0.4	-0.153		
0.4	-0.370		
0.0	0.000		

Average:
MFM:

CHORD AVERAGE CONCENTRATIONS:

POSITION y/R	C	C
0.88	-0.017	0.002
0.68	0.014	0.023
0.48	0.016	0.013
0.28	0.013	0.028
0.08	0.013	0.023
-0.12	0.039	0.054
-0.32	0.061	0.059
-0.52	0.107	0.086
-0.72	0.194	0.130
-0.92	0.266	0.174
Average	0.059	0.053
V (m/s):	2.53	3.66

PIPELINE FLOW DATA FOR 0.1 x 0.3 mm SAND-IN-WATER SLURRIES

RUN #:	S8215012	PIPE DIAMETER (m):	0.159
DATE:	12/82	SOLIDS DENSITY (g/cc):	2.65
TEMP (C):	13	SOLIDS VOL. FRACTION:	0.16
CARRIER:	Water		
SOLIDS:	0.1x0.3 mm silica sand		

PARTICLE SIZE:

SIEVE SIZE (microns)	WEIGHT% PASSING
74	0.8
105	4.5
149	24.6
177	43.4
210	55.8
297	93.7
420	100.0

PIPELINE PERFORMANCE:

VELOCITY (m/s)	HEADLOSS (m/m)	DEPOSIT
2.96	0.0860	
2.72	0.0778	INT
2.51	0.0709	INT
2.33	0.0630	INT
2.13	0.0552	STA

VELOCITY DISTRIBUTIONS:

POSITION r/R	POSITION y/R	V (m/s)	V (m/s)
0.8	0.785		
0.8	0.665		
0.8	0.444		
0.8	0.156		
0.8	-0.156		
0.8	-0.444		
0.8	-0.665		
0.8	-0.785		
0.4	0.370		
0.4	0.153		
0.4	-0.153		
0.4	-0.370		
0.0	0.000		

Average:

MFM:

CHORD AVERAGE CONCENTRATIONS:

POSITION y/R	C	C
0.88	-0.003	0.033
0.68	0.034	0.069
0.48	0.033	0.076
0.28	0.068	0.108
0.08	0.118	0.137
-0.12	0.189	0.181
-0.32	0.242	0.218
-0.52	0.279	0.227
-0.72	0.316	0.278
-0.92	0.347	0.304
Average	0.157	0.159
V (m/s):	2.74	3.66

PIPELINE FLOW DATA FOR 0.1 x 0.3 mm SAND-IN-WATER SLURRIES

RUN #: S8215013
DATE: 12/82
TEMP (C): 10
CARRIER: Water
SOLIDS: 0.1x0.3 mm silica sand

PIPE DIAMETER (m): 0.159
SOLIDS DENSITY (g/cc): 2.65
SOLIDS VOL. FRACTION: 0.30

PARTICLE SIZE:

SIEVE SIZE (microns)	WEIGHT% PASSING
74	0.8
105	4.5
149	24.6
177	43.4
210	55.8
297	93.7
420	100.0

PIPELINE PERFORMANCE:

VELOCITY (m/s)	HEADLOSS (m/m)	DEPOSIT
2.59		
2.32		INT
2.15		INT
1.96		STA

VELOCITY DISTRIBUTIONS:

POSITION r/R	y/R	V (m/s)	V (m/s)
0.8	0.785		
0.8	0.665		
0.8	0.444		
0.8	0.156		
0.8	-0.156		
0.8	-0.444		
0.8	-0.665		
0.8	-0.785		
0.4	0.370		
0.4	0.153		
0.4	-0.153		
0.4	-0.370		
0.0	0.000		

Average:
MFM:

CHORD AVERAGE CONCENTRATIONS:

POSITION y/R	C	C
0.88	0.143	0.205
0.68	0.229	0.245
0.48	0.249	0.258
0.28	0.284	0.287
0.08	0.307	0.296
-0.12	0.337	0.325
-0.32	0.363	0.342
-0.52	0.347	0.351
-0.72	0.372	0.369
-0.92	0.367	0.357
Average	0.304	0.305
V (m/s):	2.74	3.66

PIPELINE FLOW DATA FOR 0.1 x 0.3 mm SAND-IN-WATER SLURRIES

RUN #:	S8215021	PIPE DIAMETER (m):	0.159
DATE:	12/82	SOLIDS DENSITY (g/cc):	2.65
TEMP (C):	60	SOLIDS VOL. FRACTION:	0.06
CARRIER:	Water		
SOLIDS:	0.1x0.3 mm silica sand		

PARTICLE SIZE:		PIPELINE PERFORMANCE:		
SIEVE SIZE (microns)	WEIGHT% PASSING	VELOCITY (m/s)	HEADLOSS (m/m)	DEPOSIT
74	0.8	3.08		
105	4.5	2.85		INT
149	24.6	2.70		INT
177	43.4	2.59		INT
210	55.8	2.46		STA
297	93.7			
420	100.0			

VELOCITY DISTRIBUTIONS:

POSITION r/R	y/R	V (m/s)	V (m/s)
0.8	0.785		
0.8	0.665		
0.8	0.444		
0.8	0.156		
0.8	-0.156		
0.8	-0.444		
0.8	-0.665		
0.8	-0.785		
0.4	0.370		
0.4	0.153		
0.4	-0.153		
0.4	-0.370		
0.0	0.000		

Average:
MFM:

CHORD AVERAGE CONCENTRATIONS:

POSITION y/R	C	C
0.88	0.007	0.017
0.68	0.006	0.021
0.48	-0.016	0.016
0.28	0.008	0.025
0.08	-0.001	0.027
-0.12	0.016	0.051
-0.32	0.041	0.071
-0.52	0.109	0.107
-0.72	0.227	0.173
-0.92	0.385	0.245
Average	0.058	0.065
V (m/s):	2.74	3.96

PIPELINE FLOW DATA FOR 0.1 x 0.3 mm SAND-IN-WATER SLURRIES

RUN #: S8215022
DATE: 12/82
TEMP (C): 60
CARRIER: Water
SOLIDS: 0.1x0.3 mm silica sand

PIPE DIAMETER (m): 0.159
SOLIDS DENSITY (g/cc): 2.65
SOLIDS VOL. FRACTION: 0.16

PARTICLE SIZE:

SIEVE SIZE (microns)	WEIGHT% PASSING
74	0.8
105	4.5
149	24.6
177	43.4
210	55.8
297	93.7
420	100.0

PIPELINE PERFORMANCE:

VELOCITY (m/s)	HEADLOSS (m/m)	DEPOSIT
3.12		
2.87		INT
2.80		INT
2.70		STA

VELOCITY DISTRIBUTIONS:

POSITION r/R	y/R	V (m/s)	V (m/s)
0.8	0.785		
0.8	0.665		
0.8	0.444		
0.8	0.156		
0.8	-0.156		
0.8	-0.444		
0.8	-0.665		
0.8	-0.785		
0.4	0.370		
0.4	0.153		
0.4	-0.153		
0.4	-0.370		
0.0	0.000		

Average:
MFM:

CHORD AVERAGE CONCENTRATIONS:

POSITION y/R	C	C
0.88	0.012	0.020
0.68	0.013	0.038
0.48	0.011	0.045
0.28	0.046	0.083
0.08	0.098	0.119
-0.12	0.179	0.176
-0.32	0.259	0.231
-0.52	0.311	0.266
-0.72	0.353	0.313
-0.92	0.379	0.343
Average	0.157	0.157
V (m/s):	3.35	4.27

PIPELINE FLOW DATA FOR 0.1 x 0.3 mm SAND-IN-WATER SLURRIES

RUN #:	S8215023	PIPE DIAMETER (m):	0.159
DATE:	12/82	SOLIDS DENSITY (g/cc):	2.65
TEMP (C):	60	SOLIDS VOL. FRACTION:	0.30
CARRIER:	Water		
SOLIDS:	0.1x0.3 mm silica sand		

PARTICLE SIZE:		PIPELINE PERFORMANCE:		
SIEVE SIZE (microns)	WEIGHT% PASSING	VELOCITY (m/s)	HEADLOSS (m/m)	DEPOSIT
74	0.8	2.82		
105	4.5	2.81		INT
149	24.6	2.75		INT
177	43.4	2.59		STA
210	55.8			
297	93.7			
420	100.0			

VELOCITY DISTRIBUTIONS:

POSITION r/R	POSITION y/R	V (m/s)	V (m/s)
0.8	0.785		
0.8	0.665		
0.8	0.444		
0.8	0.156		
0.8	-0.156		
0.8	-0.444		
0.8	-0.665		
0.8	-0.785		
0.4	0.370		
0.4	0.153		
0.4	-0.153		
0.4	-0.370		
0.0	0.000		

Average:
MFM:

CHORD AVERAGE CONCENTRATIONS:

POSITION y/R	C	C
0.88	0.063	0.110
0.68	0.119	0.164
0.48	0.195	0.221
0.28	0.289	0.270
0.08	0.342	0.323
-0.12	0.376	0.338
-0.32	0.404	0.383
-0.52	0.379	0.379
-0.72	0.370	0.414
-0.92	0.397	0.362
Average	0.302	0.302
V (m/s):	3.35	4.27

PIPELINE FLOW DATA FOR 0.1 x 0.3 mm SAND-IN-WATER SLURRIES

RUN #:	S7950011	PIPE DIAMETER (m):	0.4953
DATE:	04/79	SOLIDS DENSITY (g/cc):	2.65
TEMP (C):	14	SOLIDS VOL. FRACTION:	0.10
CARRIER:	Water		
SOLIDS:	0.1x0.3 mm silica sand		

PARTICLE SIZE:		PIPELINE PERFORMANCE:		
SIEVE SIZE (microns)	WEIGHT% PASSING	VELOCITY (m/s)	HEADLOSS (m/m)	DEPOSIT
74	0.5	4.28	0.0239	
105	4.2	4.11	0.0219	
149	29.0	3.97	0.0207	
210	81.9	3.81	0.0190	
297	99.4	3.66	0.0176	
420	100.0	3.51	0.0166	INT
		3.35	0.0154	INT
		3.20	0.0147	INT
		3.11	0.0148	STA

PIPELINE FLOW DATA FOR 0.1 x 0.3 mm SAND-IN-WATER SLURRIES

RUN #:	S7950012	PIPE DIAMETER (m):	0.4953
DATE:	04/79	SOLIDS DENSITY (g/cc):	2.65
TEMP (C):	13	SOLIDS VOL. FRACTION:	0.15
CARRIER:	Water		
SOLIDS:	0.1x0.3 mm silica sand		

PARTICLE SIZE:		PIPELINE PERFORMANCE:		
SIEVE SIZE (microns)	WEIGHT% PASSING	VELOCITY (m/s)	HEADLOSS (m/m)	DEPOSIT
74	0.5	4.26	0.0247	
105	4.2	4.11	0.0233	
149	29.0	3.93	0.0215	
210	81.9	3.81	0.0200	
297	99.4	3.66	0.0188	
420	100.0	3.51	0.0175	INT
		3.30	0.0162	INT
		3.20	0.0155	INT
		3.02	0.0148	STA

PIPELINE FLOW DATA FOR 0.1 x 0.3 mm SAND-IN-WATER SLURRIES

RUN #: S7950013
DATE: 04/79
TEMP (C): 14
CARRIER: Water
SOLIDS: 0.1x0.3 mm silica sand

PIPE DIAMETER (m): 0.4953
SOLIDS DENSITY (g/cc): 2.65
SOLIDS VOL. FRACTION: 0.20

PARTICLE SIZE:

SIEVE SIZE (microns)	WEIGHT% PASSING
74	0.5
105	4.2
149	29.0
210	81.9
297	99.4
420	100.0

PIPELINE PERFORMANCE:

VELOCITY (m/s)	HEADLOSS (m/m)	DEPOSIT
4.26	0.0264	
4.11	0.0247	
3.97	0.0232	
3.81	0.0215	
3.66	0.0205	
3.51	0.0188	INT
3.35	0.0177	INT
3.20	0.0165	INT
3.05	0.0158	STA

VELOCITY DISTRIBUTIONS:

POSITION r/R	y/R	V (m/s)	V (m/s)
0.8	0.785		
0.8	0.665		
0.8	0.444		
0.8	0.156		
0.8	-0.156		
0.8	-0.444		
0.8	-0.665		
0.8	-0.785		
0.4	0.370		
0.4	0.153		
0.4	-0.153		
0.4	-0.370		
0.0	0.000		

Average:
MFM:

CHORD AVERAGE CONCENTRATIONS:

POSITION y/R	C	C
0.90	0.060	0.044
0.70	0.058	0.068
0.50	0.060	0.100
0.30	0.108	0.137
0.10	0.174	0.177
-0.10	0.239	0.217
-0.30	0.291	0.256
-0.50	0.327	0.292
-0.70	0.352	0.321
-0.90	0.380	0.343
V (m/s):	3.07	3.76

PIPELINE FLOW DATA FOR 0.1 x 0.3 mm SAND-IN-WATER SLURRIES

RUN #:	S7950014	PIPE DIAMETER (m):	0.4953
DATE:	04/79	SOLIDS DENSITY (g/cc):	2.65
TEMP (C):	15	SOLIDS VOL. FRACTION:	0.25
CARRIER:	Water		
SOLIDS:	0.1x0.3 mm silica sand		

PARTICLE SIZE:		PIPELINE PERFORMANCE:		
SIEVE SIZE (microns)	WEIGHT% PASSING	VELOCITY (m/s)	HEADLOSS (m/m)	DEPOSIT
74	0.5	4.30	0.0284	
105	4.2	4.11	0.0267	
149	29.0	3.94	0.0250	
210	81.9	3.81	0.0234	
297	99.4	3.66	0.0221	
420	100.0	3.49	0.0203	
		3.34	0.0191	INT
		3.20	0.0180	INT
		3.05	0.0171	INT
		2.93	0.0168	STA

PIPELINE FLOW DATA FOR 0.1 x 0.3 mm SAND-IN-WATER SLURRIES

RUN #: S7950015
DATE: 04/79
TEMP (C): 10
CARRIER: Water
SOLIDS: 0.1x0.3 mm silica sand

PIPE DIAMETER (m): 0.4953
SOLIDS DENSITY (g/cc): 2.65
SOLIDS VOL. FRACTION: 0.29

PARTICLE SIZE:

SIEVE SIZE (microns)	WEIGHT% PASSING
74	0.5
105	4.2
149	29.0
210	81.9
297	99.4
420	100.0

PIPELINE PERFORMANCE:

VELOCITY (m/s)	HEADLOSS (m/m)	DEPOSIT
4.26	0.0324	
4.11	0.0204	
3.97	0.0287	
3.81	0.0266	
3.66	0.0250	
3.51	0.0231	
3.35	0.0211	INT
3.20	0.0197	INT
3.11	0.0188	INT
3.02	0.0178	INT
2.93	0.0170	INT
2.83	0.0163	INT
2.74	0.0159	STA

VELOCITY DISTRIBUTIONS:

POSITION r/R	y/R	V (m/s)	V (m/s)
0.8	0.785		
0.8	0.665		
0.8	0.444		
0.8	0.156		
0.8	-0.156		
0.8	-0.444		
0.8	-0.665		
0.8	-0.785		
0.4	0.370		
0.4	0.153		
0.4	-0.153		
0.4	-0.370		
0.0	0.000		

CHORD AVERAGE CONCENTRATIONS:

POSITION y/R	C	C
0.90	0.042	0.096
0.70	0.109	0.162
0.50	0.185	0.216
0.30	0.256	0.260
0.10	0.312	0.294
-0.10	0.351	0.321
-0.30	0.372	0.343
-0.50	0.383	0.361
-0.70	0.393	0.378
-0.90	0.420	0.395
V (m/s):	3.16	3.76

Average:
MFM:

PIPELINE FLOW DATA FOR 0.1 x 0.3 mm SAND-IN-WATER SLURRIES

RUN #:	S7950016	PIPE DIAMETER (m):	0.4953
DATE:	04/79	SOLIDS DENSITY (g/cc):	2.65
TEMP (C):	9	SOLIDS VOL. FRACTION:	0.34
CARRIER:	Water		
SOLIDS:	0.1x0.3 mm silica sand		

PARTICLE SIZE:		PIPELINE PERFORMANCE:		
SIEVE SIZE (microns)	WEIGHT% PASSING	VELOCITY (m/s)	HEADLOSS (m/m)	DEPOSIT
74	0.5	4.26	0.0376	
105	4.2	4.11	0.0349	
149	29.0	3.97	0.0330	
210	81.9	3.81	0.0307	
297	99.4	3.66	0.0287	
420	100.0	3.51	0.0267	INT
		3.35	0.0244	INT
		3.20	0.0227	INT
		3.05	0.0208	INT
		2.89	0.0193	INT
		2.74	0.0180	INT
		2.65	0.0173	STA

PIPELINE FLOW DATA FOR 0.3 x 1 mm SAND-IN-WATER SLURRIES

RUN #: S8605041
DATE: 07/86
TEMP (C): 15
CARRIER: Water
SOLIDS: 0.3x1.0 mm silica sand

PIPE DIAMETER (m): 0.0532
SOLIDS DENSITY (g/cc): 2.65
SOLIDS VOL. FRACTION: 0.15

PARTICLE SIZE:		PIPELINE PERFORMANCE:		
SIEVE SIZE (microns)	WEIGHT% PASSING	VELOCITY (m/s)	HEADLOSS (m/m)	DEPOSIT
74	0.7	3.05	0.2117	
210	0.8	2.74	0.1923	
297	3.9	2.44	0.1753	
420	23.7	2.13	0.1468	
595	67.4	1.83	0.1327	
841	88.1	1.52	0.1210	INT
1190	96.2	1.37	0.1120	INT
2380	100.0	1.28	0.0985	STA

VELOCITY DISTRIBUTIONS:

POSITION r/R	y/R	V (m/s)	V (m/s)
0.8	0.785	1.85	2.91
0.8	0.665	1.85	2.91
0.8	0.444	1.78	2.82
0.8	0.156	1.71	2.74
0.8	-0.156	1.68	2.67
0.8	-0.444	1.31	2.40
0.8	-0.665	1.07	2.00
0.8	-0.785	0.87	1.55
0.4	0.370	2.29	3.56
0.4	0.153	2.23	3.47
0.4	-0.153	1.92	3.24
0.4	-0.370	1.52	2.74
0.0	0.000	2.29	3.43
Average:		1.70	2.78
MFM:		1.83	3.05

CHORD AVERAGE CONCENTRATIONS:

POSITION y/R	C	C
0.90	0.021	0.034
0.70	0.000	0.019
0.50	0.029	0.029
0.30	0.018	0.019
0.10	0.058	0.075
-0.10	0.107	0.145
-0.30	0.173	0.219
-0.50	0.282	0.330
-0.70	0.388	0.424
-0.90	0.498	0.427
V (m/s):	1.83	3.05

PIPELINE FLOW DATA FOR 0.3 x 1 mm SAND-IN-WATER SLURRIES

RUN #: S8605042
DATE: 07/86
TEMP (C): 15
CARRIER: Water
SOLIDS: 0.3x1.0 mm silica sand

PIPE DIAMETER (m): 0.0532
SOLIDS DENSITY (g/cc): 2.65
SOLIDS VOL. FRACTION: 0.30

PARTICLE SIZE:

SIEVE SIZE (microns)	WEIGHT% PASSING
74	0.7
210	0.8
297	3.9
420	23.7
595	67.4
841	88.1
1190	96.2
2380	100.0

PIPELINE PERFORMANCE:

VELOCITY (m/s)	HEADLOSS (m/m)	DEPOSIT
3.05	0.3181	
2.74	0.3002	
2.44	0.2949	
2.13	0.2760	
1.98	0.2579	
1.84	0.2579	
1.69	0.2356	INT
1.52	0.2218	INT
1.36	0.2296	INT
1.28	0.2171	INT
1.16	0.2017	STA

VELOCITY DISTRIBUTIONS:

POSITION r/R	y/R	V (m/s)	V (m/s)
0.8	0.785	2.53	3.27
0.8	0.665	2.53	3.27
0.8	0.444	2.67	3.13
0.8	0.156	2.23	2.91
0.8	-0.156	1.48	2.00
0.8	-0.444	1.15	1.92
0.8	-0.665	0.69	1.71
0.8	-0.785	0.58	1.45
0.4	0.370	3.31	3.93
0.4	0.153	2.59	3.50
0.4	-0.153	1.85	2.74
0.4	-0.370	0.99	2.00
0.0	0.000	2.13	3.38
Average:		1.89	2.68
MFM:		2.13	3.05

CHORD AVERAGE CONCENTRATIONS:

POSITION y/R	C	C
0.90	0.060	0.053
0.70	0.046	0.074
0.50	0.102	0.122
0.30	0.168	0.181
0.10	0.333	0.311
-0.10	0.449	0.422
-0.30	0.484	0.459
-0.50	0.504	0.472
-0.70	0.544	0.473
-0.90	0.568	0.457
V (m/s):	2.13	3.05

PIPELINE FLOW DATA FOR 0.3 x 1 mm SAND-IN-WATER SLURRIES

RUN #:	S8605043	PIPE DIAMETER (m):	0.0532
DATE:	07/86	SOLIDS DENSITY (g/cc):	2.65
TEMP (C):	15	SOLIDS VOL. FRACTION:	0.40
CARRIER:	Water		
SOLIDS:	0.3x1.0 mm silica sand		

PARTICLE SIZE:

SIEVE SIZE (microns)	WEIGHT% PASSING
74	0.7
210	0.8
297	3.9
420	23.7
595	67.4
841	88.1
1190	96.2
2380	100.0

PIPELINE PERFORMANCE:

VELOCITY (m/s)	HEADLOSS (m/m)	DEPOSIT
2.74	0.4370	
2.44	0.4400	
2.13	0.3962	
1.98	0.3680	
1.83	0.3633	
1.68	0.3586	
1.52	0.3507	INT
1.40	0.3554	INT
1.25	0.3460	STA

VELOCITY DISTRIBUTIONS:

POSITION r/R	y/R	V (m/s)	V (m/s)
0.8	0.785	3.20	
0.8	0.665	3.20	
0.8	0.444	2.74	
0.8	0.156	2.04	
0.8	-0.156	1.50	
0.8	-0.444	1.11	
0.8	-0.665	0.74	
0.8	-0.785	0.60	
0.4	0.370	3.00	
0.4	0.153	2.29	
0.4	-0.153	1.63	
0.4	-0.370	1.03	
0.0	0.000	1.92	
Average:		1.92	
MFM:		2.13	

CHORD AVERAGE CONCENTRATIONS:

POSITION y/R	C	C
0.90	0.076	
0.70	0.120	
0.50	0.292	
0.30	0.419	
0.10	0.466	
-0.10	0.526	
-0.30	0.508	
-0.50	0.511	
-0.70	0.551	
-0.90	0.553	

V (m/s): 2.13

PIPELINE FLOW DATA FOR 0.3 x 1 mm SAND-IN-WATER SLURRIES

RUN #: S8525031
DATE: 03/85
TEMP (C): 15
CARRIER: Water
SOLIDS: 0.3x1.0 mm silica sand

PIPE DIAMETER (m): 0.2631
SOLIDS DENSITY (g/cc): 2.65
SOLIDS VOL. FRACTION: 0.15

PARTICLE SIZE:		PIPELINE PERFORMANCE:		
SIEVE SIZE (microns)	WEIGHT% PASSING	VELOCITY (m/s)	HEADLOSS (m/m)	DEPOSIT
74	0.7	5.20	0.0918	
210	0.8	4.98	0.0879	
297	3.9	4.53	0.0801	
420	23.7	4.24	0.0751	
595	67.4	3.91	0.0697	
841	88.1	3.61	0.0659	
1190	96.2	3.31	0.0666	STA
2380	100.0			

VELOCITY DISTRIBUTIONS:

POSITION r/R	y/R	V (m/s)	V (m/s)
0.8	0.785	5.03	5.56
0.8	0.665	5.02	5.28
0.8	0.444	5.00	5.21
0.8	0.156	4.40	4.72
0.8	-0.156	3.64	4.06
0.8	-0.444	2.98	3.32
0.8	-0.665	2.56	2.94
0.8	-0.785	1.97	2.59
0.4	0.370	5.90	6.01
0.4	0.153	4.88	5.34
0.4	-0.153	3.98	4.47
0.4	-0.370	3.40	3.80
0.0	0.000	4.74	4.87
Average:		4.09	4.46
MFM:		4.21	4.67

CHORD AVERAGE CONCENTRATIONS:

POSITION y/R	C	C
0.90	0.013	0.010
0.70	0.008	0.014
0.50	0.011	0.015
0.30	0.019	0.021
0.10	0.043	0.050
-0.10	0.111	0.100
-0.30	0.210	0.210
-0.50	0.311	0.317
-0.70	0.430	0.423
-0.90	0.481	0.483
V (m/s):	3.94	4.37

PIPELINE FLOW DATA FOR 0.3 x 1 mm SAND-IN-WATER SLURRIES

RUN #: S8525032
DATE: 03/85
TEMP (C): 15
CARRIER: Water
SOLIDS: 0.3x1.0 mm silica sand

PIPE DIAMETER (m): 0.2631
SOLIDS DENSITY (g/cc): 2.65
SOLIDS VOL. FRACTION: 0.25

PARTICLE SIZE:

SIEVE SIZE (microns)	WEIGHT% PASSING
74	0.7
210	0.8
297	3.9
420	23.7
595	67.4
841	88.1
1190	96.2
2380	100.0

PIPELINE PERFORMANCE:

VELOCITY (m/s)	HEADLOSS (m/m)	DEPOSIT
4.92	0.1047	
4.60	0.1010	
4.35	0.0962	
4.07	0.0930	
3.83	0.0893	INT
3.45	0.0856	INT
3.60	0.0867	INT
3.41	0.0845	INT
3.32	0.0830	INT
3.12	0.0885	STA

VELOCITY DISTRIBUTIONS:

POSITION r/R	y/R	V (m/s)	V (m/s)
0.8	0.785	4.91	5.54
0.8	0.665	4.91	5.33
0.8	0.444	4.57	5.14
0.8	0.156	3.89	4.36
0.8	-0.156	3.39	3.89
0.8	-0.444	2.94	3.35
0.8	-0.665	2.48	2.77
0.8	-0.785	1.92	2.29
0.4	0.370	5.47	6.00
0.4	0.153	4.64	5.33
0.4	-0.153	3.95	4.36
0.4	-0.370	3.52	4.11
0.0	0.000	4.36	5.14
Average:		3.90	4.40
MFM:		4.17	4.68

CHORD AVERAGE CONCENTRATIONS:

POSITION y/R	C	C
0.90	0.008	0.015
0.70	0.018	0.020
0.50	0.041	0.043
0.30	0.095	0.097
0.10	0.191	0.198
-0.10	0.287	0.294
-0.30	0.369	0.365
-0.50	0.437	0.424
-0.70	0.494	0.508
-0.90	0.502	0.508
V (m/s):	3.90	4.38

PIPELINE FLOW DATA FOR 0.3 x 1 mm SAND-IN-WATER SLURRIES

RUN #: S8525033
DATE: 03/85
TEMP (C): 15
CARRIER: Water
SOLIDS: 0.3x1.0 mm silica sand

PIPE DIAMETER (m): 0.2631
SOLIDS DENSITY (g/cc): 2.65
SOLIDS VOL. FRACTION: 0.30

PARTICLE SIZE:		PIPELINE PERFORMANCE:		
SIEVE SIZE (microns)	WEIGHT% PASSING	VELOCITY (m/s)	HEADLOSS (m/m)	DEPOSIT
74	0.7	4.78	0.1145	
210	0.8	4.51	0.1122	
297	3.9	4.27	0.1071	
420	23.7	4.00	0.1040	
595	67.4	4.53	0.1120	
841	88.1	3.74	0.1022	
1190	96.2	3.62	0.1003	
2380	100.0	3.34	0.0964	
		3.23	0.0917	
		3.08	0.1041	STA

VELOCITY DISTRIBUTIONS:

POSITION r/R	y/R	V (m/s)	V (m/s)
0.8	0.785	5.14	5.54
0.8	0.665	4.97	5.30
0.8	0.444	4.57	4.93
0.8	0.156	4.00	4.36
0.8	-0.156	3.65	4.00
0.8	-0.444	3.10	3.60
0.8	-0.665	2.25	2.94
0.8	-0.785	2.16	2.28
0.4	0.370	5.33	5.92
0.4	0.153	4.72	5.12
0.4	-0.153	4.17	4.65
0.4	-0.370	3.60	4.24
0.0	0.000	4.64	5.06
Average:		4.00	4.43
MFM:		4.17	4.64

CHORD AVERAGE CONCENTRATIONS:

POSITION y/R	C	C
0.90	0.015	0.010
0.70	0.031	0.040
0.50	0.080	0.082
0.30	0.163	0.172
0.10	0.277	0.278
-0.10	0.359	0.363
-0.30	0.423	0.423
-0.50	0.469	0.463
-0.70	0.519	0.508
-0.90	0.528	0.513
V (m/s):	3.90	4.34

PIPELINE FLOW DATA FOR 0.3 x 1 mm SAND-IN-WATER SLURRIES

RUN #: S8525035
DATE: 03/85
TEMP (C): 40
CARRIER: Water
SOLIDS: 0.3x1.0 mm silica sand

PIPE DIAMETER (m): 0.2631
SOLIDS DENSITY (g/cc): 2.65
SOLIDS VOL. FRACTION: 0.30

PARTICLE SIZE:		PIPELINE PERFORMANCE:		
SIEVE SIZE (microns)	WEIGHT% PASSING	VELOCITY (m/s)	HEADLOSS (m/m)	DEPOSIT
74	0.7	5.08	0.1364	
210	0.8	4.79	0.1328	
297	3.9	4.52	0.1258	
420	23.7	4.19	0.1207	
595	67.4	3.96	0.1183	
841	88.1	3.77	0.1160	
1190	96.2	3.60	0.1145	INT
2380	100.0	3.36	0.1120	INT
		3.27	0.1113	INT
		3.15	0.1213	STA

VELOCITY DISTRIBUTIONS:

POSITION r/R	y/R	V (m/s)	V (m/s)
0.8	0.785	5.21	5.62
0.8	0.665	5.15	5.34
0.8	0.444	4.36	5.00
0.8	0.156	4.23	4.57
0.8	-0.156	3.79	4.24
0.8	-0.444	3.06	3.43
0.8	-0.665	2.54	2.80
0.8	-0.785	1.66	2.22
0.4	0.370	5.34	5.80
0.4	0.153	4.80	5.24
0.4	-0.153	4.24	4.72
0.4	-0.370	3.60	3.95
0.0	0.000	4.65	5.10
Average:		4.02	4.44
MFM:		4.22	4.68

CHORD AVERAGE CONCENTRATIONS:

POSITION y/R	C	C
0.90	0.022	0.020
0.70	0.050	0.046
0.50	0.091	0.092
0.30	0.173	0.168
0.10	0.271	0.279
-0.10	0.357	0.358
-0.30	0.440	0.428
-0.50	0.474	0.475
-0.70	0.529	0.536
-0.90	0.554	0.545
V (m/s):	3.95	4.38

PIPELINE FLOW DATA FOR 2 X 6 mm GRAVEL-IN-WATER SLURRIES

RUN #: S8605061
DATE: 08/86
TEMP (C): 15
CARRIER: Water
SOLIDS: 2x6 mm gravel

PIPE DIAMETER (m): 0.0532
SOLIDS DENSITY (g/cc): 2.65
SOLIDS VOL. FRACTION: 0.15

PARTICLE SIZE:

SIEVE SIZE (microns)	WEIGHT% PASSING
841	0.1
1190	0.4
1680	5.9
2380	44.0
3360	80.9
4760	94.4
6730	100.0

PIPELINE PERFORMANCE:

VELOCITY (m/s)	HEADLOSS (m/m)	DEPOSIT
3.05	0.2676	
2.74	0.2415	
2.44	0.2124	
2.13	0.1873	
1.83	0.1631	
1.68	0.1559	
1.52	0.1437	
1.37	0.1330	INT
1.25	0.1223	INT
1.16	0.1145	STA

VELOCITY DISTRIBUTIONS:

POSITION r/R	y/R	V (m/s)	V (m/s)
0.8	0.785	2.23	3.43
0.8	0.665	2.40	3.43
0.8	0.444	2.34	3.43
0.8	0.156	2.29	3.56
0.8	-0.156	1.81	3.20
0.8	-0.444	1.22	2.46
0.8	-0.665	0.74	1.81
0.8	-0.785	0.48	1.45
0.4	0.370	2.67	4.12
0.4	0.153	2.53	3.95
0.4	-0.153	1.88	3.31
0.4	-0.370	1.17	2.46
0.0	0.000	2.09	3.60
Average:		1.82	3.07
MFM:		1.83	3.05

CHORD AVERAGE CONCENTRATIONS:

POSITION y/R	C	C
0.90	-0.035	0.022
0.70	0.017	0.036
0.50	0.028	0.041
0.30	0.029	0.046
0.10	0.038	0.073
-0.10	0.121	0.151
-0.30	0.197	0.237
-0.50	0.296	0.316
-0.70	0.420	0.392
-0.90	0.492	0.390
V (m/s):	1.83	3.05

PIPELINE FLOW DATA FOR 2 X 6 mm GRAVEL-IN-WATER SLURRIES

RUN #: S8605062
DATE: 08/86
TEMP (C): 15
CARRIER: Water
SOLIDS: 2x6 mm gravel

PIPE DIAMETER (m): 0.0532
SOLIDS DENSITY (g/cc): 2.65
SOLIDS VOL. FRACTION: 0.30

PARTICLE SIZE:		PIPELINE PERFORMANCE:		
SIEVE SIZE (microns)	WEIGHT% PASSING	VELOCITY (m/s)	HEADLOSS (m/m)	DEPOSIT
841	0.1	3.05	0.3789	
1190	0.4	2.74	0.3419	
1680	5.9	2.44	0.3055	
2380	44.0	2.13	0.2742	
3360	80.9	1.83	0.2466	
4760	94.4	1.52	0.2271	
6730	100.0	1.37	0.2171	INT
		1.22	0.2080	INT
		1.13	0.2032	STA

VELOCITY DISTRIBUTIONS:

POSITION r/R	y/R	V (m/s)	V (m/s)
0.8	0.785	2.82	3.56
0.8	0.665	2.67	3.43
0.8	0.444	2.59	3.51
0.8	0.156	2.13	3.35
0.8	-0.156	1.60	2.91
0.8	-0.444	1.07	2.33
0.8	-0.665	0.67	1.73
0.8	-0.785	0.49	1.48
0.4	0.370	2.74	4.11
0.4	0.153	2.46	3.79
0.4	-0.153	1.66	3.00
0.4	-0.370	1.08	2.29
0.0	0.000	1.85	3.27
Average:		1.83	2.97
MFM:		1.83	3.05

CHORD AVERAGE CONCENTRATIONS:

POSITION y/R	C	C
0.90	0.088	0.114
0.70	0.089	0.116
0.50	0.114	0.131
0.30	0.179	0.196
0.10	0.232	0.291
-0.10	0.346	0.371
-0.30	0.452	0.435
-0.50	0.490	0.475
-0.70	0.553	0.510
-0.90	0.573	0.480
V (m/s):	1.83	3.05

PIPELINE FLOW DATA FOR 2 X 6 mm GRAVEL-IN-WATER SLURRIES

RUN #: S8525071
DATE: 04/85
TEMP (C): 15
CARRIER: Water
SOLIDS: 2x6 mm gravel

PIPE DIAMETER (m): 0.2631
SOLIDS DENSITY (g/cc): 2.65
SOLIDS VOL. FRACTION: 0.13

PARTICLE SIZE:

SIEVE SIZE (microns)	WEIGHT% PASSING
74	1.2
210	1.7
595	2.5
1190	3.3
1680	8.5
2380	41.4
3360	79.5
4760	94.2
6730	100.0

PIPELINE PERFORMANCE:

VELOCITY (m/s)	HEADLOSS (m/m)	DEPOSIT
4.80	0.1231	
4.49	0.1172	
4.16	0.1105	
3.87	0.1049	
3.53	0.1004	INT
3.25	0.0957	INT
2.96	0.0908	INT
2.79	0.0881	INT
2.67	0.0861	INT
2.53	0.0685	STA

VELOCITY DISTRIBUTIONS:

POSITION r/R	y/R	V (m/s)	V (m/s)
0.8	0.785	5.68	
0.8	0.665	5.60	
0.8	0.444	5.60	
0.8	0.156	5.42	
0.8	-0.156	5.03	
0.8	-0.444	4.12	
0.8	-0.665	2.46	
0.8	-0.785	1.40	
0.4	0.370	6.27	
0.4	0.153	5.92	
0.4	-0.153	5.42	
0.4	-0.370	4.77	
0.0	0.000	5.68	
Average:		4.84	
MFM:		4.83	

CHORD AVERAGE CONCENTRATIONS:

POSITION y/R	C	C
0.90	0.013	0.014
0.70	0.012	0.025
0.50	0.021	0.019
0.30	0.021	0.025
0.10	0.036	0.040
-0.10	0.068	0.063
-0.30	0.123	0.129
-0.50	0.240	0.248
-0.70	0.403	0.406
-0.90	0.482	0.476
V (m/s):	3.61	4.52

PIPELINE FLOW DATA FOR 2 X 6 mm GRAVEL-IN-WATER SLURRIES

RUN #: S8525072
DATE: 04/85
TEMP (C): 15
CARRIER: Water
SOLIDS: 2x6 mm gravel

PIPE DIAMETER (m): 0.2631
SOLIDS DENSITY (g/cc): 2.65
SOLIDS VOL. FRACTION: 0.22

PARTICLE SIZE:		PIPELINE PERFORMANCE:		
SIEVE SIZE (microns)	WEIGHT% PASSING	VELOCITY (m/s)	HEADLOSS (m/m)	DEPOSIT
74	1.2	3.92	0.1542	
210	1.7	3.60	0.1539	
595	2.5	3.56	0.1488	
1190	3.3	3.33	0.1461	
1680	8.5	3.15	0.1439	
2380	41.4	2.99	0.1423	INT
3360	79.5	2.75	0.1414	INT
4760	94.2	2.53	0.1315	INT
6730	100.0	2.37	0.1197	STA

VELOCITY DISTRIBUTIONS:

POSITION r/R	y/R	V (m/s)	V (m/s)
0.8	0.785	4.67	5.68
0.8	0.665	4.91	5.60
0.8	0.444	4.44	5.38
0.8	0.156	4.12	5.06
0.8	-0.156	3.59	4.24
0.8	-0.444	2.69	2.92
0.8	-0.665	1.17	1.99
0.8	-0.785	0.82	1.33
0.4	0.370	4.83	6.18
0.4	0.153	4.59	5.60
0.4	-0.153	3.89	4.67
0.4	-0.370	2.80	3.78
0.0	0.000	4.24	5.25
Average:		3.57	4.40
MFM:		3.47	4.36

CHORD AVERAGE CONCENTRATIONS:

POSITION y/R	C	C
0.90	0.041	0.042
0.70	0.049	0.045
0.50	0.061	0.058
0.30	0.086	0.081
0.10	0.125	0.129
-0.10	0.188	0.194
-0.30	0.289	0.296
-0.50	0.395	0.396
-0.70	0.509	0.505
-0.90	0.552	0.559
V (m/s):	3.25	4.08

PIPELINE FLOW DATA FOR 2 X 6 mm GRAVEL-IN-WATER SLURRIES

RUN #: S8525073
DATE: 04/85
TEMP (C): 40
CARRIER: Water
SOLIDS: 2x6 mm gravel

PIPE DIAMETER (m): 0.2631
SOLIDS DENSITY (g/cc): 2.65
SOLIDS VOL. FRACTION: 0.22

PARTICLE SIZE:		PIPELINE PERFORMANCE:		
SIEVE SIZE (microns)	WEIGHT% PASSING	VELOCITY (m/s)	HEADLOSS (m/m)	DEPOSIT
74	1.2	4.34	0.1465	
210	1.7	3.98	0.1401	
595	2.5	3.70	0.1359	
1190	3.3	3.44	0.1290	
1680	8.5	3.17	0.1253	INT
2380	41.4	2.87	0.1207	INT
3360	79.5	2.76	0.1230	INT
4760	94.2	2.68	0.1132	INT
6730	100.0	2.55	0.1081	STA

VELOCITY DISTRIBUTIONS:

POSITION r/R	y/R	V (m/s)	V (m/s)
0.8	0.785	5.38	
0.8	0.665	5.25	
0.8	0.444	5.22	
0.8	0.156	4.88	
0.8	-0.156	4.12	
0.8	-0.444	2.86	
0.8	-0.665	1.67	
0.8	-0.785	0.97	
0.4	0.370	5.92	
0.4	0.153	5.45	
0.4	-0.153	4.83	
0.4	-0.370	3.54	
0.0	0.000	5.12	
Average:		4.21	
MFM:		4.23	

CHORD AVERAGE CONCENTRATIONS:

POSITION y/R	C	C
0.90	0.039	0.061
0.70	0.061	0.064
0.50	0.063	0.074
0.30	0.083	0.087
0.10	0.119	0.120
-0.10	0.176	0.182
-0.30	0.279	0.289
-0.50	0.391	0.403
-0.70	0.511	0.505
-0.90	0.570	0.575
V (m/s):	3.21	3.96

PIPELINE FLOW DATA FOR 0 X 1 mm SAND-IN-WATER SLURRIES

RUN #: S8605051
DATE: 07/86
TEMP (C): 15
CARRIER: Water
SOLIDS: 0x1 mm silica sand

PIPE DIAMETER (m): 0.0532
SOLIDS DENSITY (g/cc): 2.65
SOLIDS VOL. FRACTION: 0.15

PARTICLE SIZE:		PIPELINE PERFORMANCE:		
SIEVE SIZE (microns)	WEIGHT% PASSING	VELOCITY (m/s)	HEADLOSS (m/m)	DEPOSIT
74	0.6	3.05	0.1860	
149	5.5	2.74	0.1619	
210	23.1	2.44	0.1386	
297	50.1	2.13	0.1195	
420	71.1	1.83	0.1007	
595	89.0	1.55	0.0925	INT
841	96.0	1.37	0.0866	INT
1190	98.7	1.22	0.0787	STA
1680	100.0			

VELOCITY DISTRIBUTIONS:

POSITION r/R	y/R	V (m/s)	V (m/s)
0.8	0.785	1.88	3.10
0.8	0.665	1.85	3.00
0.8	0.444	1.81	2.91
0.8	0.156	1.78	2.91
0.8	-0.156	1.78	2.91
0.8	-0.444	1.63	2.82
0.8	-0.665	1.45	2.82
0.8	-0.785	1.19	2.53
0.4	0.370	2.23	3.39
0.4	0.153	2.18	3.35
0.4	-0.153	2.04	3.28
0.4	-0.370	1.78	3.20
0.0	0.000	2.18	3.47
Average:		1.82	3.04
MFM:		1.83	3.05

CHORD AVERAGE CONCENTRATIONS:

POSITION y/R	C	C
0.90	0.013	0.026
0.70	0.026	0.065
0.50	0.033	0.079
0.30	0.033	0.086
0.10	0.042	0.097
-0.10	0.112	0.147
-0.30	0.190	0.214
-0.50	0.285	0.250
-0.70	0.392	0.362
-0.90	0.473	0.416
V (m/s):	1.83	3.05

PIPELINE FLOW DATA FOR 0 X 1 mm SAND-IN-WATER SLURRIES

RUN #: S8605052
DATE: 08/86
TEMP (C): 15
CARRIER: Water
SOLIDS: 0x1 mm silica sand

PIPE DIAMETER (m): 0.0532
SOLIDS DENSITY (g/cc): 2.65
SOLIDS VOL. FRACTION: 0.30

PARTICLE SIZE:

SIEVE SIZE (microns)	WEIGHT% PASSING
74	0.6
149	5.5
210	23.1
297	50.1
420	71.1
595	89.0
841	96.0
1190	98.7
1680	100.0

PIPELINE PERFORMANCE:

VELOCITY (m/s)	HEADLOSS (m/m)	DEPOSIT
3.05	0.2500	
2.74	0.2246	
2.44	0.2042	
2.13	0.1823	
1.83	0.1631	
1.68	0.1625	INT
1.52	0.1625	INT
1.37	0.1772	STA

VELOCITY DISTRIBUTIONS:

POSITION r/R	y/R	V (m/s)	V (m/s)
0.8	0.785	2.13	3.10
0.8	0.665	2.13	3.00
0.8	0.444	2.00	3.00
0.8	0.156	1.92	2.95
0.8	-0.156	1.81	2.91
0.8	-0.444	1.60	2.82
0.8	-0.665	1.52	2.56
0.8	-0.785	1.20	2.34
0.4	0.370	2.34	3.47
0.4	0.153	2.29	3.39
0.4	-0.153	2.04	3.24
0.4	-0.370	1.68	3.10
0.0	0.000	2.11	3.35
Average:		1.90	3.00
MFM:		1.83	3.05

CHORD AVERAGE CONCENTRATIONS:

POSITION y/R	C	C
0.90	0.037	0.114
0.70	0.093	0.178
0.50	0.151	0.204
0.30	0.223	0.257
0.10	0.278	0.287
-0.10	0.373	0.346
-0.30	0.409	0.385
-0.50	0.445	0.405
-0.70	0.472	0.440
-0.90	0.526	0.462
V (m/s):	1.83	3.05

PIPELINE FLOW DATA FOR 0 X 1 mm SAND-IN-WATER SLURRIES

RUN #: S8605053
DATE: 08/86
TEMP (C): 15
CARRIER: Water
SOLIDS: 0x1 mm silica sand

PIPE DIAMETER (m): 0.0532
SOLIDS DENSITY (g/cc): 2.65
SOLIDS VOL. FRACTION: 0.40

PARTICLE SIZE:		PIPELINE PERFORMANCE:		
SIEVE SIZE (microns)	WEIGHT% PASSING	VELOCITY (m/s)	HEADLOSS (m/m)	DEPOSIT
74	0.7	3.05	0.3165	
149	5.5	2.74	0.2971	
210	23.2	2.44	0.2880	
297	50.2	2.13	0.2748	
420	71.1	1.83	0.2503	
595	89.0	1.68	0.2359	
841	96.0	1.52	0.2456	INT
1680	100.0	1.37	0.2914	STA

VELOCITY DISTRIBUTIONS:

POSITION r/R	y/R	V (m/s)	V (m/s)
0.8	0.785	2.59	3.37
0.8	0.665	2.59	3.25
0.8	0.444	2.46	3.31
0.8	0.156	2.13	3.20
0.8	-0.156	1.41	2.91
0.8	-0.444	1.07	2.40
0.8	-0.665	0.64	1.96
0.8	-0.785	0.54	1.52
0.4	0.370	2.67	3.60
0.4	0.153	1.96	3.35
0.4	-0.153	1.55	2.87
0.4	-0.370	1.07	2.26
0.0	0.000	1.60	3.10
Average:		1.72	2.84
MFM:		1.83	3.05

CHORD AVERAGE CONCENTRATIONS:

POSITION y/R	C	C
0.90	0.125	0.268
0.70	0.183	0.301
0.50	0.297	0.349
0.30	0.407	0.390
0.10	0.441	0.417
-0.10	0.449	0.472
-0.30	0.515	0.478
-0.50	0.501	0.478
-0.70	0.535	0.482
-0.90	0.573	0.517
V (m/s):	1.83	3.05

PIPELINE FLOW DATA FOR 0 X 1 mm SAND-IN-WATER SLURRIES

RUN #: S8525041
DATE: 03/85
TEMP (C): 15
CARRIER: Water
SOLIDS: 0x1 mm silica sand

PIPE DIAMETER (m): 0.2631
SOLIDS DENSITY (g/cc): 2.65
SOLIDS VOL. FRACTION: 0.16

PARTICLE SIZE:		PIPELINE PERFORMANCE:		
SIEVE SIZE (microns)	WEIGHT% PASSING	VELOCITY (m/s)	HEADLOSS (m/m)	DEPOSIT
74	0.7	5.27	0.0760	
149	5.5	4.82	0.0669	
210	23.2	4.38	0.0590	
297	50.2	4.10	0.0545	
420	71.1	3.77	0.0494	
595	89.0	3.46	0.0451	INT
841	96.0	3.23	0.0424	INT
1680	100.0	3.01	0.0424	STA

VELOCITY DISTRIBUTIONS:

POSITION r/R	y/R	V (m/s)	V (m/s)
0.8	0.785	4.59	5.26
0.8	0.665	4.52	5.10
0.8	0.444	4.44	5.01
0.8	0.156	4.24	4.90
0.8	-0.156	3.84	4.52
0.8	-0.444	3.37	4.18
0.8	-0.665	3.01	3.89
0.8	-0.785	2.92	3.78
0.4	0.370	5.26	6.01
0.4	0.153	4.95	5.68
0.4	-0.153	4.38	5.19
0.4	-0.370	3.89	4.86
0.0	0.000	4.80	5.76
Average:		4.14	4.90
MFM:		4.21	5.00

CHORD AVERAGE CONCENTRATIONS:

POSITION y/R	C	C
0.90	0.025	0.024
0.70	0.028	0.029
0.50	0.033	0.038
0.30	0.045	0.053
0.10	0.073	0.086
-0.10	0.131	0.131
-0.30	0.221	0.211
-0.50	0.307	0.282
-0.70	0.399	0.356
-0.90	0.435	0.408
V (m/s):	3.94	4.68

PIPELINE FLOW DATA FOR 0 X 1 mm SAND-IN-WATER SLURRIES

RUN #: S8525042
DATE: 03/85
TEMP (C): 15
CARRIER: Water
SOLIDS: 0x1 mm silica sand

PIPE DIAMETER (m): 0.2631
SOLIDS DENSITY (g/cc): 2.65
SOLIDS VOL. FRACTION: 0.25

PARTICLE SIZE:

SIEVE SIZE (microns)	WEIGHT% PASSING
74	0.7
149	5.5
210	23.2
297	50.2
420	71.1
595	89.0
841	96.0
1680	100.0

PIPELINE PERFORMANCE:

VELOCITY (m/s)	HEADLOSS (m/m)	DEPOSIT
5.22	0.0846	
4.79	0.0753	
4.39	0.0678	
4.09	0.0629	
3.76	0.0582	
3.49	0.0545	
3.22	0.0507	INT
3.07	0.0506	INT
2.97	0.0512	STA

VELOCITY DISTRIBUTIONS:

POSITION r/R	y/R	V (m/s)	V (m/s)
0.8	0.785	4.87	5.32
0.8	0.665	4.79	5.28
0.8	0.444	4.55	5.09
0.8	0.156	4.04	4.62
0.8	-0.156	3.63	4.52
0.8	-0.444	3.45	4.24
0.8	-0.665	3.16	4.06
0.8	-0.785	3.12	4.00
0.4	0.370	5.51	6.18
0.4	0.153	4.86	5.60
0.4	-0.153	4.34	5.15
0.4	-0.370	3.99	4.94
0.0	0.000	4.79	5.68
Average:		4.22	4.95
MFM:		4.22	4.97

CHORD AVERAGE CONCENTRATIONS:

POSITION y/R	C	C
0.90	0.029	0.046
0.70	0.038	0.057
0.50	0.062	0.089
0.30	0.120	0.137
0.10	0.222	0.209
-0.10	0.292	0.273
-0.30	0.367	0.342
-0.50	0.401	0.378
-0.70	0.447	0.431
-0.90	0.470	0.440
V (m/s):	3.95	4.65

PIPELINE FLOW DATA FOR 0 X 1 mm SAND-IN-WATER SLURRIES

RUN #: S8525043
DATE: 03/85
TEMP (C): 15
CARRIER: Water
SOLIDS: 0x1 mm silica sand

PIPE DIAMETER (m): 0.2631
SOLIDS DENSITY (g/cc): 2.65
SOLIDS VOL. FRACTION: 0.34

PARTICLE SIZE:

SIEVE SIZE (microns)	WEIGHT% PASSING
74	0.7
149	5.5
210	23.2
297	50.2
420	71.1
595	89.0
841	96.0
1680	100.0

PIPELINE PERFORMANCE:

VELOCITY (m/s)	HEADLOSS (m/m)	DEPOSIT
5.22	0.0954	
4.84	0.0872	
4.55	0.0818	
4.13	0.0737	
3.83	0.0690	
3.60	0.0653	
3.34	0.0619	
3.19	0.0602	INT
3.06	0.0588	INT
2.88	0.0583	STA

VELOCITY DISTRIBUTIONS:

POSITION r/R	y/R	V (m/s)	V (m/s)
0.8	0.785	4.67	5.25
0.8	0.665	4.44	5.09
0.8	0.444	4.24	4.88
0.8	0.156	4.00	4.49
0.8	-0.156	3.84	4.59
0.8	-0.444	3.59	4.31
0.8	-0.665	3.41	4.24
0.8	-0.785	3.37	4.12
0.4	0.370	5.12	5.96
0.4	0.153	4.69	5.45
0.4	-0.153	4.44	5.22
0.4	-0.370	4.31	5.09
0.0	0.000	4.83	5.64
Average:		4.20	4.92
MFM:		4.25	5.00

CHORD AVERAGE CONCENTRATIONS:

POSITION y/R	C	C
0.90	0.074	0.097
0.70	0.111	0.153
0.50	0.198	0.208
0.30	0.294	0.282
0.10	0.365	0.335
-0.10	0.385	0.384
-0.30	0.432	0.415
-0.50	0.446	0.429
-0.70	0.485	0.458
-0.90	0.482	0.460
V (m/s):	3.98	4.68

PIPELINE FLOW DATA FOR 0 X 1 mm SAND-IN-WATER SLURRIES

RUN #: S8525045
DATE: 03/85
TEMP (C): 40
CARRIER: Water
SOLIDS: 0x1 mm silica sand

PIPE DIAMETER (m): 0.2631
SOLIDS DENSITY (g/cc): 2.65
SOLIDS VOL. FRACTION: 0.34

PARTICLE SIZE:		PIPELINE PERFORMANCE:		
SIEVE SIZE (microns)	WEIGHT% PASSING	VELOCITY (m/s)	HEADLOSS (m/m)	DEPOSIT
74	0.7	5.22	0.0956	
149	5.5	4.82	0.0878	
210	23.2	4.48	0.0833	
297	50.2	4.13	0.0776	
420	71.1	3.78	0.0744	
595	89.0	3.48	0.0691	INT
841	96.0	3.21	0.0632	INT
1680	100.0	3.02	0.0765	STA

VELOCITY DISTRIBUTIONS:

POSITION r/R	y/R	V (m/s)	V (m/s)
0.8	0.785	5.25	5.71
0.8	0.665	4.94	5.35
0.8	0.444	4.38	4.94
0.8	0.156	3.94	4.64
0.8	-0.156	3.78	4.38
0.8	-0.444	3.50	4.18
0.8	-0.665	3.08	4.00
0.8	-0.785	2.80	3.68
0.4	0.370	5.19	5.75
0.4	0.153	4.67	5.49
0.4	-0.153	4.38	5.00
0.4	-0.370	4.12	4.69
0.0	0.000	4.62	5.45
Average:		4.19	4.84
MFM:		4.21	4.92

CHORD AVERAGE CONCENTRATIONS:

POSITION y/R	C	C
0.90	0.050	0.054
0.70	0.078	0.087
0.50	0.148	0.168
0.30	0.278	0.271
0.10	0.379	0.353
-0.10	0.415	0.405
-0.30	0.475	0.451
-0.50	0.474	0.466
-0.70	0.527	0.515
-0.90	0.540	0.530
V (m/s):	3.94	4.60

PIPELINE FLOW DATA FOR 0 X 6 mm GRAVEL-IN-WATER SLURRIES

RUN #: S8525051
DATE: 04/85
TEMP (C): 15
CARRIER: Water
SOLIDS: 0x6 mm gravel

PIPE DIAMETER (m): 0.2631
SOLIDS DENSITY (g/cc): 2.65
SOLIDS VOL. FRACTION: 0.15

PARTICLE SIZE:		PIPELINE PERFORMANCE:		
SIEVE SIZE (microns)	WEIGHT% PASSING	VELOCITY (m/s)	HEADLOSS (m/m)	DEPOSIT
74	0.9	5.23	0.0808	
149	4.5	4.95	0.0754	
210	17.8	4.64	0.0700	
297	38.2	4.37	0.0654	
420	53.9	4.14	0.0623	INT
595	67.4	3.98	0.0607	INT
841	72.7	3.83	0.0582	INT
1680	77.1	3.75	0.0594	INT
2380	85.3	3.40	0.0507	INT
3360	94.9	3.22	0.0481	STA
4760	98.5			
9510	100.0			

VELOCITY DISTRIBUTIONS:

POSITION r/R	y/R	V (m/s)	V (m/s)
0.8	0.785	4.86	5.60
0.8	0.665	4.83	5.60
0.8	0.444	4.72	5.45
0.8	0.156	4.64	5.38
0.8	-0.156	4.44	5.00
0.8	-0.444	4.00	4.67
0.8	-0.665	3.33	4.24
0.8	-0.785	2.46	3.68
0.4	0.370	5.60	6.61
0.4	0.153	5.45	6.22
0.4	-0.153	4.94	5.83
0.4	-0.370	4.24	5.03
0.0	0.000	5.28	6.18
Average:		4.49	5.31
MFM:		4.41	5.21

CHORD AVERAGE CONCENTRATIONS:

POSITION y/R	C	C
0.90	0.018	0.029
0.70	0.024	0.025
0.50	0.027	0.035
0.30	0.042	0.046
0.10	0.060	0.071
-0.10	0.098	0.098
-0.30	0.161	0.155
-0.50	0.252	0.249
-0.70	0.411	0.403
-0.90	0.523	0.525
V (m/s):	4.13	4.87

PIPELINE FLOW DATA FOR 0 X 6 mm GRAVEL-IN-WATER SLURRIES

RUN #: S8525052
DATE: 04/85
TEMP (C): 15
CARRIER: Water
SOLIDS: 0x6 mm gravel

PIPE DIAMETER (m): 0.2631
SOLIDS DENSITY (g/cc): 2.65
SOLIDS VOL. FRACTION: 0.25

PARTICLE SIZE:		PIPELINE PERFORMANCE:		
SIEVE SIZE (microns)	WEIGHT% PASSING	VELOCITY (m/s)	HEADLOSS (m/m)	DEPOSIT
74	0.9	5.19	0.0903	
149	4.5	4.92	0.0859	
210	17.8	4.67	0.0826	
297	38.2	4.41	0.0758	
420	53.9	4.15	0.0740	
595	67.4	3.84	0.0735	INT
841	72.7	3.60	0.0667	INT
1680	77.1	3.34	0.0694	STA
2380	85.3			
3360	94.9			
4760	98.5			
9510	100.0			

VELOCITY DISTRIBUTIONS:

POSITION r/R	y/R	V (m/s)	V (m/s)
0.8	0.785	5.00	5.60
0.8	0.665	4.91	5.53
0.8	0.444	4.69	5.42
0.8	0.156	4.52	5.19
0.8	-0.156	4.24	4.91
0.8	-0.444	3.84	4.62
0.8	-0.665	3.11	4.08
0.8	-0.785	2.19	3.54
0.4	0.370	5.75	6.56
0.4	0.153	5.35	6.09
0.4	-0.153	4.67	5.56
0.4	-0.370	4.18	5.00
0.0	0.000	5.06	5.87
Average:		4.40	5.20
MFM:		4.41	5.16

CHORD AVERAGE CONCENTRATIONS:

POSITION y/R	C	C
0.90	0.043	0.054
0.70	0.056	0.066
0.50	0.071	0.082
0.30	0.117	0.128
0.10	0.183	0.181
-0.10	0.255	0.233
-0.30	0.321	0.310
-0.50	0.402	0.396
-0.70	0.522	0.501
-0.90	0.562	0.545
V (m/s):	4.13	4.83

PIPELINE FLOW DATA FOR 0 X 6 mm GRAVEL-IN-WATER SLURRIES

RUN #: S8525053
DATE: 04/85
TEMP (C): 15
CARRIER: Water
SOLIDS: 0x6 mm gravel

PIPE DIAMETER (m): 0.2631
SOLIDS DENSITY (g/cc): 2.65
SOLIDS VOL. FRACTION: 0.35

PARTICLE SIZE:		PIPELINE PERFORMANCE:		
SIEVE SIZE (microns)	WEIGHT% PASSING	VELOCITY (m/s)	HEADLOSS (m/m)	DEPOSIT
74	0.9	5.26	0.1022	
149	4.5	4.92	0.0951	
210	17.8	4.67	0.0891	
297	38.2	4.39	0.0832	
420	53.9	4.13	0.0796	
595	67.4	3.86	0.0734	
841	72.7	3.72	0.0696	INT
1680	77.1	3.54	0.0639	INT
2380	85.3	3.34	0.0725	INT
3360	94.9	3.16	0.0763	STA
4760	98.5			
9510	100.0			

VELOCITY DISTRIBUTIONS:

POSITION r/R	y/R	V (m/s)	V (m/s)
0.8	0.785	5.06	5.49
0.8	0.665	4.86	5.42
0.8	0.444	4.57	5.28
0.8	0.156	4.38	5.00
0.8	-0.156	4.12	4.91
0.8	-0.444	3.78	4.57
0.8	-0.665	3.26	4.18
0.8	-0.785	2.86	3.50
0.4	0.370	5.53	6.27
0.4	0.153	5.12	6.00
0.4	-0.153	4.62	5.60
0.4	-0.370	4.24	5.06
0.0	0.000	4.88	5.87
Average:		4.39	5.14
MFM:		4.38	5.16

CHORD AVERAGE CONCENTRATIONS:

POSITION y/R	C	C
0.90	0.096	0.116
0.70	0.124	0.147
0.50	0.165	0.195
0.30	0.238	0.242
0.10	0.319	0.304
-0.10	0.379	0.366
-0.30	0.446	0.443
-0.50	0.500	0.479
-0.70	0.562	0.550
-0.90	0.584	0.560
V (m/s):	4.10	4.83

PIPELINE FLOW DATA FOR 0 X 6 mm GRAVEL-IN-WATER SLURRIES

RUN #: S8525054
DATE: 04/85
TEMP (C): 40
CARRIER: Water
SOLIDS: 0x6 mm gravel

PIPE DIAMETER (m): 0.2631
SOLIDS DENSITY (g/cc): 2.65
SOLIDS VOL. FRACTION: 0.35

PARTICLE SIZE:		PIPELINE PERFORMANCE:		
SIEVE SIZE (microns)	WEIGHT% PASSING	VELOCITY (m/s)	HEADLOSS (m/m)	DEPOSIT
74	0.9	5.26	0.0979	
149	4.5	4.93	0.0918	
210	17.8	4.69	0.0881	
297	38.2	4.40	0.0883	
420	53.9	4.10	0.0797	
595	67.4	3.86	0.0748	
841	72.7	3.59	0.0713	INT
1680	77.1	3.58	0.0691	INT
2380	85.3	3.42	0.0861	INT
3360	94.9	3.21	0.0883	STA
4760	98.5			
9510	100.0			

VELOCITY DISTRIBUTIONS:

POSITION r/R	y/R	V (m/s)	V (m/s)
0.8	0.785	5.12	5.75
0.8	0.665	4.94	5.68
0.8	0.444	4.62	5.35
0.8	0.156	4.38	5.05
0.8	-0.156	4.18	4.88
0.8	-0.444	3.84	4.62
0.8	-0.665	3.22	3.94
0.8	-0.785	2.46	3.33
0.4	0.370	5.68	6.51
0.4	0.153	5.00	6.00
0.4	-0.153	4.52	5.53
0.4	-0.370	4.12	5.00
0.0	0.000	4.83	5.75
Average:		4.36	5.16
MFM:		4.38	5.17

CHORD AVERAGE CONCENTRATIONS:

POSITION y/R	C	C
0.90	0.067	0.071
0.70	0.102	0.098
0.50	0.154	0.144
0.30	0.232	0.221
0.10	0.326	0.313
-0.10	0.385	0.383
-0.30	0.441	0.464
-0.50	0.471	0.504
-0.70	0.522	0.587
-0.90	0.588	0.611
V (m/s):	3.41	4.10

PIPELINE FLOW DATA FOR 0 X 10 mm COAL-IN-WATER SLURRIES

RUN #: S8525011
DATE: 02/85
TEMP (C): 23
CARRIER: Water
SOLIDS: 0 x 10 mm Westar coal

PIPE DIAMETER (m): 0.263
SOLIDS DENSITY (g/cc): 1.374
SOLIDS VOL. FRACTION: 0.23

PARTICLE SIZE:		PIPELINE PERFORMANCE:		
SIEVE SIZE (microns)	WEIGHT% PASSING	VELOCITY (m/s)	HEADLOSS (m/m)	DEPOSIT
74	4.0	4.07	0.0428	
210	19.3	3.58	0.0355	
420	41.1	3.14	0.0290	
841	53.0	2.61	0.0231	
2380	74.3	2.14	0.0177	
6730	92.1	1.77	0.0167	INT
12700	100.0	1.57	0.0150	STA

VELOCITY DISTRIBUTIONS:

POSITION r/R	y/R	V (m/s)	V (m/s)
0.8	0.785		
0.8	0.665		
0.8	0.444		
0.8	0.156		
0.8	-0.156		
0.8	-0.444		
0.8	-0.665		
0.8	-0.785		
0.4	0.370		
0.4	0.153		
0.4	-0.153		
0.4	-0.370		
0.0	0.000		

Average:
MFM:

CHORD AVERAGE CONCENTRATIONS:

POSITION y/R	C	C
0.90	0.114	0.185
0.70	0.145	0.126
0.50	0.115	0.123
0.30	0.108	0.145
0.10	0.181	0.178
-0.10	0.195	0.164
-0.30	0.176	0.203
-0.50	0.299	0.286
-0.70	0.489	0.443
-0.90	0.627	0.600
V (m/s):	2.40	3.10

PIPELINE FLOW DATA FOR 0 X 10 mm COAL-IN-WATER SLURRIES

RUN #:	S8525012	PIPE DIAMETER (m):	0.263
DATE:	02/85	SOLIDS DENSITY (g/cc):	1.374
TEMP (C):	23	SOLIDS VOL. FRACTION:	0.35
CARRIER:	Water		
SOLIDS:	0 x 10 mm Westar coal		

PARTICLE SIZE:		PIPELINE PERFORMANCE:		
SIEVE SIZE (microns)	WEIGHT% PASSING	VELOCITY (m/s)	HEADLOSS (m/m)	DEPOSIT
74	33.5	4.17	0.0483	
210	43.1	3.68	0.0383	
420	57.2	3.19	0.0326	
841	66.5	2.69	0.0261	
2380	83.4	2.27	0.0215	
6730	95.6	1.96	0.0192	
12700	100.0	1.69	0.0190	STA

VELOCITY DISTRIBUTIONS:

POSITION r/R	y/R	V (m/s)	V (m/s)
0.8	0.785	2.49	3.27
0.8	0.665	2.45	3.19
0.8	0.444	2.42	3.22
0.8	0.156	2.42	3.17
0.8	-0.156	2.37	3.18
0.8	-0.444	2.20	3.14
0.8	-0.665	1.59	2.75
0.8	-0.785	1.20	2.07
0.4	0.370	2.85	3.72
0.4	0.153	2.85	3.73
0.4	-0.153	2.74	3.69
0.4	-0.370	2.52	3.50
0.0	0.000	2.94	3.93
Average:		2.37	3.25
MFM:		2.43	3.26

CHORD AVERAGE CONCENTRATIONS:

POSITION y/R	C	C
0.90	0.264	0.297
0.70	0.227	0.274
0.50	0.231	0.223
0.30	0.257	0.270
0.10	0.283	0.307
-0.10	0.328	0.318
-0.30	0.327	0.321
-0.50	0.464	0.450
-0.70	0.580	0.548
-0.90	0.702	0.696
V (m/s):	2.40	3.10

PIPELINE FLOW DATA FOR 0 X 10 mm COAL-IN-WATER SLURRIES

RUN #:	S8525013	PIPE DIAMETER (m):	0.263
DATE:	02/85	SOLIDS DENSITY (g/cc):	1.374
TEMP (C):	22	SOLIDS VOL. FRACTION:	0.48
CARRIER:	Water		
SOLIDS:	0 x 10 mm Westar coal		

PARTICLE SIZE:		PIPELINE PERFORMANCE:		
SIEVE SIZE (microns)	WEIGHT% PASSING	VELOCITY (m/s)	HEADLOSS (m/m)	DEPOSIT
74	36.7	3.90	0.0466	
210	46.4	3.43	0.0385	
420	56.7	3.04	0.0333	
841	64.2	2.61	0.0284	
2380	80.8	2.20	0.0224	
6730	95.2	1.93	0.0203	
12700	100.0	1.69	0.0169	
		1.54	0.0175	STA

VELOCITY DISTRIBUTIONS:

POSITION r/R	y/R	V (m/s)	V (m/s)
0.8	0.785	2.27	2.98
0.8	0.665	2.28	2.97
0.8	0.444	2.34	3.00
0.8	0.156	2.33	3.03
0.8	-0.156	2.31	3.03
0.8	-0.444	2.15	3.03
0.8	-0.665	1.73	2.81
0.8	-0.785	1.21	2.34
0.4	0.370	2.71	3.47
0.4	0.153	2.71	3.50
0.4	-0.153	2.65	3.47
0.4	-0.370	2.45	3.34
0.0	0.000	2.81	3.67
Average:		2.28	3.10
MFM:		2.29	3.13

CHORD AVERAGE CONCENTRATIONS:

POSITION y/R	C	C
0.90	0.395	0.391
0.70	0.395	0.430
0.50	0.426	0.405
0.30	0.419	0.419
0.10	0.453	0.468
-0.10	0.459	0.477
-0.30	0.484	0.476
-0.50	0.557	0.525
-0.70	0.590	0.567
-0.90	0.758	0.664
V (m/s):	2.20	2.90

APPENDIX B

CONCENTRATION DISTRIBUTION PLOTS

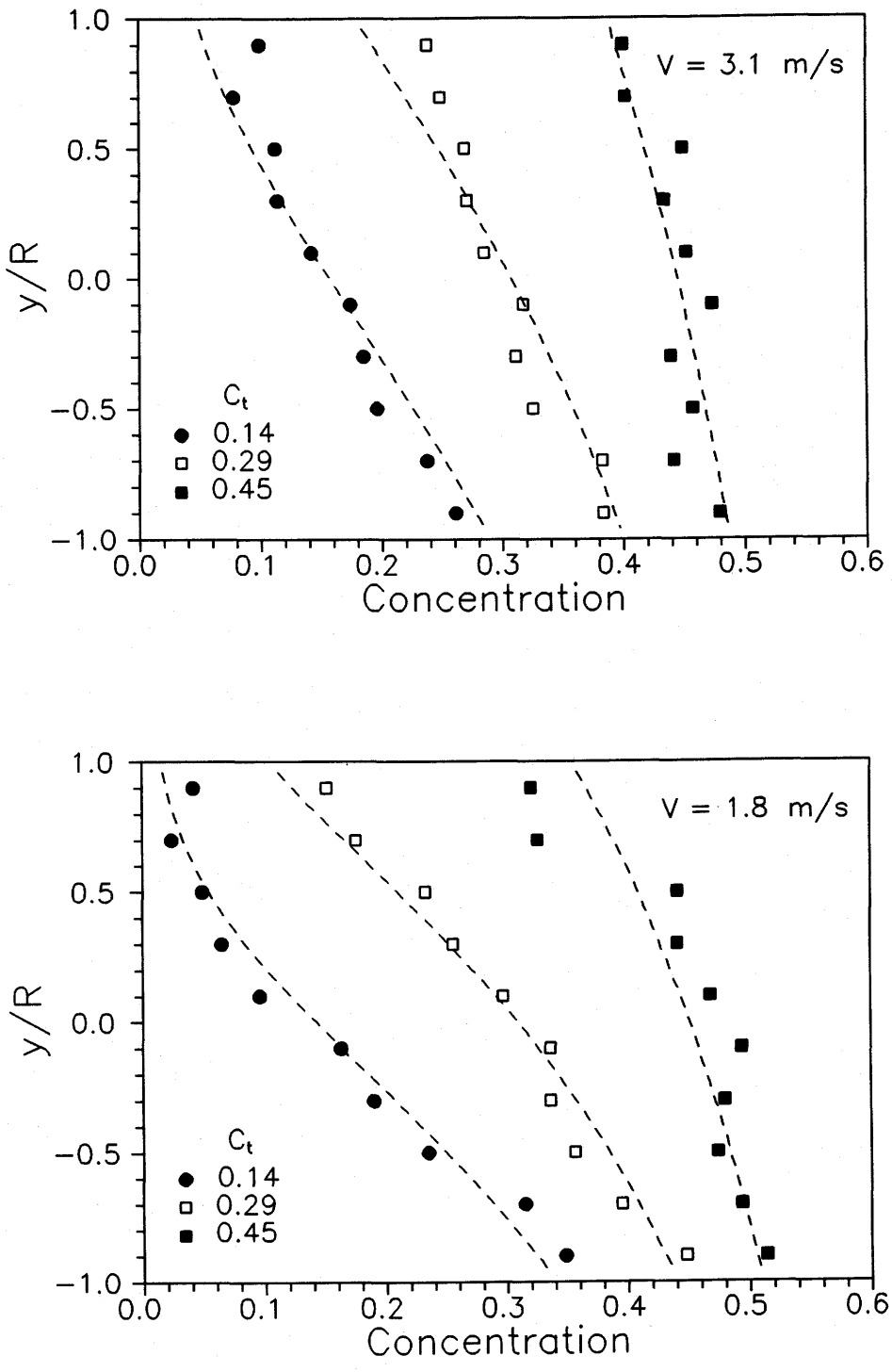

Figure B1: Concentration distributions for 0.18 mm sand slurries flowing in a 53.2 mm pipe. T = 15°C.

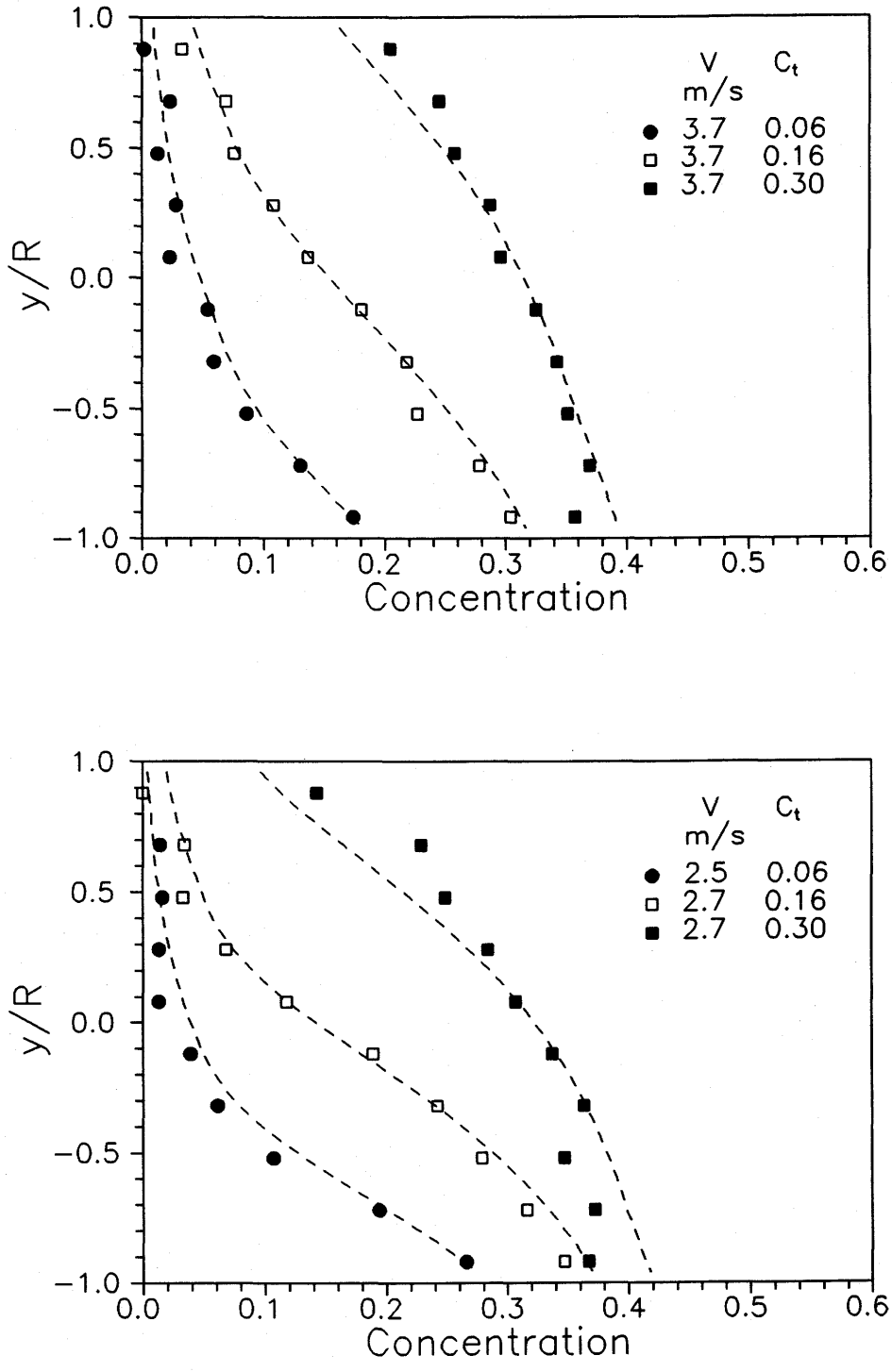

Figure B2: Concentration distributions for 0.19 mm sand slurries flowing in a 159 mm pipe. T = 10°C.

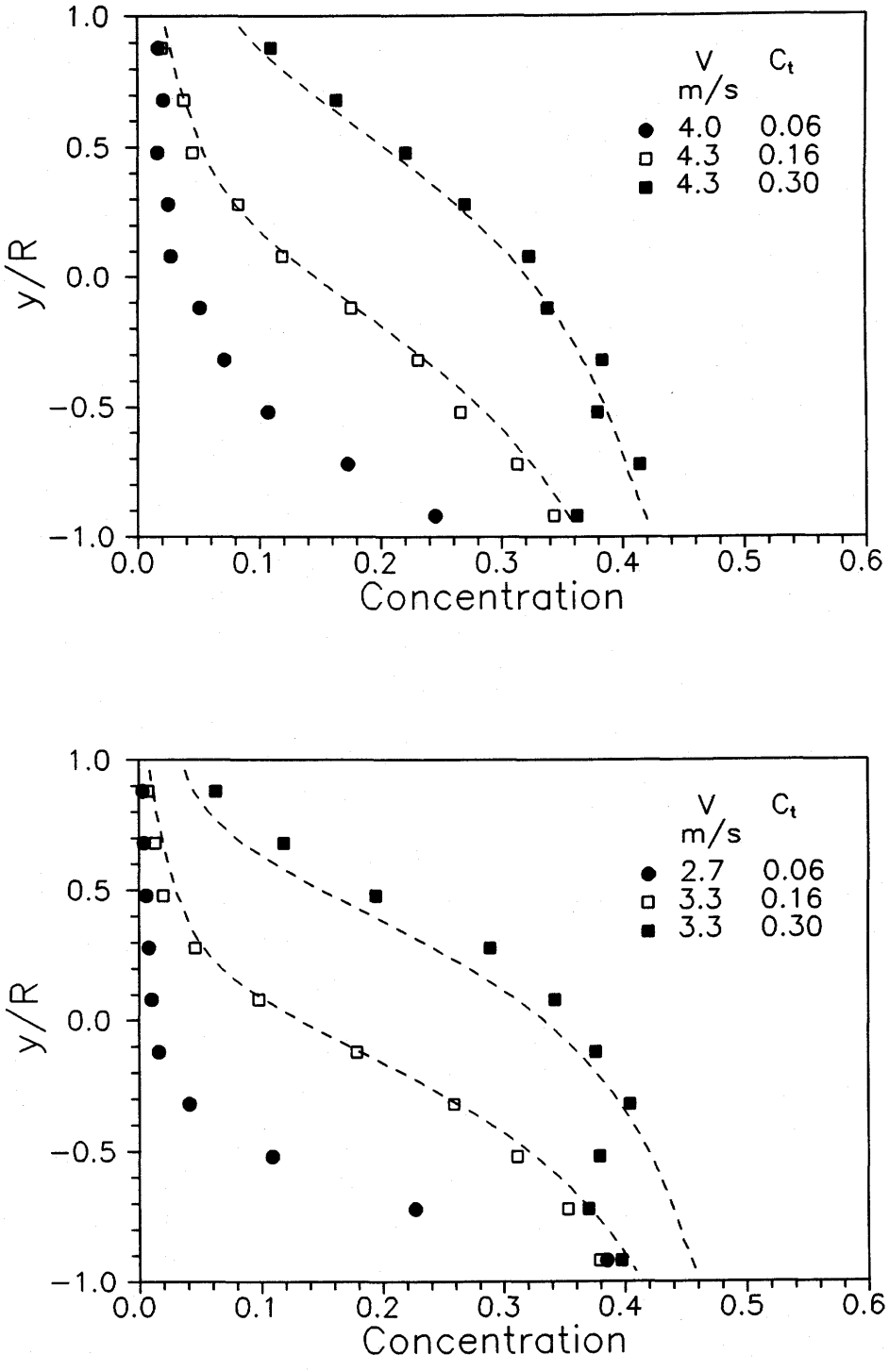

Figure B3: Concentration distributions for 0.19 mm sand slurries flowing in a 159 mm pipe. T = 60°C.

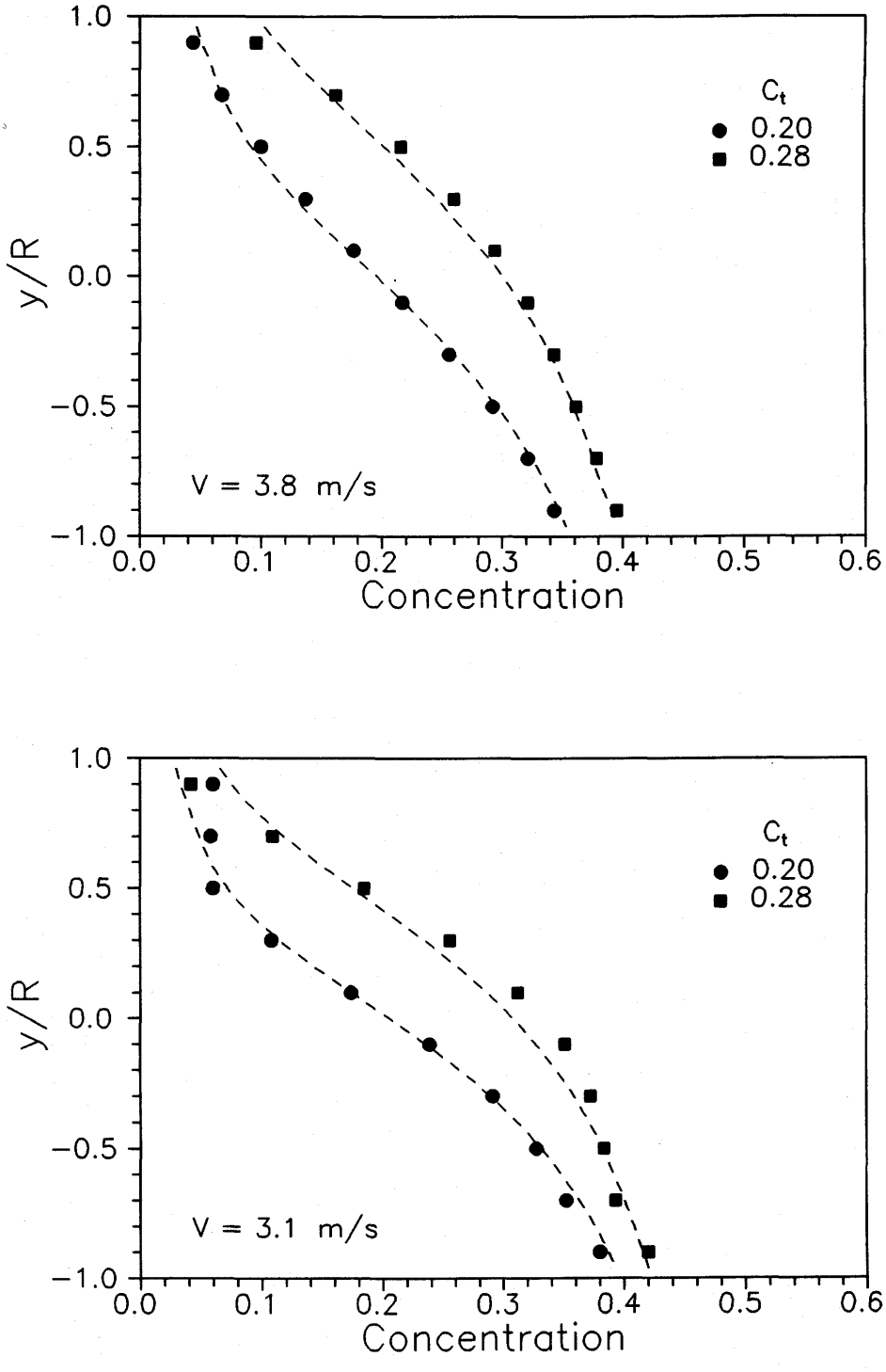

Figure B4: Concentration distributions for 0.18 mm sand slurries flowing in a 495 mm pipe. T = 13°C.

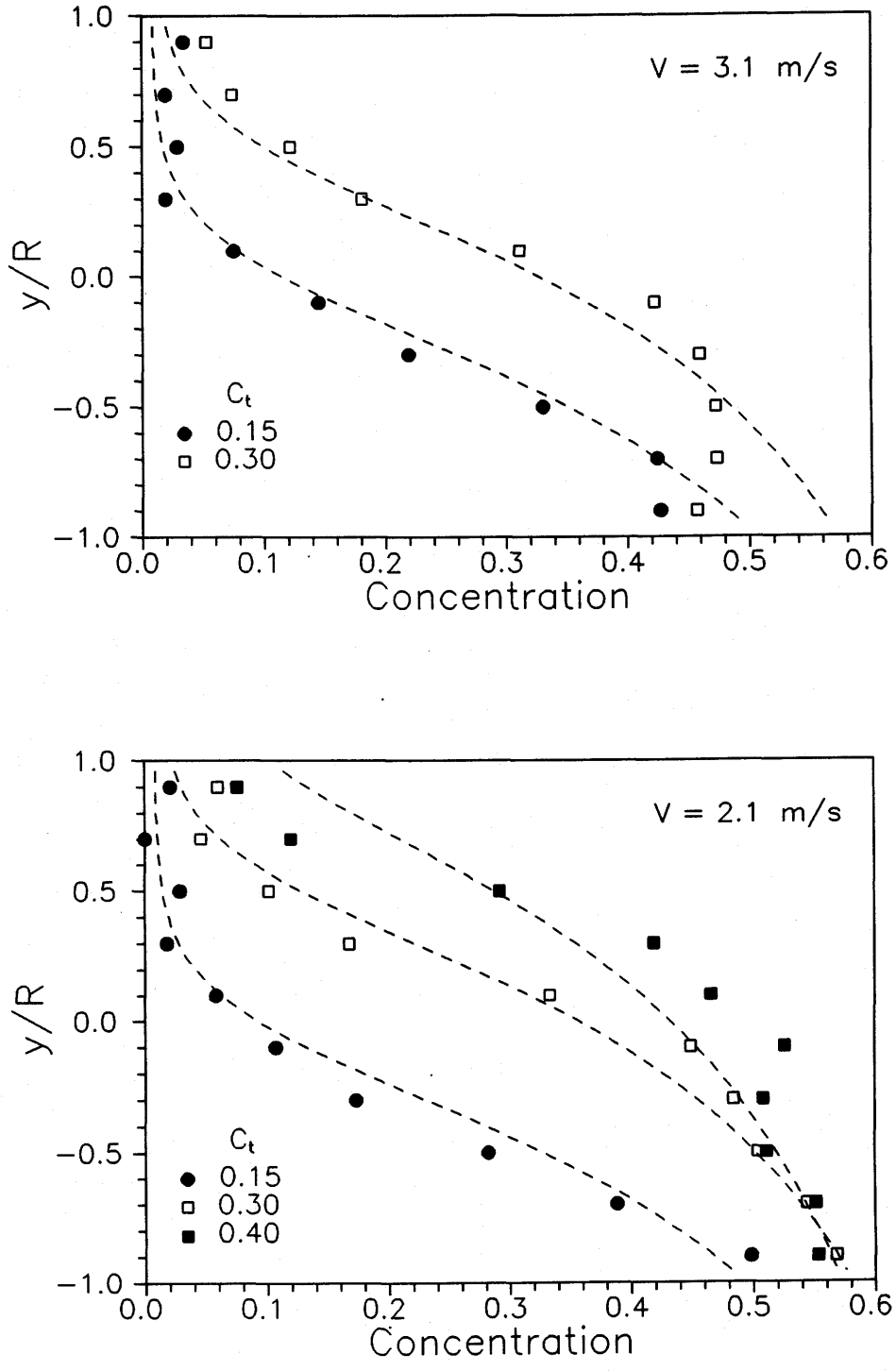

Figure B5: Concentration distributions for 0.55 mm sand slurries flowing in a 53.2 mm pipe. T = 15°C.

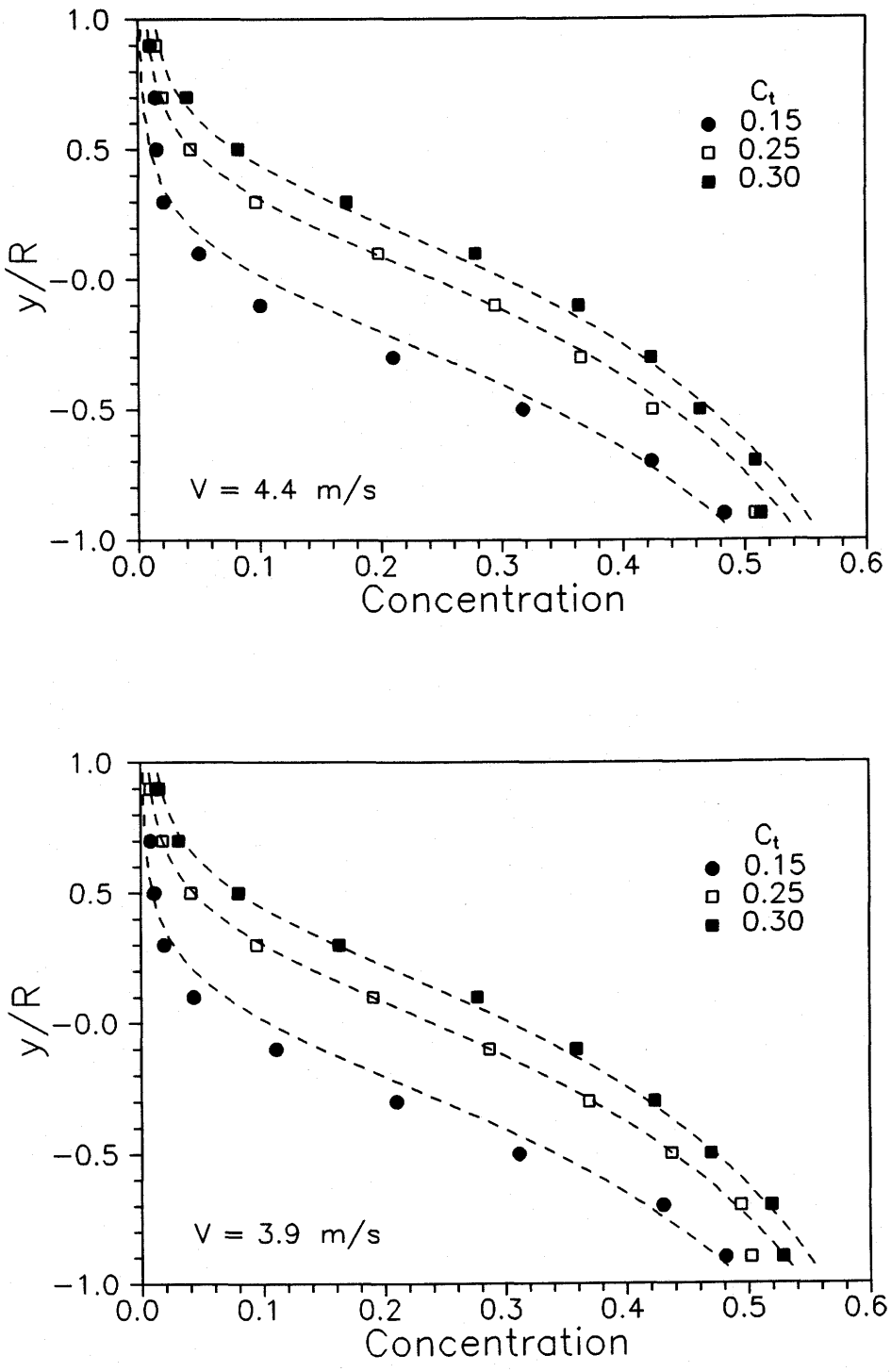

Figure B6: Concentration distributions for 0.55 mm sand slurries flowing in a 263 mm pipe. T = 15 °C.

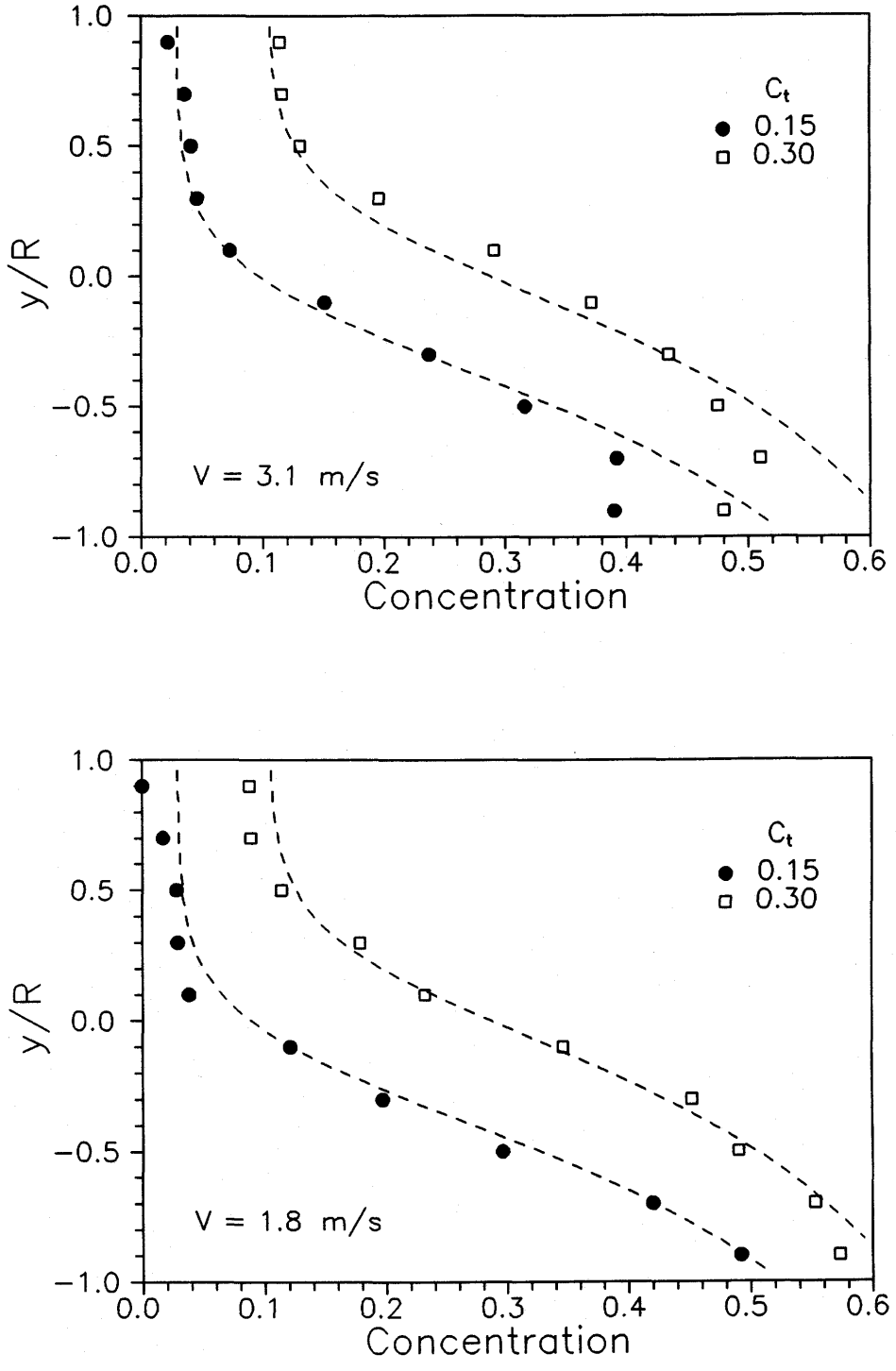

Figure B7: Concentration distributions for 2.4 mm sand slurries flowing in a 53.2 mm pipe. T = 15°C.

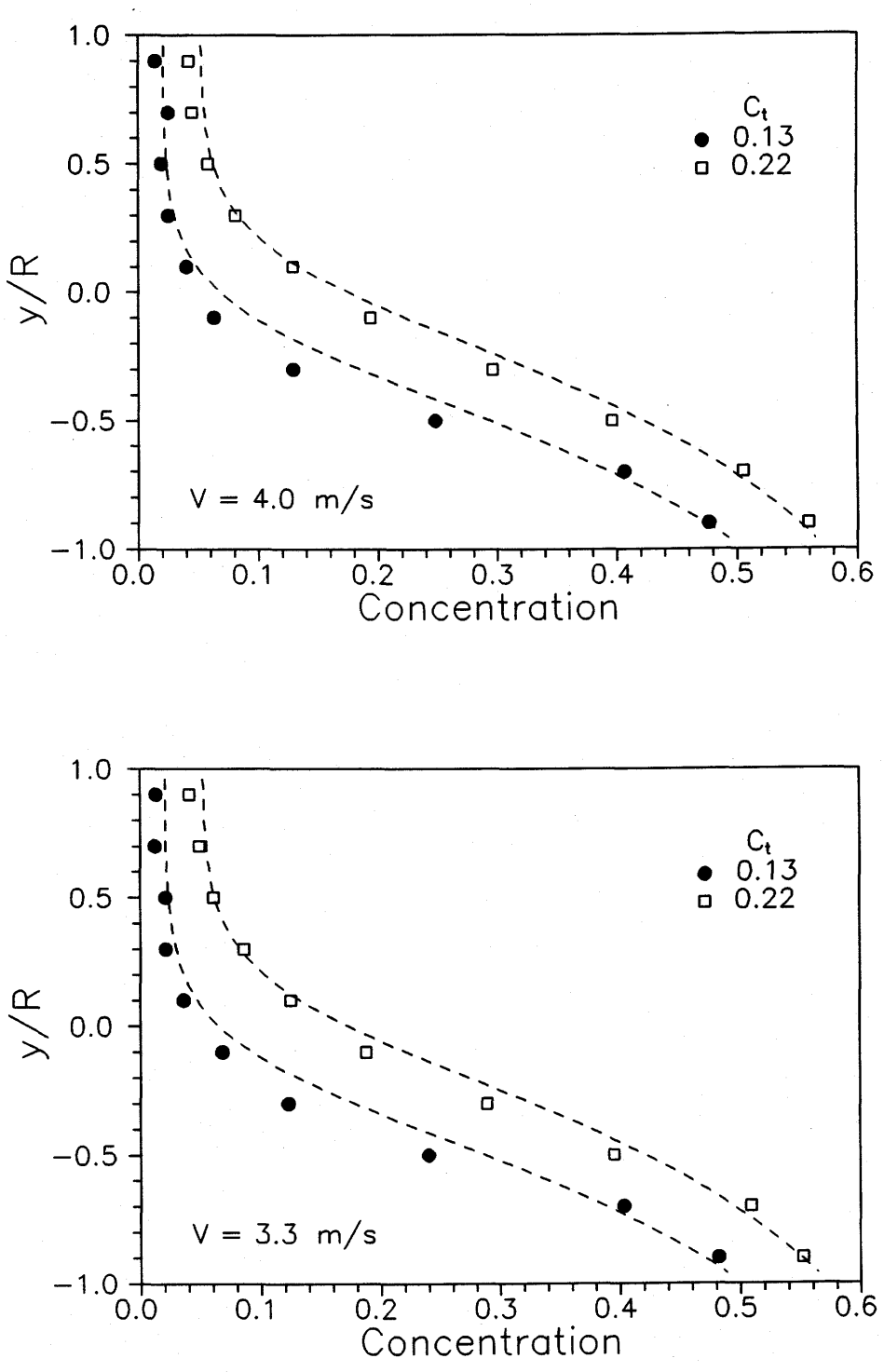

Figure B8: Concentration distributions for 2.4 mm sand slurries flowing in a 263.1 mm pipe. T = 15 °C.

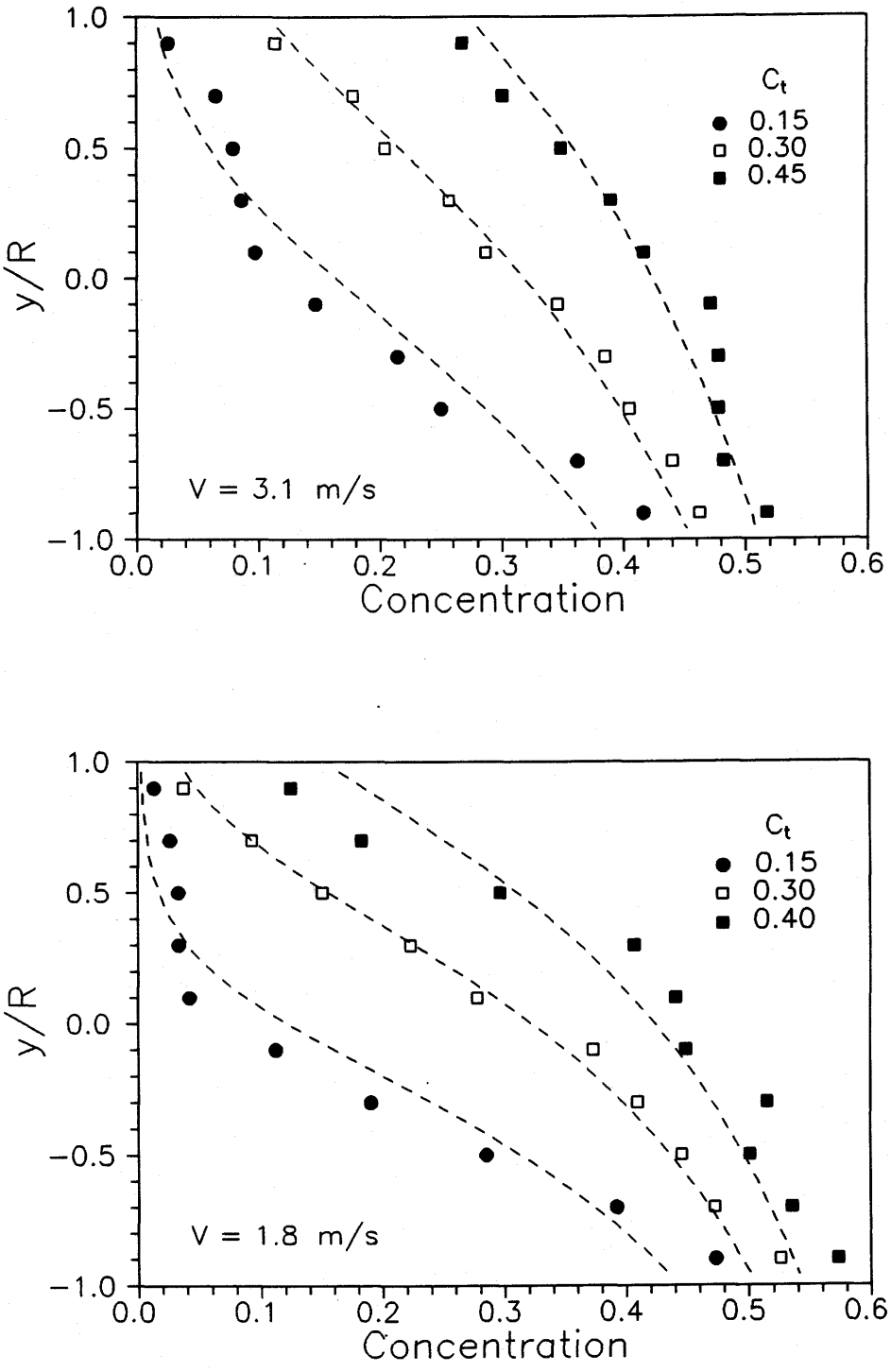

Figure B9: Concentration distributions for 0.29 mm sand slurries flowing in a 53.2 mm pipe. T = 15°C.

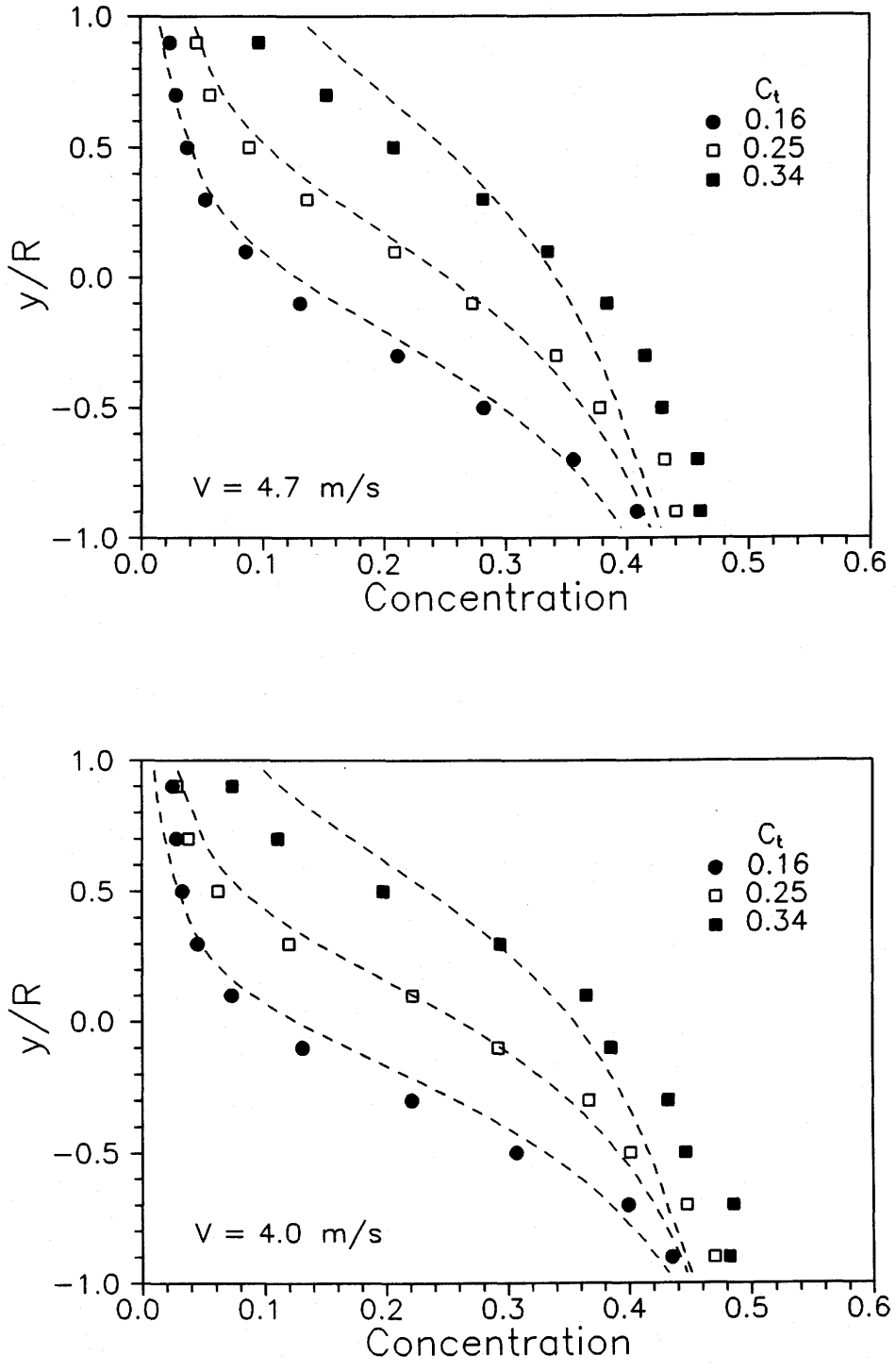

Figure B10: Concentration distributions for 0.29 mm sand slurries flowing in a 263 mm pipe. T = 15 °C.

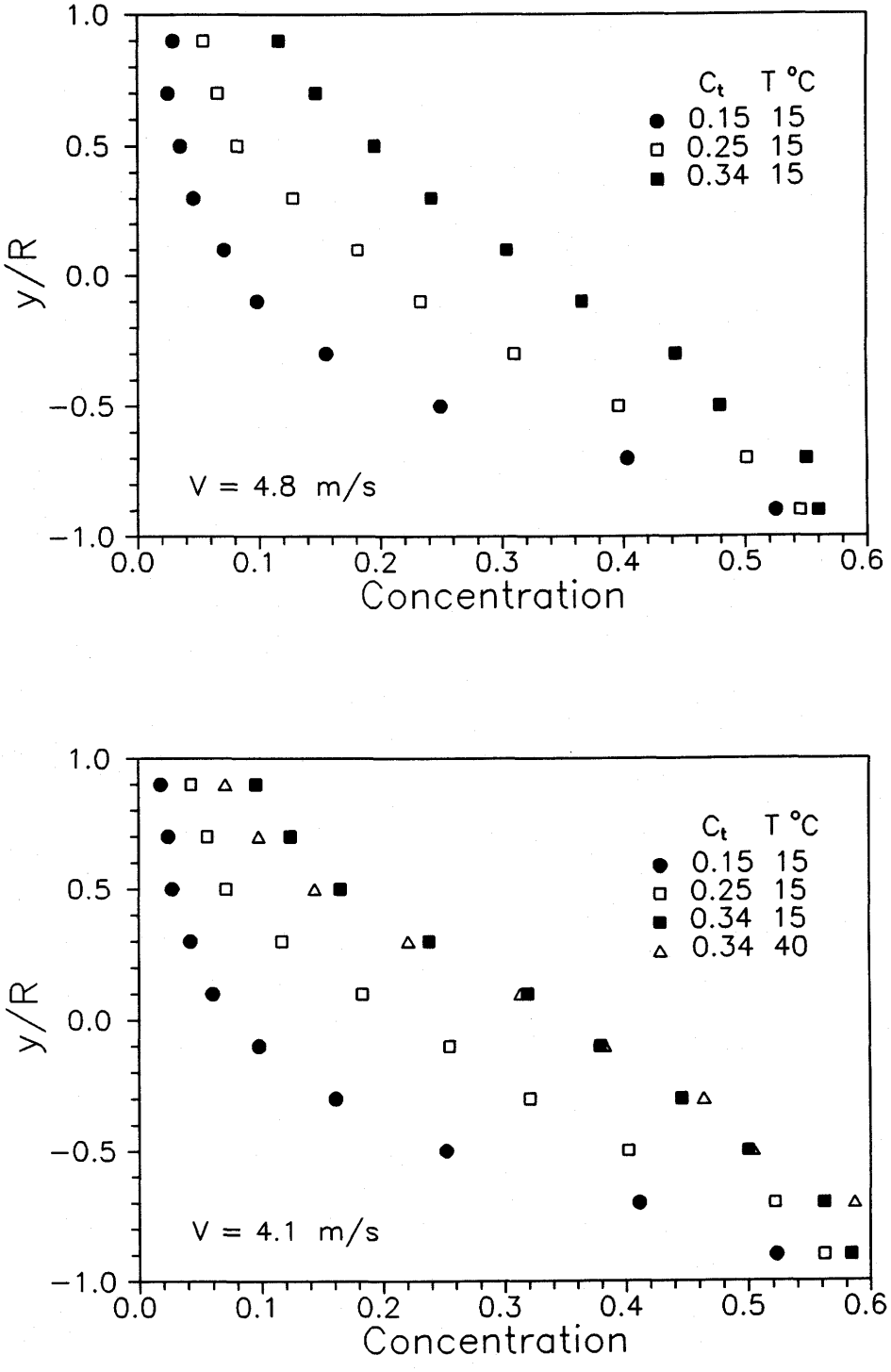

Figure B11: Concentration distributions for 0.38 mm sand slurries flowing in a 263 mm pipe. T = 15°C.

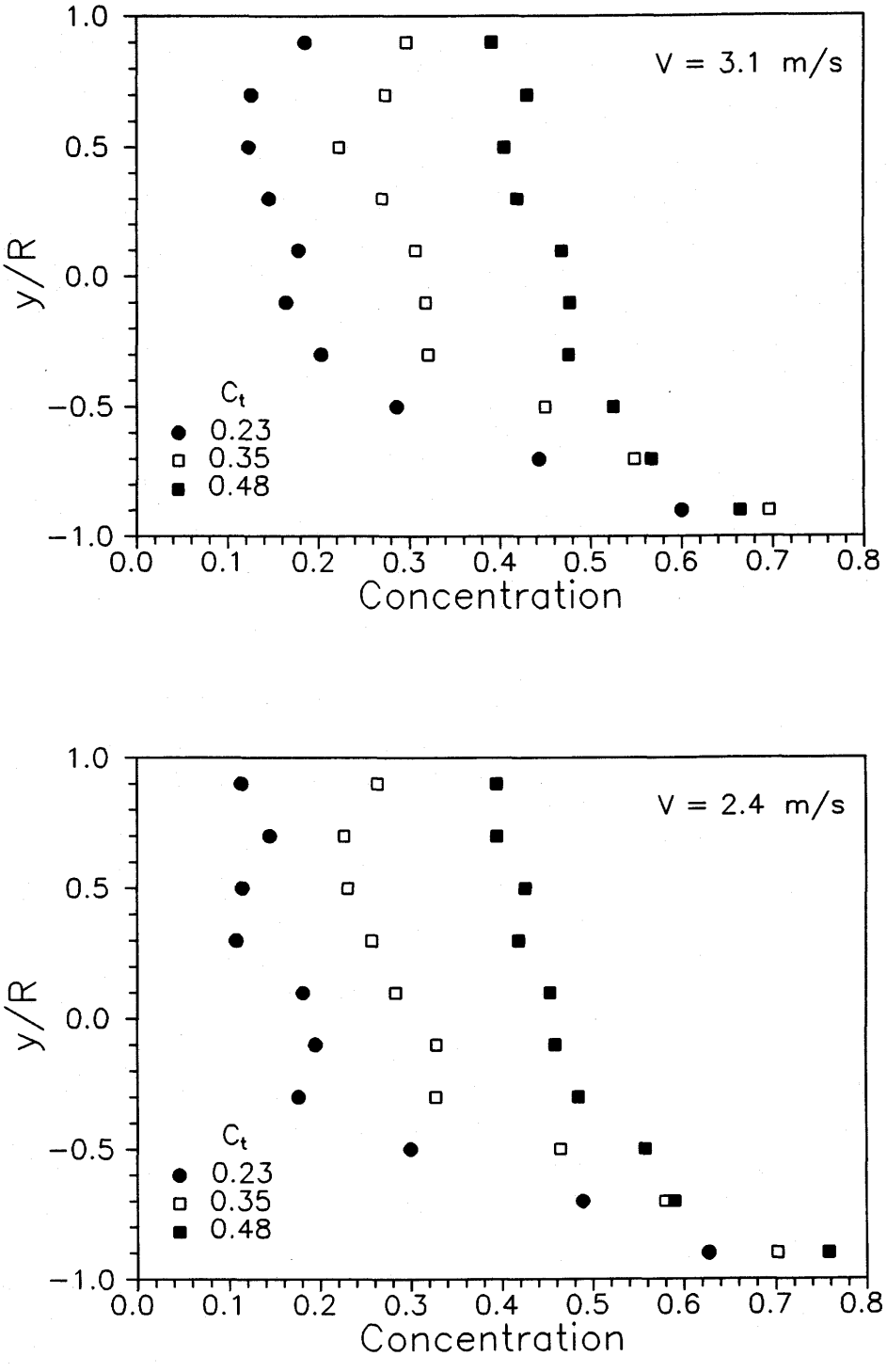

Figure B12: Concentration distributions for 0 to 10 mm coal slurries flowing in a 263 mm pipe. T = 23°C.

APPENDIX C

VELOCITY DISTRIBUTION PLOTS

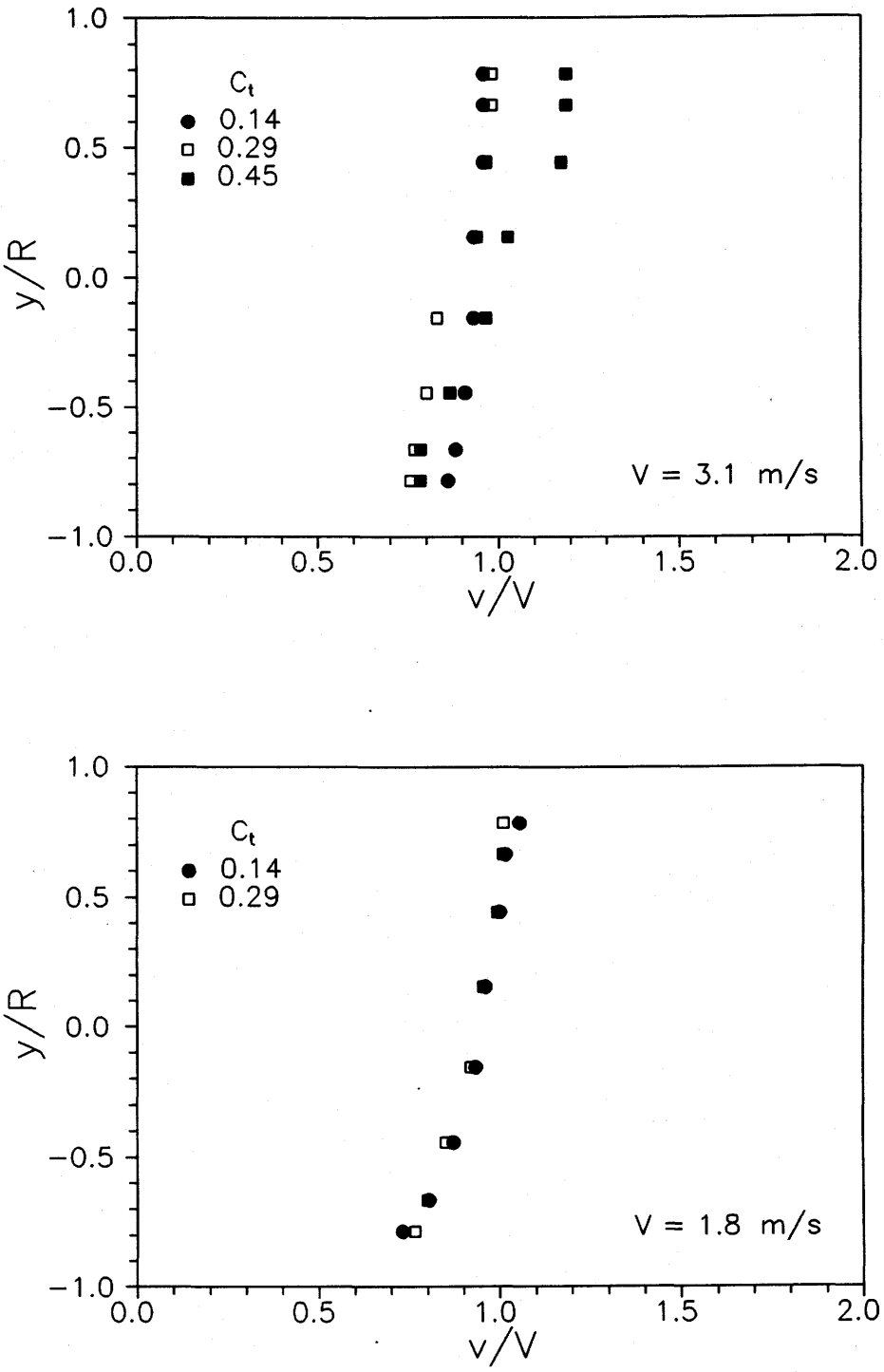

Figure C1: Velocity distributions for 0.18 mm sand slurries flowing in a 53.2 mm pipe. r/R = 0.8. T = 15°C.

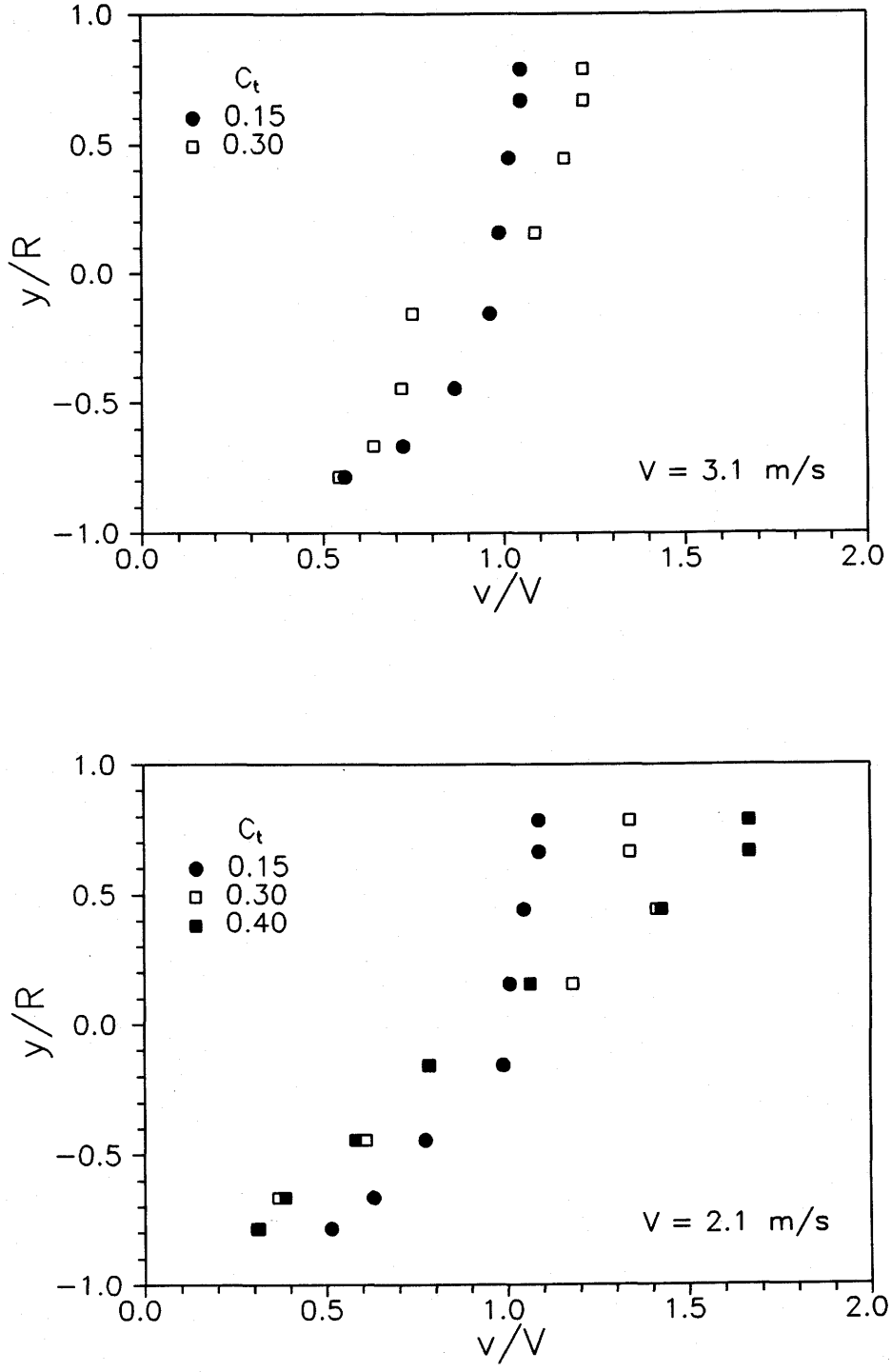

Figure C2: Velocity distributions for 0.55 mm sand slurries flowing in a 53.2 mm pipe. r/R = 0.8. T = 15°C.

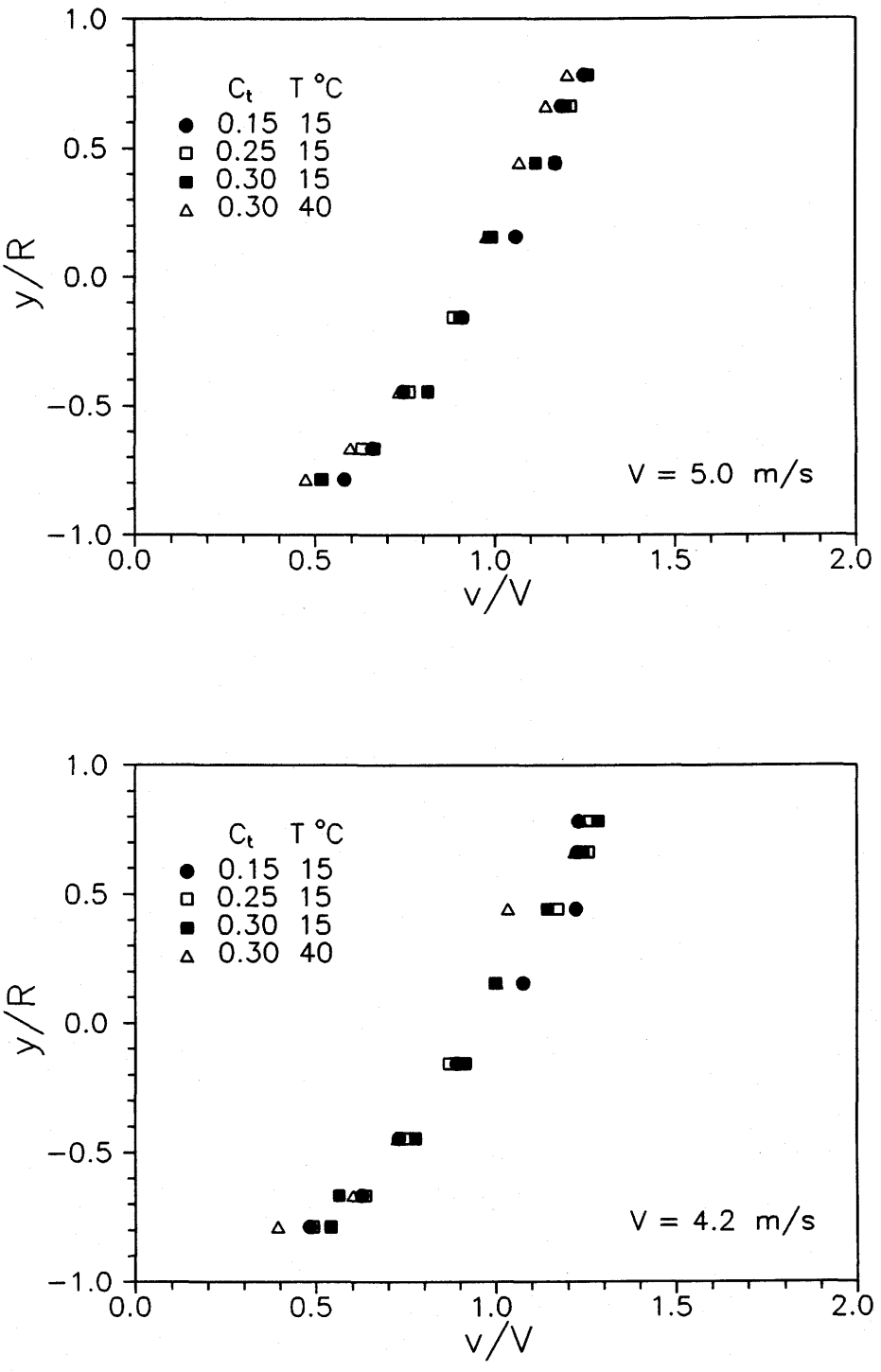

Figure C3: Velocity distributions for 0.55 mm sand slurries flowing in a 263 mm pipe. r/R = 0.8.

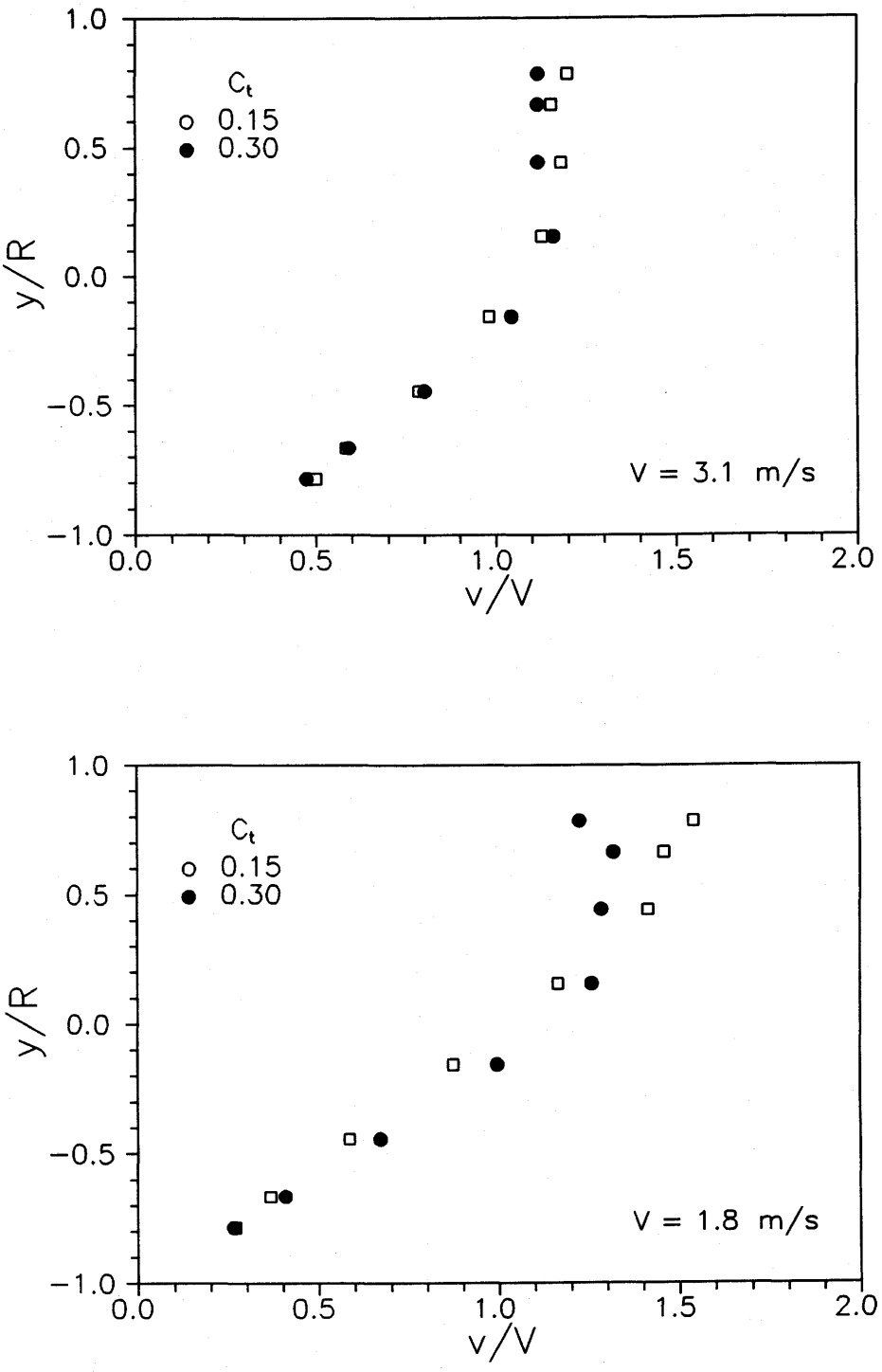

Figure C4: Velocity distributions for 2.4 mm sand slurries flowing in a 53.2 mm pipe. r/R = 0.8. T = 15°C.

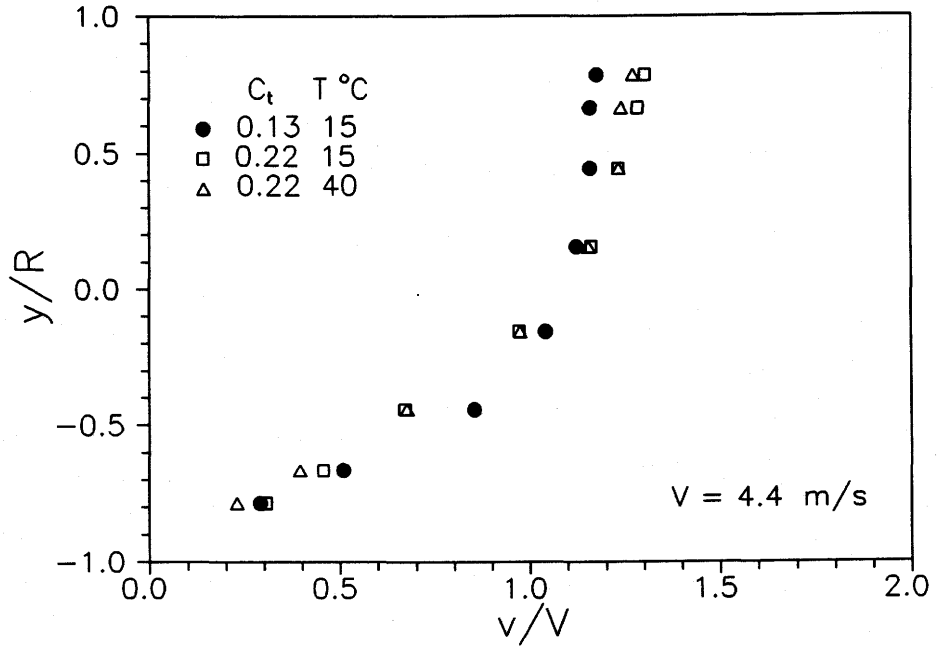

Figure C5: Velocity distributions for 2.4 mm sand slurries flowing in a 263 mm pipe. r/R = 0.8.

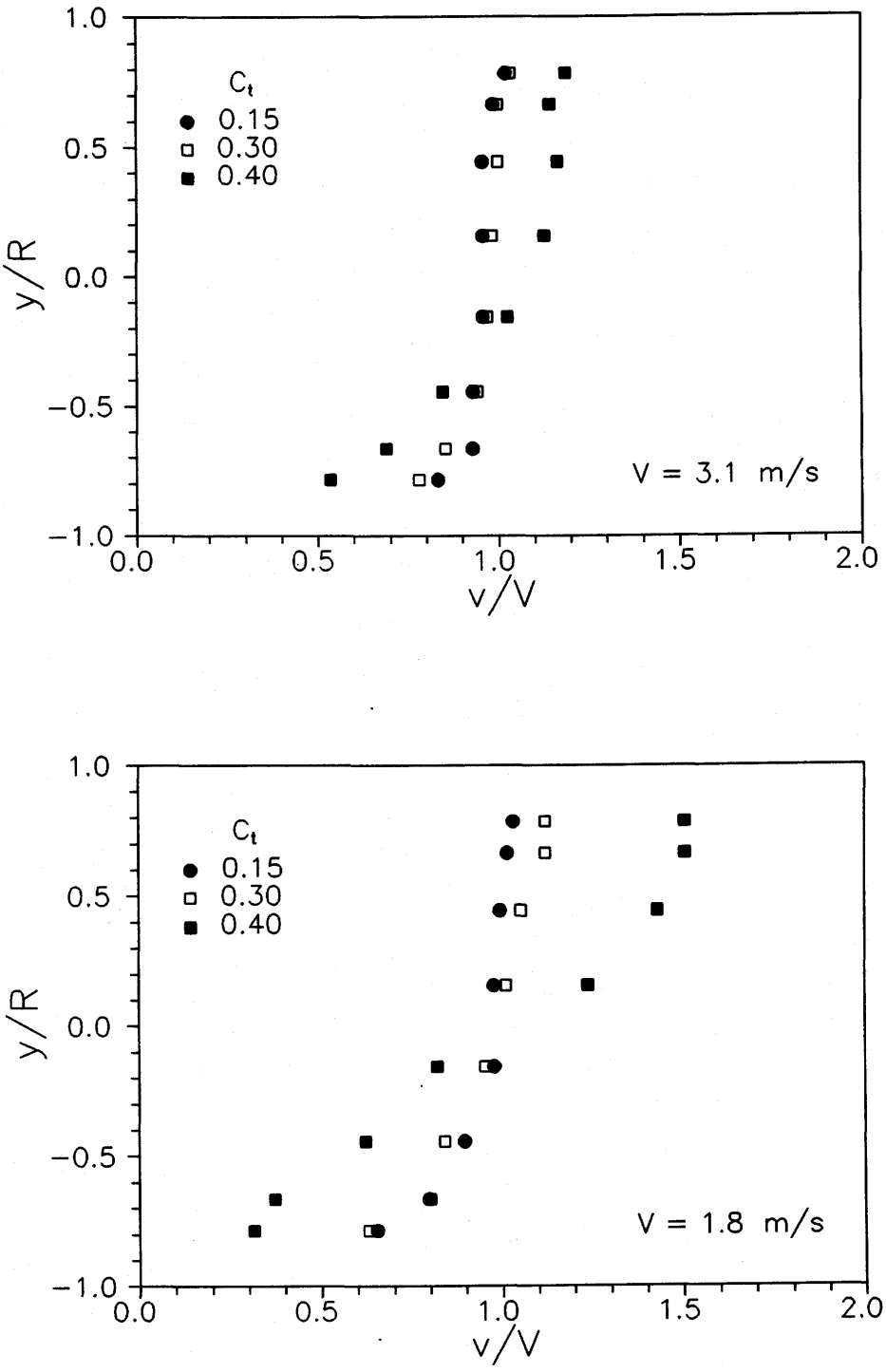

Figure C6: Velocity distributions for 0.29 mm sand slurries flowing in a 53.2 mm pipe. r/R = 0.8. T = 15°C.

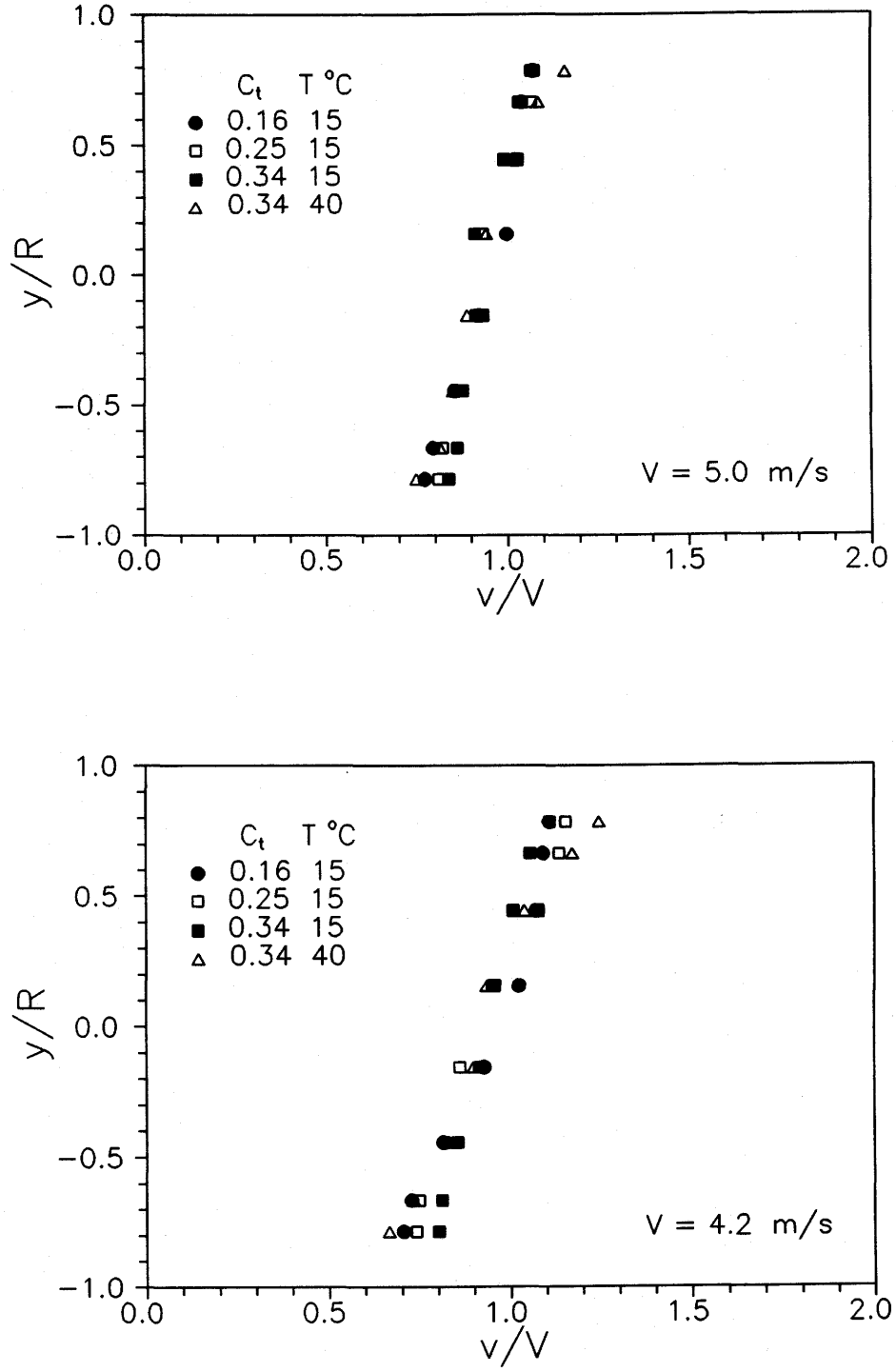

Figure C7: Velocity distributions for 0.29 mm sand slurries flowing in a 263 mm pipe. r/R = 0.8.

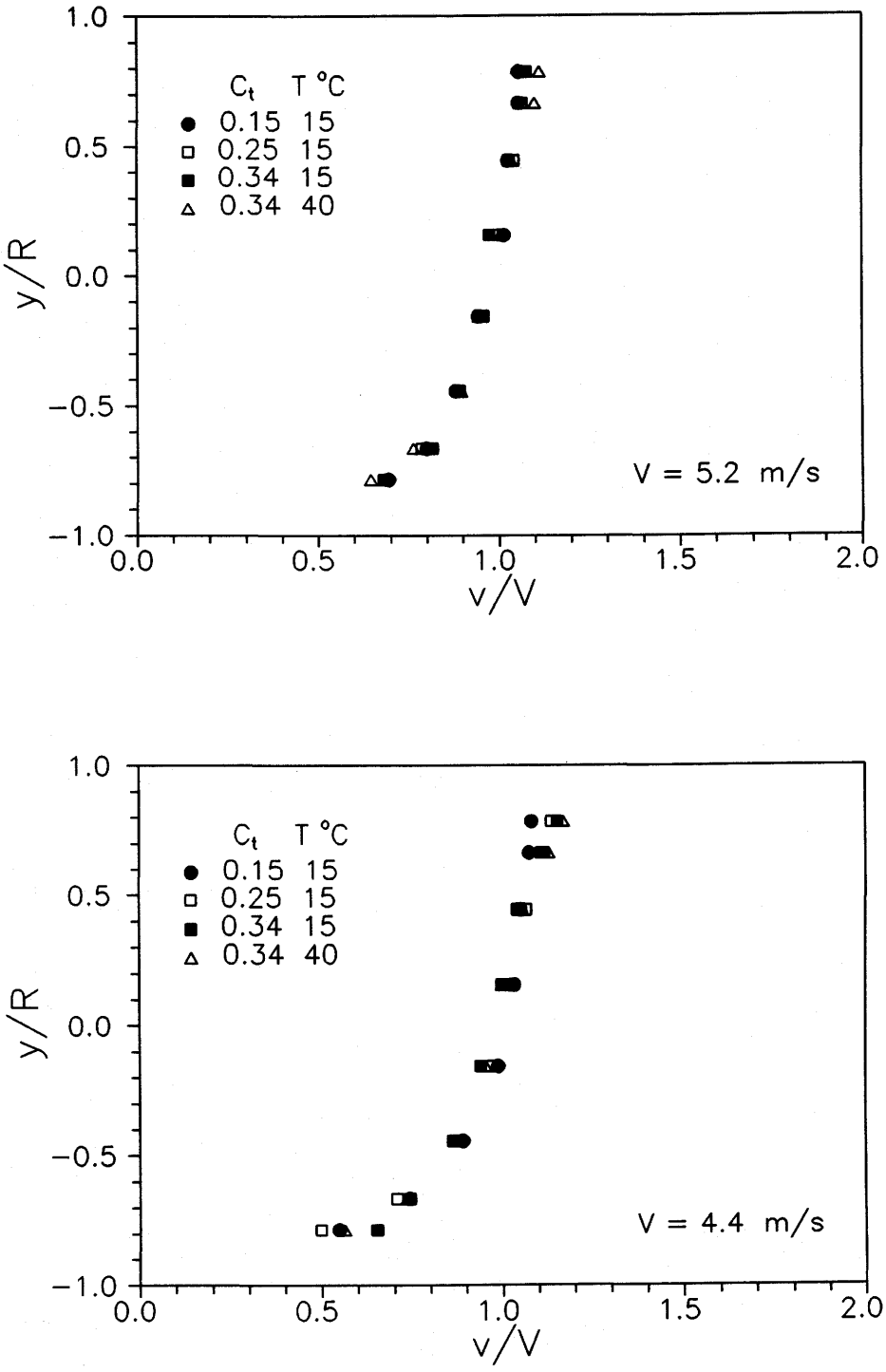

Figure C8: Velocity distributions for 0.38 mm sand slurries flowing in a 263 mm pipe. r/R = 0.8.

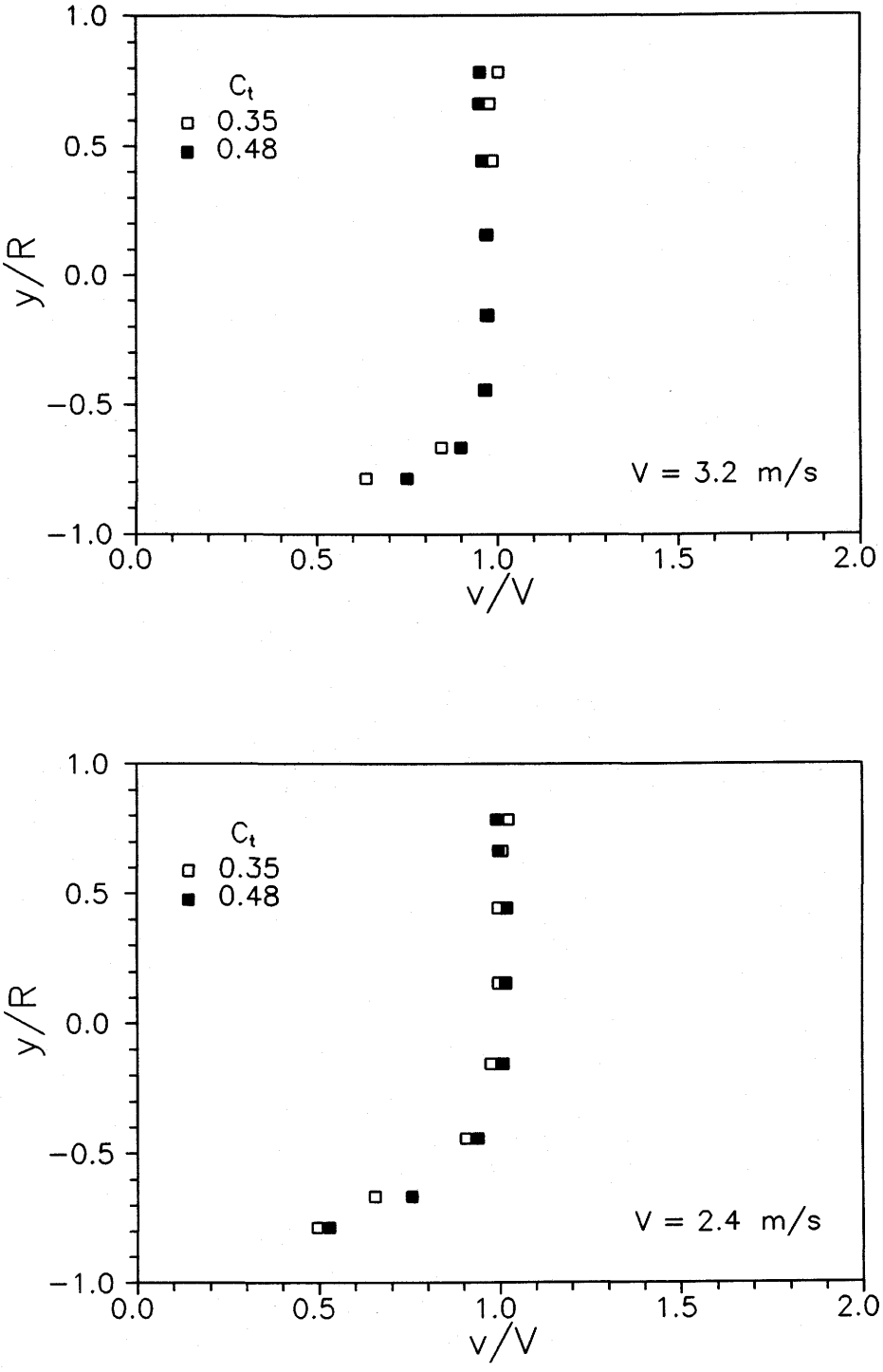

Figure C9: Velocity distributions for 0 to 10 mm coal slurries flowing in a 263 mm pipe. r/R = 0.8. T = 23°C.

APPENDIX D

DATABASE FOR CONTACT LOAD CORRELATIONS

Table D.1 Data Included in the First Contact Load Correlation (Equation 6.16).

D (mm)	d_{50} (mm)	ρ_s (kg/m^3)	ρ_f (kg/m^3)	μ_f (mPa.s)	C_r
53	0.19	2650	984	0.5	0.18
53	0.19	2650	984	0.5	0.36
53	0.19	2650	998	1.0	0.18
53	0.19	2650	998	1.0	0.36
53	0.19	2650	1000	1.3	0.18
53	0.19	2650	1000	1.3	0.36
53	0.49	2650	999	1.0	0.18
53	0.49	2650	999	1.0	0.30
263	0.19	2650	999	1.1	0.29
263	0.19	2650	999	1.0	0.38
263	0.29	2650	1000	1.3	0.16
263	0.29	2650	1004	1.5	0.25
263	0.29	2650	1007	1.8	0.34
263	0.29	2650	999	1.0	0.34
263	0.38	2650	1004	1.3	0.15
263	0.38	2650	1019	1.3	0.24
263	0.38	2650	1034	1.8	0.33
263	0.38	2650	1045	1.0	0.32
263	0.55	2650	1003	1.3	0.15
263	0.55	2650	1010	1.5	0.25
263	0.55	2650	1009	1.6	0.30
263	0.55	2650	1007	0.9	0.29
263	2.40	2650	1029	1.5	0.11
263	2.40	2650	1068	2.0	0.19
263	2.40	2650	1058	1.2	0.19
263	0.80	1374	1001	0.9	0.22
263	0.85	1374	1042	2.1	0.23
263	1.10	1374	1064	3.2	0.30
495	0.19	2650	999	1.2	0.35
495	0.19	2650	985	0.5	0.21
495	0.19	2650	985	0.5	0.28
495	0.19	2650	985	0.5	0.36

Table D.2 Data Included in the Revised Contact Load Correlation (Equation 6.19).

D (mm)	d_{50} (mm)	ρ_s (kg/m^3)	ρ_f (kg/m^3)	μ_f (mPa.s)	C_r
53	0.19	2650	999	1.2	0.15
53	0.19	2650	999	1.2	0.30
53	0.29	2650	1001	1.2	0.15
53	0.19	2650	1004	1.4	0.30
53	0.55	2650	1001	1.2	0.15
53	0.55	2650	1013	1.6	0.30
53	2.4	2650	1041	1.3	0.14
53	2.4	2650	1173	2.1	0.22
159	3.0	1668	1026	1.6	0.19
159	3.1	1668	1063	2.3	0.34
263	0.29	2650	1000	1.3	0.16
263	0.29	2650	1004	1.5	0.25
263	0.29	2650	1007	1.8	0.34
263	0.29	2650	999	1.0	0.34
263	0.38	2650	1004	1.3	0.15
263	0.38	2650	1019	1.3	0.24
263	0.38	2650	1034	1.8	0.33
263	0.38	2650	1045	1.0	0.32
263	0.55	2650	1003	1.3	0.15
263	0.55	2650	1010	1.5	0.25
263	0.55	2650	1009	1.6	0.30
263	0.55	2650	1007	0.9	0.29
263	2.40	2650	1029	1.5	0.11
263	2.40	2650	1068	2.0	0.19
263	2.40	2650	1058	1.2	0.19
263	0.80	1374	1003	0.9	0.22
263	0.85	1374	1057	2.1	0.23
263	1.10	1374	1095	3.2	0.30
495	0.18	2650	1000	1.2	0.15
495	0.18	2650	1000	1.2	0.20
495	0.18	2650	1000	1.2	0.25
495	0.18	2650	1000	1.3	0.29
495	0.19	2650	985	0.5	0.21
495	0.19	2650	985	0.5	0.28